Universitá degli Studi di Ferrara

Facoltà di Scienze Matematiche Fisiche e Naturali

INFLUENCE OF ACCIDENTAL EVENTS ON DIRECT CP VIOLATION MEASUREMENT IN K^0 DECAYS

$\sim \circ \sim$

Relatore: Dott. F. PETRUCCI

Correlatore: Chiar.mo Prof. P. DALPIAZ

Tesi di Dottorato di:

Dott.ssa Marcella SCARPA

Dottorato di Ricerca in Fisica, XV ciclo

Abstract

Re(ϵ'/ϵ) is an important parameter to establish the direct CP violation. CERN NA48 experiment took data, for Re(ϵ'/ϵ), from 1997 to 2001. The decay rates of neutral kaons ($K_{L,S}$) in two pions were measured using two collinear beams and the four decay modes were collected simultaneously. The experimental design allows the cancellation of symmetrically contributing systematic effects on the double ratio R defined as

$$\mathrm{R}=\frac{\Gamma(K_L\to\pi^0\pi^0)\Gamma(K_S\to\pi^+\pi^-)}{\Gamma(K_S\to\pi^0\pi^0)\Gamma(K_L\to\pi^+\pi^-)} \approx 1-6Re(\epsilon'/\epsilon)$$

2001 data taking was devoted to take additional data, check the stability of the measure with respect to preceding years (different duty cycle and longer spill of the SPS beam, lower primary proton momentum, new drift chambers), and perform refined studies on accidental activity and beam intensity variations.

The installation of two new beam monitors was required with integrated output in four different time windows from 200ns to 15μs. With these simple new devices a better understanding has been achieved on the accidental activity related to the beams and, as a consequence, the error on the corresponding correction to R has been lowered as expected.

Main subject of this dissertation is my work on:

- new beam monitors installation, their performances and data quality
- study of beam intensity variations
- analysis on beam-induced accidental activity.

Both last two items are based on beam monitors data and other techniques such as Overlay Monte Carlo.

Dedication

To my mum - 2nd time, the revenge

Acknowledgements

It has been really a pleasure to work within the Ferrara group on the NA48 experiment. First of all I would like to thank my supervisors Piero Dalpiaz and Ferruccio Petrucci for their support and kindliness of disposition. To the rest of Ferrara group: Jean Duclos and Alberto Gianoli, the INFN Ferrara electronics team also called *dream team* Angelo Cotta Ramusino, Stefano Chiozzi, Roberto Malaguti and Chiara Damiani, Pier Luigi Frabetti and Mara Martini thank-you to have shared your knowledge and your time with me in a fruitfully and kindly way.

Special thank to the NA48 collaboration as a whole for being like it is. I would like to thank all the NA48 members and in particular, for their hints, Lydia Fayard and Guillame Unal and the other analysis coordinators: Ivan Mikulec, Massimo Lenti, Cristina Lazzeroni. To our spokesmen, Heinrich Wahl and Augusto Ceccucci, and to Italo Mannelli thank-you for the useful suggestions given to all of us. Thank to the CERN-fellowship: Roberta, Roberto (alias Saccobello), Marco (alias Contalb), Giangi, Il Prof, Lucia e Marco (alias Clemenciccio). for their introduction to the experiment and the nice time we have spent together.

Thanks to my family and all the friends in Ferrara and Milan that have bear me with patience and sympathy. And special thanks to the 'Koncus' Tito and Marianna. Lastly I would like to thank Elena Tininini who lighted my interest in physics in a very special way: 'You will like it and have funny time: physicists are crazy people'.

Contents

Tables

Table

Figures

Figure

Introduction

Contents NA48 is a CERN experiment located on K12 SPS beam line. Until year 2001 the $Re(\epsilon'/\epsilon)$ measurement in $K_{L,S} \to \pi\pi^{00,+-}$ decays was its primary goal [3, 2, 1]. During 2002 the experiment, named NA48/1 [4], took data according to the K_S rare decays program and in 2003 NA48/2 [5] will run with K^+K^- beams.

$Re(\epsilon'/\epsilon)$ determination is achieved through the double ratio of decay rates:

$$R = \frac{\Gamma(K_L \to \pi^0\pi^0)\Gamma(K_S \to \pi^+\pi^-)}{\Gamma(K_S \to \pi^0\pi^0)\Gamma(K_L \to \pi^+\pi^-)} \approx 1 - 6Re(\epsilon'/\epsilon) \tag{1}$$

As K_L and K_S beams are collinear and the four decay modes are simultaneously collected in the same fiducial volume, it is possible to cancel systematic effects with symmetric contributions on Long/Short or Charge/Neutral modes. After background subtraction we are led to a *counting experiment* in which only the number of good events enter in the double ratio:

$$R = \frac{N(K_L \to \pi^0\pi^0)N(K_S \to \pi^+\pi^-)}{N(K_S \to \pi^0\pi^0)N(K_L \to \pi^+\pi^-)} \tag{2}$$

and the further effort is evaluating the systematics effects due to residual asymmetries.

2001 was the last year devoted to $Re(\epsilon'/\epsilon)$ measure. This last run was very important to reach a precise understanding of beam related accidental activity and its influence on $Re(\epsilon'/\epsilon)$. It was also a stability test on previous measures since there were significant differences and improvements with respect to the past:

- the primary proton beam intensity and the accelerator duty cycle were different: the end of LEP activities granted a longer spill delivered to NA48 with lower momentum protons. These conditions give lower instantaneous intensity in the detector.

- new drift chambers, rebuild after the 1999 beam pipe implosion in which all the four chambers were damaged.

  The 2000 run was devoted to systematic checks and others K_S and K_L decays.

I report here the NA48 results for the different data taking periods:

sample	Re(ϵ'/ϵ)
1997	(15.3 ± 2.3)x10^{-4} [1]
199-99	(15.0 ± 2.7)x10^{-4} [2]
2001	(13.7 ± 3.1)x10^{-4} [3]

and the NA48 $Re(\epsilon'/\epsilon)$ result on overall data taking from 1997 to 2001:
Re(ϵ'/ϵ) $= (14.7 \pm 2.2)$x10^{-4}[3]

First part of this thesis is devoted to theory and experimental setup: CP violation in Standard Model with particular attention to the kaon system (Chapter 1), NA48 experimental method, beam lines and detector (Chapter 2). The second part is focused on beam intensity and accidental activity effects. The beam monitors and their data quality are introduced (Chapter 3), the way of studying the different effects due to accidental activity and intensity variations (Chapter 4) are then inspected and finally (Chapter 5) the beam monitors applications alone and related to other techniques to determine the relative correction to R are presented.

In App.A we will see a particular case of event losses: the overflows in drift chambers read-out and the test on the new read-out prototype. The new read-out, that is overflow free, has been commissioned and installed during the 2002 run.

Chapter 1

CP violation

1.1 Discrete symmetries P, C, T

Even if continuous symmetries are very important, being related to generalized current conservation, we will ignore them to concentrate on the discrete symmetries. The fundamental discrete symmetries are correlated to the following operation:

- Parity P: inversion of space coordinates $\overrightarrow{x}$ to $-\overrightarrow{x}$
- Charge conjugation C: exchange a particle to its anti-particle (e.g. $e^- \rightarrow e^+$, $q \rightarrow \overline{q}$).
- Time reversal: exchanges t to $-t$

The mathematics underlying to symmetry treatment is the group theory. We make use, to describe discrete symmetries, of a finite group containing only two elements: the identity e and an element g satisfying $g^2 = e$ (e.g. g=P,C,T). The invariance under g means that its representative unitary (P and C case) or anti-unitary (T case) operator $U(g)$ commutes with the physical state Hamiltonian H: $[U, H] = 0$.[9]

Strong and electromagnetic interactions are both P and C invariant, while weak interactions violate both P and C and also their product CP, even if this last one is a very small violation. CP violation, manifests itself as an asymmetry in the properties of matter and anti-matter, and may concur to explain the enhancement of matter over anti-matter evolved in the early stage of the Universe [1] .

[1] Sakharov, in 1967, postulated that it was possible to start with a Universe symmetric in matter and antimatter amounts, and make an asymmetrical one if three conditions are satisfied: 1) baryon number violation, 2) C and CP violation and 3) deviation from thermal equilibrium [12].

We will ignore for the time being this small CP violation effect. All hadrons and leptons experience weak interactions hence they can undergo weak decay, but are often hidden by the much more rapid strong or electromagnetic decays (e.g. $\pi^0 \to \gamma\gamma$). However, $\pi^\pm$ and μ are special cases: the π is the lightest hadron and $\pi^\pm$ can not decay in 2γ as π^0 (charge conservation). For this reason the weak decay $\pi^- \to \mu^- \overline{\nu_\mu}$ is the dominant one [1] .

Neutrinos experience only weak interactions (are colorless and electrically neutral) and only Left-Handed neutrino (ν_L) and Right-Handed anti-neutrino ($\overline{\nu}_R$) are observed: the absence of the 'mirror' images (ν_R) and ($\overline{\nu}_L$) is a violation of parity invariance and we say that weak interactions violate P maximally. The fact that neutrino is massless [2] (or if massive its mass can be ignored in this contest) force it to be in a defined helicity state: negative for ν_L and positive for $\overline{\nu}_R$.

The decay $\pi^- \to \mu^- \overline{\nu_\mu}$ is drawn in Fig. (1.1)(d). Performing a parity (momentum inversion, spin unaltered) or charge conjugation transformation (spin inversion, momentum unaltered, particle to anti-particle) we obtain a neutrino, or anti-neutrino, in a wrong helicity state.

This is the reason why we can have $\pi^+ \to \mu^+ \nu_{\mu L}$ but not the:

- P transformed process $\pi^+ \to \mu^+ \nu_{\mu R}$ Fig. (1.1)(b): P violation
- C transformed process $\pi^- \to \mu^- \overline{\nu}_{\mu L}$ Fig. (1.1)(c): C violation

while the CP process $\pi^- \to \mu^- \overline{\nu}_{\mu R}$ Fig. (1.1)(d) is allowed and
$\Gamma(\pi^+ \to \mu^+ \nu_{\mu L}) = \Gamma(\pi^- \to \mu^- \overline{\nu}_{\mu R})$ because of CP invariance.[9]

1.2 CP violation in neutral kaon system

1.2.1 A bit of history

In 1964 CP violation has been observed in neutral kaons' decays [6]. At that time Christenson, Cronin, Fitch and Turlay recorded the K_L , supposed to be a CP

[1] Due to lepton number conservation the μ^- does not decay in the electromagnetic process $\mu^- \to e^- \gamma$, its dominant decay is thus the weak $\mu^- \to e^- \overline{\nu}_e \nu_\mu$

[2] otherwise performing a Lorentz transformation it is possible to change a $\nu_L$to ν_R

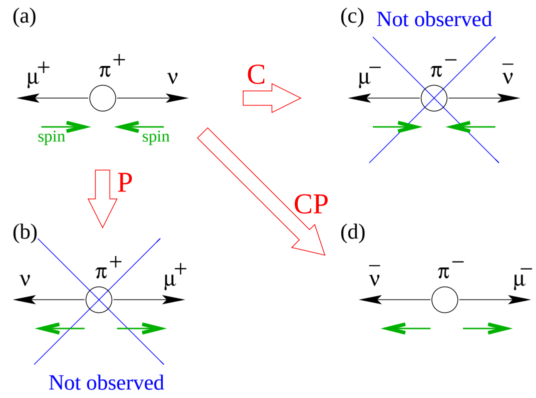

Figure 1.1: CP example: pion decay

eigenstate, decaying in the opposite CP state $\pi^+\pi^-$ thus showing a CP violation effect of order $\approx 2 \times 10^{-3}$.

The observed violation is now known as *indirect CP violation* because it occurs via the mixing of CP eigenstates K_1 (CP= $+1$) and K_2 (CP= -1): K_L and K_S , the mass eigenstates, are not the CP eigenstates but a mixture of them. Since $K_L \approx K_2 + \epsilon K_1$ the observed indirect violation is a consequence of the $K_{1\ (CP=+1)} \rightarrow \pi\pi_{\ (CP=+1)}$ and $\epsilon = (2.271 \pm 0.017)\text{x}10^{-3}$[7] is the indirect CP violation parameter.

1.2.2 CP in the Kaon system [10, 14]

Without the weak interaction the kaon system follows the simple two-state quantum mechanical description and the two strong eigenstates are

$|K^0>$: (d$\overline{s}$), strangeness quantum number S= $+1$

and its antiparticle CP conjugate

$|\overline{K}^0>$: (s$\overline{d}$), S= -1

The strangeness eigenstates $|K^0>$ and $|\overline{K}^0>$ are produced by strong interaction, that is flavour conserving. On the contrary weak interactions allow flavour changing thus K^0-$\overline{K}^0$mixing. The observed mass eigenstates are K_S and K_L and $m_{S,L}$ and $\tau_{S,L}$ are their masses and lifetimes, therefore the $K^0(\overline{K}^0)$ produced by strong interactions seem to be different kind of particles ($K_{S,L}$) when we study their weak decays.

To describe the quantum mechanical behavior of the physical states K_L and K_S , we start from the strong eigenstates base. Since weak interactions allow their mixing, the time evolution of the K^0-$\overline{K}^0$system is described by

$$i\frac{\partial\psi(t)}{\partial t} = H\psi(t) \qquad \psi(t) = \begin{pmatrix} |K^0> \\ |\overline{K}^0> \end{pmatrix} \tag{1.1}$$

The effective Hamiltonian H, representing the decay, is not hermitian but it is always possible its decomposition into two hermitian matrices M and Γ

- $H = M - \frac{i}{2}\Gamma$, where M and Γ are respectively mass and decay width matrices

$$H = \begin{pmatrix} M_{11} - \frac{i}{2}\Gamma_{11} & M_{12} - \frac{i}{2}\Gamma_{12} \\ M_{21} - \frac{i}{2}\Gamma_{21} & M_{22} - \frac{i}{2}\Gamma_{22} \end{pmatrix} \tag{1.2}$$

Moreover H can also be written as the sum of strangeness conserving ($H^{(0)}$) and strangeness violating ($H^{(2)}$) parts

- $H = H^{(0)} + H^{(2)}$. In in the strangeness eigenstate base:

$$H = \begin{pmatrix} < K^0|H^{(0)}|K^0 > & < K^0|H^{(2)}|\overline{K^0} > \\ < \overline{K^0}|H^{(2)}|K^0 > & < \overline{K^0}|H^{(0)}|\overline{K^0} > \end{pmatrix} \tag{1.3}$$

$K^0$and $\overline{K}^0$are particle and antiparticle so, they have the same mass M_0 and decay width Γ_0 because of CPT invariance. Looking at the diagonal elements in Eq. (1.2) and Eq. (1.3), we can conclude that

- $M_{11} = M_{22} = M_0$ and $\Gamma_{11} = \Gamma_{22} = \Gamma_0$

- $M(\Gamma)_0$ real and $M(\Gamma)_{21} = M(\Gamma)^*_{12}$ as the hermicity of the matrix require

Finally we can write:

$$H = \begin{pmatrix} M_0 - \frac{i}{2}\Gamma_0 & M_{12} - \frac{i}{2}\Gamma_{12} \\ M^*_{12} - \frac{i}{2}\Gamma^*_{12} & M_0 - \frac{i}{2}\Gamma_0 \end{pmatrix} \tag{1.4}$$

and diagonalizing H the physical states are found to be:

$$|K_{S,L}>=\frac{1}{\sqrt{|p|^2+|q|^2}}[p|K^0>\pm q|\overline{K}^0>] \tag{1.5}$$

where

$$\begin{aligned} |p|^2+|q|^2 &= 1 \\ \frac{q}{p} &\equiv \frac{1-\overline{\epsilon}}{1+\overline{\epsilon}}=\sqrt{\frac{M_{12}^*-\Gamma_{12}^*}{M_{12}-\Gamma_{12}}} \qquad (1.6) \\ \overline{\epsilon} &= \frac{\sqrt{M_{12}-\Gamma_{12}}-\sqrt{M_{12}^*-\Gamma_{12}^*}}{\sqrt{M_{12}-\Gamma_{12}}+\sqrt{M_{12}^*-\Gamma_{12}^*}} \qquad (1.7) \end{aligned}$$

The corresponding eigenvalues are

$$m_{S,L}-i\gamma_{S,L}=(M_0-\frac{i}{2}\Gamma_0)\pm\sqrt{(M_{12}-\Gamma_{12})(M_{12}^*-\Gamma_{12}^*)} \tag{1.8}$$

with experimental values $\Delta m = m_S - m_L \sim -3.57 \times 10^{-6}$eV and Δm$\approx -\frac{1}{2}\Delta\gamma$.

If $H^{(2)}$ were T invariant, CP conservation would hold, and its out-diagonal elements would be real: $M_{12}^*=M_{12}$ and $\Gamma_{12}^*=\Gamma_{12}$ leading to

- q/p=1 and $\overline{\epsilon}=0$
- K_S =K_1 and K_L =K_2 : physical states would correspond to CP eigenstates $|K_{S,L}>=|K_{1,2}>=(|K^0>\pm|\overline{K}^0>)/\sqrt{2}$

but this is not the case, as we have seen.

We can choose the phase of $|K^0>$ and $|\overline{K}^0>$ such that

- $CP|K^0>=|\overline{K}^0>$
- if the angular momentum is zero (L=0) the parity of two and three pions final state are: $P(2\pi)=(-1)^2(-1)^0$ and $P(3\pi)=(-1)^3(-1)^0$. The 2π and 3π final states are CP eigenstates with eigenvalues +1 and -1 respectively [1]
- CP(K_1)= +1, CP(K_2)= −1.

[1] if L≠0 it is possible to have CP(3π)=+1 and in this case K_1 can decay also in 3π, but 3π is in any case phase-space suppressed with respect to 2π

$$K_S = \frac{K_1 + \bar{\epsilon} K_2}{\sqrt{1 + |\bar{\epsilon}|^2}} \tag{1.9}$$

$$K_L = \frac{K_2 + \bar{\epsilon} K_1}{\sqrt{1 + |\bar{\epsilon}|^2}} \tag{1.10}$$

Because $K_1 \rightarrow 2\pi$ and $K_2 \rightarrow 3\pi$ are CP permitted, the phase space suppression of the 3π explains the longer lifetime of K_L : $\tau_S = 0.9 \times 10^{-10}s$, $\tau_L = 0.5 \times 10^{-7}s$.

So far we have seen that the indirect CP violation is related to the K^0-$\overline{K}^0$ mixing and the out-coming $2\pi(3\pi)$ from K_L (K_S) decays are, in this scenario, due to the K_1 (K_2) component. The weak interaction mixing K^0-$\overline{K}^0$ is described by the box diagrams in Fig. (1.2). Since the transition involves the change in strangeness by two units these diagrams are also known as $\Delta S = 2$ diagrams.

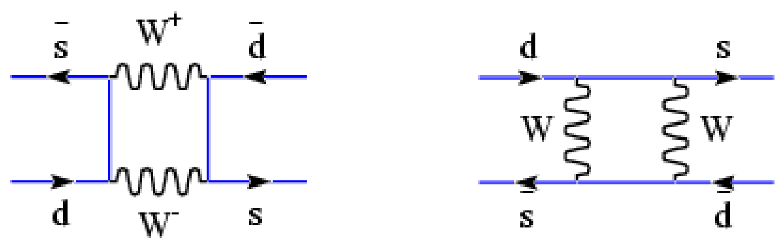

Figure 1.2: box diagrams $|\Delta S| = 2$

CP violation in neutral kaon system is dominated by mixing and the possibility that this is the only source of violation is referred as superweak theory. We can ask if there is also a *direct CP violation*, i.e. a violation in the decay process itself: when a CP-even(odd) state decays into a CP-odd(even) one.

$$K_L \propto K_2 + \bar{\epsilon} K_1 \tag{1.11}$$

$$\begin{array}{ccc} \text{Direct}(\epsilon') \swarrow & & \searrow \text{Indirect}(\bar{\epsilon}) \\ \pi\pi & & \pi\pi \end{array}$$

To understand this process, first of all we define the ratio between CP violation and CP conserving amplitudes:

$$\eta_{+-} = \frac{A(K_L \to \pi^+\pi^-)}{A(K_S \to \pi^+\pi^-)} = |\eta_{+-}|e^{i\phi_{+-}} \tag{1.12}$$

$$\eta_{00} = \frac{A(K_L \to \pi^0\pi^0)}{A(K_S \to \pi^0\pi^0)} = |\eta_{00}|e^{i\phi_{00}} \tag{1.13}$$

The actual experimental data are $|\eta_{+-}| \approx |\eta_{00}| = 2.2.8 \times 10^{-3}$ and $\phi_{+-} \approx \phi_{00} = 44°$

If direct CP violation occurs, a difference between the amplitudes $|A(K^0 \to F)| \neq |A(\overline{K}^0 \to \overline{F})|$ is observed [13]. In general if we have an initial state P and a final state F and A(P→F)$\neq A(\overline{P} \to \overline{F})$ we should observe a difference in the corresponding decay rates and therefore have a measurable asymmetry:

$$\mathcal{A} = \frac{\Gamma(P \to F) - \Gamma(\overline{P} \to \overline{F})}{\Gamma(P \to F) + \Gamma(\overline{P} \to \overline{F})} \tag{1.14}$$

We write the amplitudes as the sum of two terms

$$A(P \to F) = Ae^{i\phi}e^{i\delta} + A'e^{i\phi'}e^{i\delta'}$$

$$A(\overline{P} \to \overline{F}) = Ae^{-i\phi}e^{i\delta} + A'e^{-i\phi'}e^{i\delta'}$$

where $e^{i\phi}$, $e^{i\phi'}$ and $e^{i\delta}$, $e^{i\delta'}$ describe the weak and strong phase-shifts respectively. The rate asymmetry:

$$\mathcal{A} = \frac{-2AA'\sin(\phi - \phi')\sin(\delta - \delta')}{|A|^2 + |A'|^2 + 2AA'\cos(\phi - \phi')\cos(\delta - \delta')} \tag{1.15}$$

shows that in order to generate direct CP violation the following requirements have to be satisfied:

- at least two interfering amplitudes
- two different weak phase-shifts: $\sin(\phi - \phi') \neq 0$
- two different strong phase-shifts: $\sin(\delta - \delta') \neq 0$

Looking at K($I_K = 1/2$)→2π($I_\pi = 1$) the total isospin of the final state can be I=0,2 (Q=0, B=0, S=0, $I_3 = 0$) since I=1 is excluded by Bose symmetry. There are three kind of $\Delta S = 1$ diagrams contributing to the K→$\pi\pi$ transitions: penguin, exchange and spectator (Fig. (1.3)).

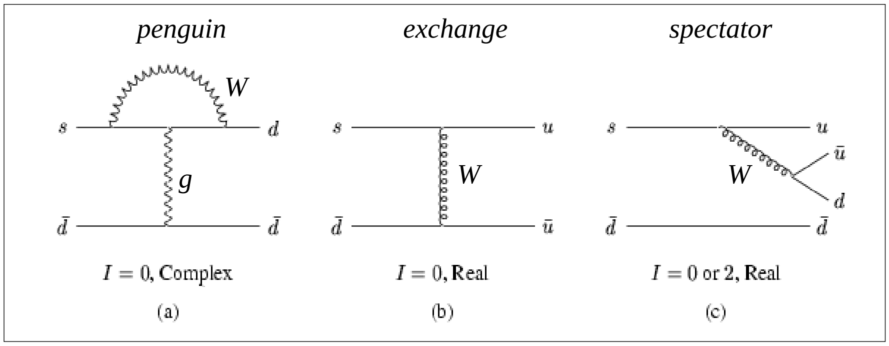

Figure 1.3: Three subprocesses contributing to K $\rightarrow \pi\pi$ $|\Delta S| = 1$

The final states in (a)(*penguin*) and (b)(*exchange*) have I=0, whereas in (c) (*spectator*) we can have either I=0 or I=2. Direct CP violation manifests itself as a non-zero relative phase between I=0 and I=2 amplitudes. In the K$\rightarrow \pi\pi$ diagrams the penguin introduces the *non zero relative phase* between $I_{\pi\pi} = 0$ and $I_{\pi\pi} = 2$ amplitudes, thus allowing direct CP violation. This is due to the fact that:

- the *penguin graph* involves three different quark generations in the intermediate state, as a consequence it can give rise to a decay amplitude which is complex at the quark level.

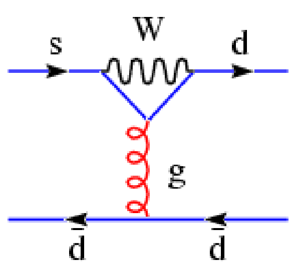

Transitions $s \rightarrow d$ with emission of at least one gluon lead only to I=0 final state since it can only change isospin by 1/2 unit

  * $A(s \rightarrow d\ c\bar{c}) \propto V_{cs}V_{cd}^*$
  * $A(s \rightarrow d\ t\bar{t}) \propto V_{ts}V_{td}^*$

Where V_{ij} are the quark mixing matrix elements (see next section).

- since $q\overline{q}$ can not have I=2 the *W exchange diagram* ($s\overline{d}{\rightarrow}u\overline{u}$) leads only to a $I_{\pi\pi} = 0$ final state with real amplitude A_0.

- the *free quark transitions* ($s \rightarrow u\overline{u}d$) in which the $\overline{d}$ of the initial Kaon acts as a spectator can contribute in the real part of A_0 and A_2.

In a graphical way we can represent, in the complex plane, the amplitudes A_0 and A_2 as [11]:

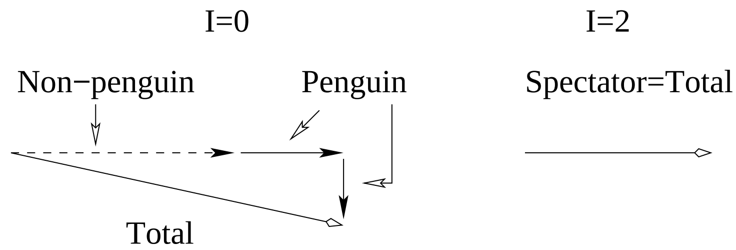

The gluonic corrections to these diagrams generate strong phases, denoted by δ, independent of the weak Hamiltonian form.

$$A(K^0 \rightarrow \pi\pi(I)) = A_I e^{i\delta_I} \qquad A(\overline{K}^0 \rightarrow \pi\pi(I)) = A_I^* e^{i\delta_I} \tag{1.16}$$

The weak amplitude A_I would be real if CP invariance held. Using the Clebsch-Gordan coefficients for the combinations of the two I=1 pions

$$|\pi^+\pi^- > \;=\; \sqrt{\frac{2}{3}}|\pi\pi, I = 0 > + \sqrt{\frac{1}{3}}|\pi\pi, I = 2 > \tag{1.17}$$

$$|\pi^0\pi^0 > \;=\; -\sqrt{\frac{1}{3}}|\pi\pi, I = 0 > + \sqrt{\frac{2}{3}}|\pi\pi, I = 2 > \tag{1.18}$$

the amplitudes for the k$\rightarrow\pi\pi$ transitions can be written as:

$$A(K^0 \rightarrow \pi^+\pi^-) \;=\; \sqrt{\frac{2}{3}}A_0 e^{i\delta_0} + \sqrt{\frac{1}{3}}A_2 e^{i\delta_2} \tag{1.19}$$

$$A(K^0 \rightarrow \pi^0\pi^0) \;=\; -\sqrt{\frac{1}{3}}A_0 e^{i\delta_0} + \sqrt{\frac{2}{3}}A_2 e^{i\delta_2} \tag{1.20}$$

From $\pi - \pi$ scattering analysis evidence of strongly enhancement of I=0 channel with respect to I=2 is found: in the I=0 channel interactions are attractive while they are repulsive for I=2. Despite of the experimental evidence this rule, also called $\Delta I = 1/2$ rule, is not justified by any general symmetry consideration and there is no derivation of it from QCD's first principles. As a consequence of the $\Delta I > 1/2$ suppression with respect to $\Delta I = 1/2$

$$\frac{A(K_s \to \pi^+\pi^-)}{A(K_s \to \pi^0\pi^0)} = \frac{\sqrt{2}A(K_s \to \pi^+\pi^-(0)) + A(K_s \to \pi^+\pi^-(2))}{-A(K_s \to \pi^0\pi^0(0)) + \sqrt{2}A(K_s \to \pi^0\pi^0(2))} \quad (1.21)$$

$$\frac{\Gamma(K_s \to \pi^+\pi^-)}{\Gamma(K_s \to \pi^0\pi^0)} = 2 \quad (1.22)$$

and the measured value is 2.18 ± 0.3, thus confirming that the $\Delta I = 1/2$ rule is approximately valid at this level [15].

In the following we will show that direct CP violation is strictly related to:

$$\frac{A(\overline{K^0} \to \pi\pi(I=2))}{A(K^0 \to \pi\pi(I=2))} \neq \frac{A(\overline{K^0} \to \pi\pi(I=0))}{A(K^0 \to \pi\pi(I=0))} \quad (1.23)$$

To simplify the notation we will use [15]

- $|0>=|\pi\pi(I=0)>, \quad |2>=|\pi\pi(I=2)>$
- weak transition matrix T: $<I|T|P>=A_I e^{i\delta_I} \qquad <I|T|\overline{P}>=A_I^* e^{i\delta_I}$

such that the previous equation is given by:

$$\frac{<2|T|\overline{K^0}>}{<2|T|K^0>} \neq \frac{<0|T|\overline{K^0}>}{<0|T|K^0>} \quad (1.24)$$

and the CP violating/CP conserving ratio $\eta_{+-,00}$ are described by:

$$\eta_{+-} = \frac{<\pi^+\pi^-|T|K_L>}{<\pi^+\pi^-|T|K_S>}$$

$$\eta_{00} = \frac{<\pi^0\pi^0|T|K_L>}{<\pi^0\pi^0|T|K_S>}$$

Introducing now

$$\omega = \frac{<2|T|K_s>}{<0|T|K_s>} \quad (1.25)$$

$$\epsilon_I = \frac{<I|T|K_L>}{<I|T|K_S>} \quad I=0,2 \quad (1.26)$$

and by means of the Isospin decomposition as defined in Eq. (1.17)

$$
\begin{aligned}
\eta_{+-} &= \frac{\sqrt{2} < 0|T|K_L > + < 2|T|K_L >}{\sqrt{2} < 0|T|K_S > + < 2|T|K_S >} = \\
&\frac{\frac{<0|T|K_L>}{<0|T|K_S>} + \frac{1}{\sqrt{2}}\frac{<2|T|K_L>}{<0|T|K_S>}}{1 + \frac{1}{\sqrt{2}}\frac{<2|T|K_S>}{<0|T|K_S>}} = \frac{\epsilon_0 + \frac{1}{\sqrt{2}}\frac{<2|T|K_L>}{<0|T|K_S>}}{1 + \frac{\omega}{\sqrt{2}}} = \\
&\frac{\epsilon_0 + \frac{1}{\sqrt{2}}\frac{<2|T|K_L>}{<0|T|K_S>}\frac{<2|T|K_S>}{<2|T|K_S>}}{1 + \frac{\omega}{\sqrt{2}}} = \\
&\frac{\epsilon_0 + \frac{1}{\sqrt{2}}\omega\epsilon_2}{1 + \frac{\omega}{\sqrt{2}}} = \frac{\epsilon_0 + \frac{1}{\sqrt{2}}\omega\epsilon_2}{1 + \frac{\omega}{\sqrt{2}}} + \epsilon_0 - \epsilon_0 = \\
&\epsilon_0 + \frac{1}{1 + \frac{\omega}{\sqrt{2}}}\frac{\omega}{\sqrt{2}}(\epsilon_2 - \epsilon_0)
\end{aligned} \tag{1.27}
$$

In the same way

$$
\begin{aligned}
\eta_{00} &= \frac{- < 0|T|K_L > + \sqrt{2} < 2|T|K_L >}{- < 0|T|K_S > + \sqrt{2} < 2|T|K_S >} = \\
&\frac{\frac{<0|T|K_L>}{<0|T|K_S>} - \sqrt{2}\frac{<2|T|K_L>}{<0|T|K_S>}}{1 - \sqrt{2}\frac{<2|T|K_S>}{<0|T|K_S>}} = \frac{\epsilon_0 - \sqrt{2}\frac{<2|T|K_L>}{<0|T|K_S>}}{1 - \sqrt{2}\omega} = \\
&\frac{\epsilon_0 - \sqrt{2}\omega\epsilon_2}{1 - \sqrt{2}\omega} = \\
&\epsilon_0 - \frac{1}{1 - \sqrt{2}\omega}\sqrt{2}\omega(\epsilon_2 - \epsilon_0)
\end{aligned} \tag{1.28}
$$

The universally adopted notation is the following:

$$
\epsilon \equiv \epsilon_0 \qquad \epsilon' \equiv \frac{\omega}{\sqrt{2}}(\epsilon_2 - \epsilon_0) \tag{1.29}
$$

in which ϵ and ϵ' are respectively the direct and indirect CP violation parameter. To have direct CP violation we need $\epsilon_2 \neq \epsilon_0$. We can see how this is related to the $K^0$and $\overline{K}^0$transition amplitudes taking into account the relations between mass and strong eigenstates

$$
\begin{aligned}
|K_S > &= p|K^0 > + q|\overline{K}^0 > \\
|K_L > &= p|K^0 > - q|\overline{K}^0 >
\end{aligned}
$$

we can write the new quantities as

$$\omega = \frac{1+\frac{q}{p}\frac{<2|T|\overline{K}^0>}{<2|T|K^0>}}{1+\frac{q}{p}\frac{<0|T|\overline{K}^0>}{<0|T|K^0>}}\frac{<2|T|K^0>}{<0|T|K^0>} \tag{1.30}$$

$$\epsilon_I = \frac{1-\frac{q}{p}\frac{<I|T|\overline{K}^0>}{<I|T|K^0>}}{1+\frac{q}{p}\frac{<I|T|\overline{K}^0>}{<I|T|K^0>}} \tag{1.31}$$

$$\epsilon_2-\epsilon_0 = \frac{q}{p}\left(\frac{<2|T|\overline{K}^0>}{<2|T|K^0>}-\frac{<0|T|\overline{K}^0>}{<0|T|K^0>}\right) \tag{1.32}$$

From these equations is evident that to have direct CP violation we need

$$\frac{<2|T|\overline{K}^0>}{<2|T|K^0>} \neq \frac{<0|T|\overline{K}^0>}{<0|T|K^0>} \quad direct \;\; CP \;\; violation \tag{1.33}$$

In terms of weak amplitudes and strong phases referring to Eq. (1.16) decomposition the following relations are valid:

$$\begin{aligned}
\epsilon_I &= \frac{pA_I-qA_I^*}{pA_I+qA_I^*} = \frac{i\frac{\Im(A_I)}{\Re(A_I)}+\frac{p-q}{p+q}}{1+i\frac{\Im(A_I)}{\Re(A_I)}\frac{p-q}{p+q}} = \frac{i\frac{\Im(A_I)}{\Re(A_I)}+\overline{\epsilon}}{1+i\frac{\Im(A_I)}{\Re(A_I)}\overline{\epsilon}} \approx i\frac{\Im A_I}{\Re A_I} \\
\omega &= \frac{(pA_2+qA_2^*)e^{i\delta_2}}{(pA_0+qA_0^*)e^{i\delta_0}} = \frac{\frac{\Re(A_2)}{\Re(A_0)}+i\frac{\Im(A_2)}{\Re(A_0)}\overline{\epsilon}}{1+i\frac{\Im(A_0)}{\Re(A_0)}\overline{\epsilon}}e^{i(\delta_2-\delta_0)} \approx \frac{\Re A_2}{\Re A_0}e^{i(\delta_2-\delta_0)} \quad ; \quad |\omega| \simeq 1/22 \\
\phi &= \frac{\pi}{2}+\delta_2-\delta_0 \approx \frac{\pi}{4} \\
\epsilon' &= \frac{\omega}{\sqrt{2}}(\epsilon_2-\epsilon_0) \approx \frac{ie^{(\delta_2-\delta_0)}}{\sqrt{2}}\frac{\Re A_2}{\Re A_0}\left(\frac{\Im A_2}{\Re A_2}-\frac{\Im A_0}{\Re A_0}\right) = \\
& \frac{e^{i\phi}}{\sqrt{2}}\frac{\Re A_2}{\Re A_0}\left(\frac{\Im A_2}{\Re A_2}-\frac{\Im A_0}{\Re A_0}\right)
\end{aligned} \tag{1.34}$$

From the expression of ϵ' in this form is also possible to notice the requirements on weak (from $A_I = \mathcal{A}_I e^{i\phi_I}$) and strong phase shifts, to allow direct CP violation, as seen in Eq. (1.15):

$$\Re(\epsilon') \quad \longleftrightarrow \quad \sin(\phi_2-\phi_0)\sin(\delta_2-\delta_0) \neq 0 \Leftrightarrow \phi_2 \neq \phi_0 \; and \; \delta_2 \neq \delta_0$$

$$\Im(\epsilon') \quad \longleftrightarrow \quad \sin(\phi_2-\phi_0)\cos(\delta_2-\delta_0) \neq 0 \Leftrightarrow \phi_2 \neq \phi_0$$

The indirect CP violation parameter ϵ is related to $\overline{\epsilon}$ by [17]:

$$\epsilon = \epsilon_0 \simeq \overline{\epsilon} + i\frac{\Im A_0}{\Re A_0} \tag{1.35}$$

thus $\epsilon = \overline{\epsilon}$ only in the Wu-Yang phase convention $\Im A_0 = 0$ [1]

The CP violating/CP conserving ratio η_{+-} and η_{00} can be expressed in terms of indirect ϵ and direct ϵ' ($\epsilon' \ll \epsilon$) parameters:

$$\eta_{+-} = \epsilon + \epsilon'(\frac{1}{1+\omega/\sqrt{2}}) \simeq \epsilon + \epsilon' \tag{1.36}$$

$$\eta_{00} = \epsilon - 2\epsilon'(\frac{1}{1-\omega\sqrt{2}}) \simeq \epsilon - 2\epsilon' \tag{1.37}$$

The direct CP violation parameter ϵ', due to ω, is strongly suppressed and in fact from the measures of $\eta_{+-} \approx \eta_{00} = 2.28 \times 10^{-3}$ we expect ϵ' of order $10^{-3}\epsilon$. It is interesting to notice that the ϵ' phase $(\delta_2 - \delta_0 + \pi/2) \approx (48 \pm 4)^\circ$ [7] is nearly equal to the ϵ phase $\phi(\epsilon) = (43.48 \pm 0.08)^\circ$ [7] thus

$$\Re(\frac{\epsilon'}{\epsilon}) \approx \frac{\epsilon'}{\epsilon}$$

and from this follow that

$$\begin{aligned} |\eta_{00}| &\approx |\epsilon|[1 + \Re(\frac{\epsilon'}{\epsilon})] \\ |\eta_{+-}| &\approx |\epsilon|[1 - 2\Re(\frac{\epsilon'}{\epsilon})] \end{aligned} \tag{1.38}$$

In NA48 we measure the double ratio $R = |\eta_{00}/\eta_{+-}|^2$. Recalling the $\eta_{+-,00}$ definition in Eq. (1.13), R is simply related to $Re(\epsilon'/\epsilon)$ by (Eq. (1.39)):

$$R = |\frac{\eta_{00}}{\eta_{+-}}|^2 = \frac{\Gamma(K_L \to \pi^0\pi^0)\Gamma(K_S \to \pi^+\pi^-)}{\Gamma(K_S \to \pi^0\pi^0)\Gamma(K_L \to \pi^+\pi^-)} \simeq 1 - 6\Re(\frac{\epsilon'}{\epsilon}) \tag{1.39}$$

1.3 CP violation in the Standard Model

In the Standard Model all matter fields (quarks and leptons) are fermions while the gauge fields are spin 1 bosons. The coupling between fermions and gauge bosons can not connect Left-handed to Right-handed fields [2] and the absence of right handed coupling to W bosons implies that the right handed fields are SU(2) singlets while the

[1] $\Im A_0$ $\Im A_2$ $\Im\epsilon$ depend on the phase convention choice since the phases on $K^0$and $\overline{K}^0$change by a transformation of $|s\rangle = |s\rangle e^{i\alpha}$ [7]

[2] the fermion ψ coupling to gauge fields is proportional to $\psi^\dagger\gamma_0\gamma_\mu\psi$. A fermion field can be projected, via projectors $P_{L,R} = \frac{1\pm\gamma_5}{2}$, in left and right handed components. But $P_L\gamma_0\gamma_\mu P_R = 0$ ...

left handed are doublets (two fields) [10, 13, 14]. Since masses are associates to left and right handed fields, the particles are massless if the gauge symmetry is unbroken. To generate the fermions' masses in SM the Higgs mechanism is needed to preserve $SU(2)_L \times U(1)_Y$. For three generations of quarks, the general Yukawa coupling (Y) produces general non-diagonal mass 3x3 matrix M.

$$\mathcal{L}_{mass} = \overline{d'}_{Li} M^d_{ij} d_j + \overline{u'}_{Li} M^u_{ij} u_j + h.c. \quad M_{ij} = Y_{ij}\frac{v}{\sqrt{2}} \tag{1.40}$$

where u'_i, d'_i are the quarks belonging to SU(2) doublet of i-th generation (i=1,2,3), Y_{ij} are the Yukawa coupling constants with i=u,c,t and j=d,s,b and v is the Higgs field vacuum expectation value. The mass terms (terms quadratic in fields) give the physical masses when they are diagonalized in flavour. To find another basis in which the M matrices are diagonal, the up quark mass matrix M^u_{ij} can be chosen diagonal and the down quark M^d_{ij} is then diagonalized by a unitary transformation (change of basis) demanding that $V^\dagger M M^\dagger V$ be real and diagonal [13]. This unitary matrix is the Cabibbo-Kobayashi-Maskawa matrix which relates the weak and mass eigenstates: $(q_{weak})_i = V_{ik}(q_{mass})_k$

$$\begin{pmatrix} d' \\ s' \\ b' \end{pmatrix} = \begin{pmatrix} V_{ud} & V_{us} & V_{ub} \\ V_{cd} & V_{cs} & V_{cb} \\ V_{td} & V_{ts} & V_{tb} \end{pmatrix} \begin{pmatrix} d \\ s \\ b \end{pmatrix} \tag{1.41}$$

We have, adapted to their SU(2) properties, the three generations:

$$\begin{pmatrix} \nu_{eL} \\ e^-_L \end{pmatrix} \quad \begin{pmatrix} u_L \\ d'_L \end{pmatrix} \quad e_R \quad u_R \quad d_R \tag{1.42}$$

$$\begin{pmatrix} \nu_{\mu L} \\ \mu^-_L \end{pmatrix} \quad \begin{pmatrix} c_L \\ s'_L \end{pmatrix} \quad \mu_R \quad c_R \quad s_R \tag{1.43}$$

$$\begin{pmatrix} \nu_{\tau L} \\ \tau^-_L \end{pmatrix} \quad \begin{pmatrix} b_L \\ t'_L \end{pmatrix} \quad \tau_R \quad t_R \quad b_R \tag{1.44}$$

$$\tag{1.45}$$

If we do not choose M^u_{ij} diagonal then $V = V_u V_d^\dagger$ where V_d and V_u diagonalize the respective mass matrix. Only the coupling to $W^\pm$ includes the mixing between families, allowing the flavour violation or transition from one flavour to another; the coupling to Z (neutral current) is diagonal in flavour (V and $V^\dagger$ cancel due to unitarity) giving the absence of flavour-changing-neutral-current (FCNC) or GIM mechanism. [13]

$$\mathcal{L}_{int} = \mathcal{L}_{CC} + \mathcal{L}_{NC} \tag{1.46}$$

$$\mathcal{L}_{CC} \longleftrightarrow \sum \overline{u}_{Li}(V_u^\dagger V_d)_{ik}(W)d_{Lk} \tag{1.47}$$

$$\mathcal{L}_{NC} \longleftrightarrow \sum \overline{u}_{Li}(V_u^\dagger V_u)_{ik}(Z,\gamma,...)d_{Lk} \quad V_u^\dagger V_u = \delta_{ik} \tag{1.48}$$

$$\tag{1.49}$$

If there are N_g generations then V is a $N_g \times N_g$ unitary matrix. Therefore it has N_g^2 parameters but $(2N_g - 1)$ can be absorbed in unphysical phases redefining the left-handed quark fields. In fact there are N_g up-type quarks and N_g down-type quarks that can be rotated to eliminate one phase of one row and one column, but the entry corresponding to the intersection of row and column can not be rotated twice thus we can eliminate $(2N_g - 1)$ phases.

Part of the parameters can be thought as rotation angles. In an N_g dimension space there are as many angles as the coordinate planes[16]:

$$N_{angles} = \binom{N_g}{2} = \frac{1}{2}N_g(N_g - 1) \tag{1.50}$$

The unphysical phases excluded, there are still $(N_g - 1)^2$ physical parameters to be determined: $\frac{1}{2}N_g(N_g - 1)$ mixing angles and $\frac{1}{2}(N_g - 1)(N_g - 2)$ phases.
As an example we take Ng=2: there is only one angle, the Cabibbo angle θ_C, and there are no phases:

$$V = \begin{pmatrix} \cos\theta_c & \sin\theta_c \\ -\sin\theta_c & \cos\theta_c \end{pmatrix} \tag{1.51}$$

While if $N_g = 3$, the V_{CKM} case, there are 3 angles and 1 phase. In the standard parametrization recommended by Particle Data Group [7], θ_{ij} $(i, j = 1, 2, 3)$ are the mixing angles, δ is the irreducible phase and V_{CKM} is written as:

$$V_{CKM} = \begin{pmatrix} c_{12}c_{13} & s_{12}c_{13} & s_{13}e^{-i\delta} \\ -s_{12}c_{23} - c_{12}s_{23}s_{13}e^{i\delta} & c_{12}c_{23} - s_{12}s_{23}s_{13}e^{i\delta} & s_{23}c_{13} \\ s_{12}s_{23} - c_{12}c_{23}s_{13}e^{i\delta} & -s_{23}c_{12} - s_{12}c_{23}s_{13}e^{i\delta} & c_{23}c_{13} \end{pmatrix} \tag{1.52}$$

where $c_{ij} = \cos\theta_{ij}$, $s_{ij} = \sin\theta_{ij}$ $(i, j = 1, 2, 3)$ can all be chosen to be positive; δ may vary in the range $[0, 2\pi]$ but CP violation measurements in K decays force it in the range $[0, \pi]$. The advantages of this parametrization are basically the following [22]:

- s_{13} and s_{23} are small numbers ($\mathcal{O}(10^{-3})$ and $\mathcal{O}(10^{-2})$ respectively), consequently $c_{13} = c_{23} = 1$ with good accuracy and the four independent parameters are $s_{12} = |V_{us}|$, $s_{13} = |V_{ub}|$, $s_{23} = |V_{cb}|$, δ. These simple relations allow to measure s_{12}, s_{13}, s_{23} independently in three decays.

- the CP violation phase δ is always multiplied by a very small number (s_{13}): this shows clearly the CP suppression independently of the actual size of δ

The Cabibbo-Kobayashi-Maskawa matrix elements are free parameters to be measured. According to PDG[7] the experimentally measured values, of the angles of s_{12}, s_{23}, s_{13}, are at 90% CL :

$$V_{CKM} = \begin{pmatrix} 0.9745 \text{ to } 0.9757 & 0.219 \text{ to } 0.224 & 0.002 \text{ to } 0.005 \\ 0.218 \text{ to } 0.224 & 0.9736 \text{ to } 0.9750 & 0.036 \text{ to } 0.046 \\ 0.004 \text{ to } 0.014 & 0.034 \text{ to } 0.046 & 0.9989 \text{ to } 0.9993 \end{pmatrix} \tag{1.53}$$

V_{ub} is the smallest elements in CKM matrix but its knowledge with small uncertainty is crucial for CP violation since it provides a bound in the upper vertex of the unitarity triangle (see forward Fig. (1.4)), which area is related to CP violation. The easiest way to obtain V_{ub} and V_{cb} is through semileptonic B decays, anyway V_{ub} is not easy to measure since $\sim$ 99% of B decays occurs through b$\rightarrow$c transition (V_{cb}) while only $\sim$ 1% through b$\rightarrow$u transitions. There are many experimental measures of these elements: while there is agreement on V_{cb}, the analysis of V_{ub} individually approaches a 15% uncertainty. The different analyzes agree within this number, but there are yet uncontrolled uncertainties[8]. The theoretical predictions are also difficult due to the strong interactions: at these decay energies the strong coupling is large and difficult to predict with perturbative QCD methods.

The requirement of the matrix unitarity is stated as $V^\dagger_{CKM} V_{CKM} = \mathbf{1}$ and unitarity constraints follows from it: $\sum_{i=1}^{3} |V_{ij}|^2 = \sum_{j=1}^{3} |V_{ij}|^2 = 1$[1] , where the orthogonality between any two columns is expressed by [18]

- $V_{ud}V^*_{us} + V_{cd}V^*_{cs} + V_{td}V^*_{ts} = 0$ 1^{st} and 2^{nd} columns
- $V_{us}V^*_{ub} + V_{cs}V^*_{cb} + V_{ts}V^*_{tb} = 0$ 2^{nd} and 3^{th}
- $V_{ud}V^*_{ub} + V_{cd}V^*_{cb} + V_{td}V^*_{tb} = 0$ 1^{st} and 3^{th} most important for us

and between rows:

- $V_{ud}V^*_{cd} + V_{us}V^*_{cs} + V_{ub}V^*_{cb} = 0$ 1^{st} and 2^{nd} rows
- $V_{cd}V^*_{td} + V_{cs}V^*_{ts} + V_{cb}V^*_{tb} = 0$ 2^{nd} and 3^{th}
- $V_{ud}V^*_{td} + V_{us}V^*_{ts} + V_{ub}V^*_{tb} = 0$ 1^{st} and 3^{th}

The six orthogonality conditions can be drawn as triangles in the complex plane, requiring the sum of three complex numbers V_{ij} to vanish. Due to unitarity, for any choice of $i, j, k, l = 1, 2, 3$ it is possible to define a quantity $\mathcal{J}$ [20] such that

$$\Im(V_{ij}V^*_{ik}V_{lk}V^*_{lj}) = \mathcal{J} \sum_{m,n=1}^{3} \epsilon_{ilm}\epsilon_{jkn} \tag{1.54}$$

where $\mathcal{J}$ is the Jarslkog invariant and it is related to unitarity triangles and CKM elements by:

$$|\mathcal{J}| = 2\mathcal{A}_T \tag{1.55}$$

$$\mathcal{J} = c_{12}c_{23}c^2_{13}s_{12}s_{23}s_{13}\sin\delta \tag{1.56}$$

while the sign of $\mathcal{J}$ gives the direction of the complex vectors around the triangle.[19] Therefore in the Standard Model CP is violated if $\mathcal{J} \neq 0$ and $\mathcal{A}_T$ is equal for each triangle, due to its relation with $\mathcal{J}$.

To have CP violation it necessary to avoid that the CKM phase could be removed by a redefinition of the quark fields: this requirement conditions arise on quark masses and CKM angles and phase: [19, 20]:

[1] where a useful relation is $|V_{ub}|^2 + |V_{cb}|^2 + |V_{tb}|^2 = 1$ that, due to the small values of $|V_{ub}|$ and $|Vcb|$ implies $|V_{tb}| \approx 1$

- $m_u \neq m_c, \quad m_c \neq m_t, \quad m_t \neq m_u, \quad m_d \neq m_s, \quad m_s \neq m_b, \quad m_b \neq m_d$

  since if two quarks of the same charge have same masses, one mixing angle and the phase could be removed from CKM: 6 conditions

- the angles must be $\neq 0, \frac{\pi}{2}$ otherwise again the phase can be removed: 6 conditions

- from $\mathcal{J} \leftrightarrow \sin\delta$ the δ must be $\neq 0, \pi$: 2 conditions

The eight conditions on angles and phase are incorporated into $\mathcal{J} \neq 0$ and all the 14 conditions are unified in the single relation $det(C) \neq 0$ [21, 7] where

$$\begin{aligned} iC &= [M^u M^{u^\dagger}, M^d M^{d^\dagger}] & (1.57) \\ det(C) &= -2(m_c^2 - m_u^2)(m_t^2 - m_c^2)(m_t^2 - m_u^2) * \\ &\quad (m_s^2 - m_d^2)(m_b^2 - m_s^2)(m_b^2 - m_d^2) * \mathcal{J} & (1.58) \end{aligned}$$

CP is violated if $det(C) \neq 0$. This follows from the observation that the mass matrices commutator gives indications if they can be diagonalized simultaneously.

To have a graphical view of V_{CKM} proprieties and CP violation, we introduce the Wolfenstein parametrization $V_{CKM} = V_{CKM}^{(w)} + \delta V_{CKM}$ in which each element is expanded as a power series of $\lambda = |V_{us}| \simeq \sin\theta_C \approx 0.22$:

$$V_{CKM}^{(w)} = \begin{pmatrix} 1 - \frac{\lambda^2}{2} & \lambda & A\lambda^3(\rho - i\eta) \\ -\lambda & 1 - \frac{\lambda^2}{2} & A\lambda^2 \\ A\lambda^3(1 - \rho - i\eta) & -A\lambda^2 & 1 \end{pmatrix} + \mathcal{O}(\lambda^4) \qquad (1.59)$$

The set of four independent parameters is given by λ, ρ, η and A ($A \approx 1$). It is evident that the elements get smaller moving away from the diagonal and the hierarchy between families where elements connecting the first two generations have size $\simeq \lambda$, the ones connecting second and third of order λ^2 and the others connecting first and third of or size smaller than λ^3. In this contest

$$|\mathcal{J}| = \Im(V_{ts}^* V_{td} V_{us}^* V_{ud}) = \Im(V_{ts}^* V_{td})\lambda(1 - \frac{\lambda^2}{2}) \approx \lambda(1 - \frac{\lambda^2}{2})A^2\lambda^5\eta \qquad (1.60)$$

hence we need $\eta \neq 0$ to have CP violation.

This is an approximate parametrization; an efficient way to find higher order terms in λ is to define the parameters (A, λ, ρ, η) through

$$s_{12} = \lambda, \quad s_{23} = A\lambda^2, \quad s_{13}e^{-i\delta} = A\lambda^3(\rho - i\eta) \tag{1.61}$$

therefore to *all orders* in λ

$$\rho = \frac{s_{13}}{s_{12}s_{23}} \cos\delta, \quad \eta = \frac{s_{13}}{s_{12}s_{23}} \sin\delta \tag{1.62}$$

Making this change of variables in the standard parametrization we find the CKM matrix as a function of (A, λ, ρ, η) which satisfy unitarity exactly. In this representation

$$\begin{aligned}
V_{us} &= \lambda \\
V_{ud} &= 1 - \frac{1}{2}\lambda^2 - \frac{1}{8}\lambda^4 + \mathcal{O}(\lambda^6) \\
V_{ub} &= A\lambda^3(\rho - i\eta) \\
V_{cd} &= -\lambda + \frac{1}{2}A^2\lambda^5[1 - 2(\rho - i\eta)] + \mathcal{O}(\lambda^7) \\
V_{cb} &= A\lambda^2 + \mathcal{O}(\lambda^8) \\
V_{tb} &= 1 - \frac{1}{2}A^2\lambda^4 + \mathcal{O}(\lambda^6) \\
V_{td} &= A\lambda^3[1 - (\rho - i\eta)(1 - \frac{1}{2}\lambda^2)] + \mathcal{O}(\lambda^7)
\end{aligned}$$

The unitarity $V_{ud}V_{ub}^* + V_{cd}V_{cb}^* + V_{td}V_{tb}^* = 0$condition's elements then became:

- $V_{ud}V_{ub}^* = A\lambda^3[\overline{\rho} + i\overline{\eta}] + \mathcal{O}(\lambda^7)$
- $V_{cd}V_{cb}^* = -A\lambda^3 + \mathcal{O}(\lambda^7)$
- $V_{td}V_{tb}^* = A\lambda^3[1 - (\overline{\rho} + i\overline{\eta})] + \mathcal{O}(\lambda^7)$

where $\overline{\rho} = \rho(1 - \lambda^2/2)$ and $\overline{\eta} = \eta(1 - \lambda^2/2)$.[22]

It is possible to express $\sin(2\phi_i)$, $\phi_i = \alpha,\ \beta,\ \gamma$, in terms of $(\overline{\rho}, \overline{\eta})$ [22]

$$sin(2\alpha) = \frac{2\overline{\eta}(\overline{\eta}^2 + \overline{\rho}^2 - \overline{\rho})}{(\overline{\rho}^2 + \overline{\eta}^2)((1-\overline{\rho})^2 + \overline{\eta}^2)} \tag{1.63}$$

$$sin(2\beta) = \frac{2\overline{\eta}(1-\overline{\rho})}{(1-\overline{\rho})^2 + \overline{\eta}^2} \tag{1.64}$$

$$sin(2\gamma) = \frac{2\overline{\rho\eta}}{\overline{\rho}^2 + \overline{\eta}^2} = \frac{2\rho\eta}{\rho^2 + \eta^2} \tag{1.65}$$

$$\overline{CA} = \frac{|V_{ud}V_{ub}^*|}{|V_{cd}V_{cb}^*|} = \sqrt{\overline{\rho}^2 + \overline{\eta}^2} = (1 - \frac{\lambda^2}{2})\frac{1}{\lambda}|\frac{V_{ub}}{V_{cb}}| \tag{1.66}$$

$$\overline{BA} = \frac{|V_{td}V_{tb}^*|}{|V_{cd}V_{cb}^*|} = \sqrt{(1-\overline{\rho})^2 + \overline{\eta}^2} = \frac{1}{\lambda}|\frac{V_{td}}{V_{cb}}| \tag{1.67}$$

By a graphical point of view the unitarity condition can be represented by a triangle in the $(\overline{\rho}, \overline{\eta})$ complex plane: the "unitarity triangle" in $\overline{\rho} - \overline{\eta}$ plane shown in Fig. (1.4).

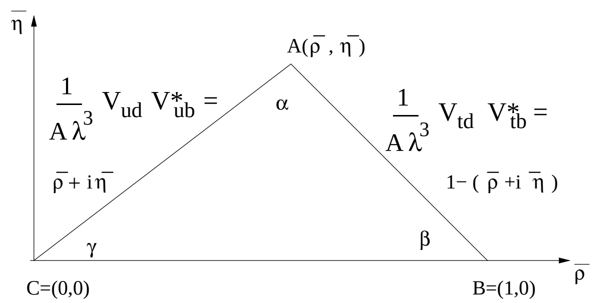

Figure 1.4: unitarity triangle in $(\overline{\rho}, \overline{\eta})$ complex plane

As we have seen before, CP violation is related e.g. to $\mathcal{J} = \Im(V_{ud}V_{tb}V_{ub}^*V_{td}^*)$ and $\mathcal{J} = 2\mathcal{A}_T \leftrightarrow \eta$, so CP is violated if $\eta \neq 0$ and that is true if (Eq. (1.62)) $\delta \neq 0$.

While if there are only two generations there is no place for CP violation, as shown by the orthogonality relation between the two columns $V_{ud}V_{us}^* + V_{cd}V_{cs}^* = 0$, represented in Fig. (1.5).

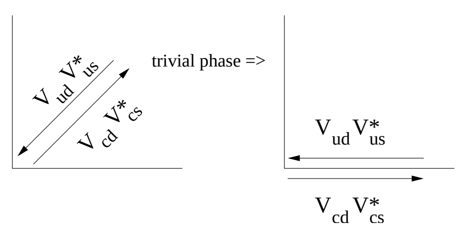

Figure 1.5: two generations 'triangle'

Chapter 2

NA48 the CERN experiment

2.1 NA48 experimental method

The relation between the double ratio R and the CP violation parameters, as we have seen in the first chapter, is given by:

$$R = |\frac{\eta_{00}}{\eta_{+-}}|^2 = \frac{\Gamma(K_L \to \pi^0\pi^0)\Gamma(K_S \to \pi^+\pi^-)}{\Gamma(K_S \to \pi^0\pi^0)\Gamma(K_L \to \pi^+\pi^-)} \simeq 1 - 6Re(\frac{\epsilon'}{\epsilon}) \tag{2.1}$$

and this is the way NA48 and other experiments (KTev and the 'first generation' experiments NA31, E731) derives $Re(\epsilon'/\epsilon)$ from R. For a single decay rate $\Gamma(K_{L,S} \to \pi\pi^{+-,00})$ we have to consider not only our data sample and its background but also the detector acceptance and the overall efficiency therefore:

$$\Gamma_{km} = \frac{N_{km} - N_{bkg,\ km}}{\Phi_k\ \mathcal{E}\mathcal{A}_{km}\ \tau_k} \quad k = \text{L,S},\ m = \text{C,N} = \pi^+\pi^-, \pi^0\pi^0 \tag{2.2}$$

where

- N_{km}: number of events we are looking for
- $N_{bkg,\ km}$: number of background events
- Φ_k: total kaon flux to which we have to normalize
- $\mathcal{E}\mathcal{A}_{k,m}$: total acceptance and efficiency
- τ_k: lifetime

After background subtraction, fluxes and lifetimes cancel in the double ratio, between Long and Short modes. Charged and Neutral efficiencies ($\mathcal{E}$) cancel between K_L and

K_S decays if $\mathcal{E}_L(\pi^+\pi^-) = \mathcal{E}_S(\pi^+\pi^-)$ and $\mathcal{E}_L(\pi^0\pi^0) = \mathcal{E}_S(\pi^0\pi^0)$. If these conditions are satisfied:

$$R = \frac{N(K_L \to \pi^0\pi^0)N(K_S \to \pi^+\pi^-)}{N(K_S \to \pi^0\pi^0)N(K_L \to \pi^+\pi^-)}\frac{\mathcal{A}_S^{00}\mathcal{A}_L^{+-}}{\mathcal{A}_L^{00}\mathcal{A}_S^{+-}} \tag{2.3}$$

and if Long-Short symmetry holds also for acceptance ($\mathcal{A}$) we obtain a sort of *counting experiment*:

$$R = \frac{N(K_L \to \pi^0\pi^0)N(K_S \to \pi^+\pi^-)}{N(K_S \to \pi^0\pi^0)N(K_L \to \pi^+\pi^-)} \tag{2.4}$$

Nevertheless acceptance depends on the vertex coordinate z and on the $K_{L,S}$ momentum. This in general causes differences leading to a sizeable correction to R. The asymmetry between Long and Short acceptance is reduced selecting the Kaon (L,S) momentum in a defined range where they have similar spectra (Fig. (2.1)).

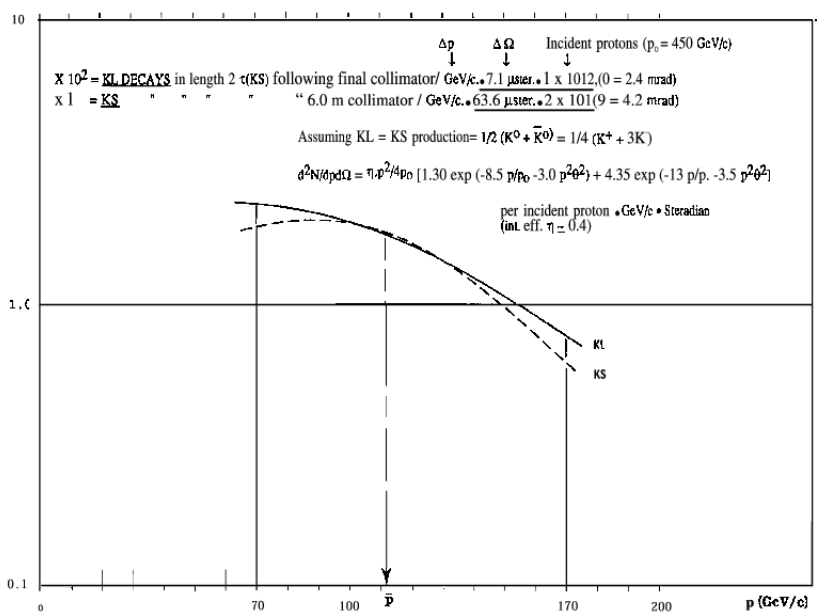

Figure 2.1: K_L and K_S decay spectra in the selected range

This can be done choosing an appropriate K_S production angle, given the K_L one, and a short (6m$\approx$ $1c\tau_S$) distance between the K_S target and collimator to maximize the K_S flux with respect to the collimator produced background[25].

To be insensitive to remaining energy differences in the K_L and K_S spectra, the analysis is performed in twenty bins (5GeV each) of kaon energy and the resulting

R is plotted for each bin (Fig. (2.2)). The number of 2001 good decays in the four modes versus the energy bins are shown in Fig. (2.3), where the

- 1.55×10^6 $K_L \to \pi^0\pi^0$
- 2.16×10^6 $K_S \to \pi^0\pi^0$
- 7.14×10^6 $K_L \to \pi^+\pi^-$
- 9.61×10^6 $K_S \to \pi^+\pi^-$

are obtained in 93 days of run (and $\approx$ 190·000 good bursts).

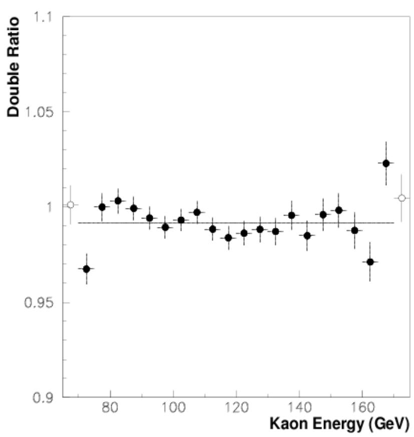

Figure 2.2: The double ratio R in 20 energy bins, 5GeV each

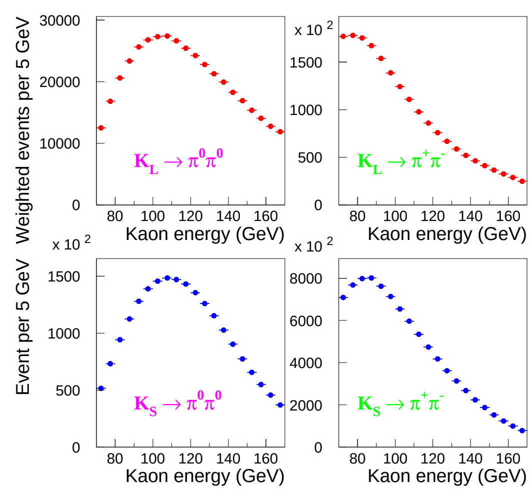

Figure 2.3: K_L (weighted) and K_S decay events in 20 energy bins

Reaching the required acceptance symmetry in z is a bit more difficult: at the same z the collinear K_L and K_S have the same acceptance but their very different lifetimes lead to huge difference in the decay lengths. The solution is to weight the K_L with a proper lifetime function such that after the weighting the two shapes are very similar as shown in Fig. (2.4).

The weighting function, derived from $K_{L,S} \to \pi\pi$ ratio, is given by:

$$W(\tau) = \frac{I(\tau) \text{ from } K_S \text{ target}}{I(\tau) \text{ from } K_L \text{ target}} \tag{2.5}$$

$$= e^{-\frac{z}{\beta\gamma c}\left(\frac{1}{\tau_S}-\frac{1}{\tau_L}\right)} \approx e^{-\frac{z}{\beta\gamma c}\frac{1}{\tau_S}} \tag{2.6}$$

Now acceptance is fairly symmetric between K_L and K_S and we are in Eq. (2.4) conditions. The acceptance symmetrization through the weighting procedure is not

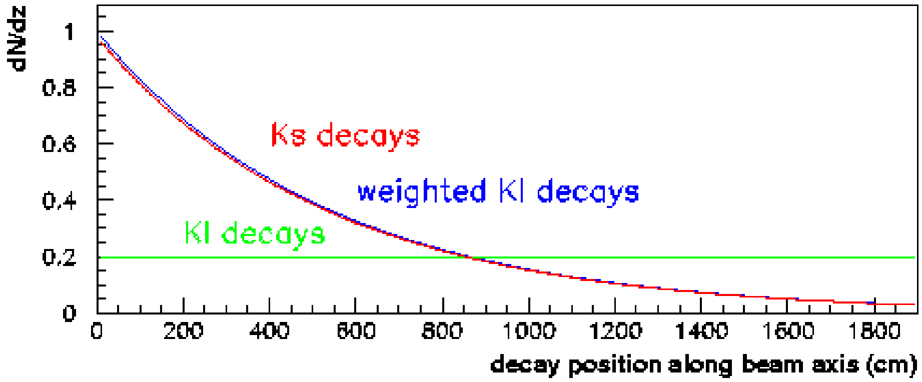

Figure 2.4: K_L , K_L weighted and K_S decays position

for free and the price to pay is a decrease in the effective K_L statistics within the $3.5\tau_S$ fiducial region, increasing of $\approx 35\%$ the statistical error of R [2]. But, as an advantage, the analysis in not Monte-Carlo dependent.

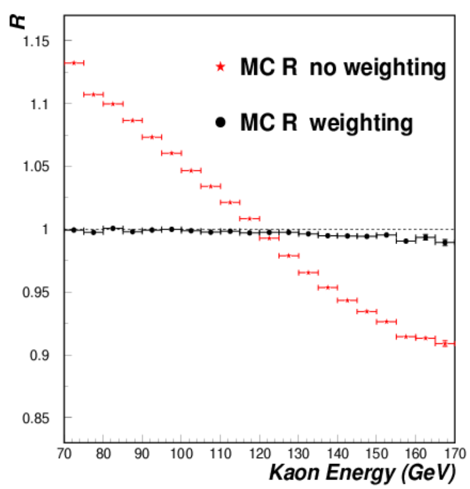

Figure 2.5: Acceptance effect on R (20 energy bins, 5 Gev each) computed from MC

Without the weighting procedure we should have to apply a large correction to R as can be seen in Fig. (2.5), while a flat distribution is obtained weighting the K_L decays. Only small remaining differences, on beam divergences and beam sizes, need to be corrected. This is done using a high statistics Monte-Carlo simulation.

One step back, there are other possible sources of errors and asymmetries that have been taken into account. According to the NA48 proposal [25] the dominant error sources are:

- statistics on $K_L \to 2\pi^0$
- possible differences in $\pi^0\pi^0$ and $\pi^+\pi^-$ reconstructed kaon energy scale
- background to $K_L \to 2\pi^0$ from $K_L \to 3\pi^0$ if only 4 photons are detected
- background to $K_L \to \pi^+\pi^-$ from three body decays K_{e3}, $K_{\mu 3}$
- different effects of accidental activity in the detector between K_S and K_L

For a precise measure of $Re(\epsilon'/\epsilon)$ it is necessary to collect enough CP violating decays and to minimize every difference between Charge-Neutral and Short-Long that can yield appreciable errors on R. In this way it is possible to reach the proposed $\approx 2 \times 10^{-4}$, statistical and systematic combined, on $Re(\epsilon'/\epsilon)$.

To minimize the sensitivity on accidental activity and beam intensity variations the four decay modes ($K_{L,S} \to \pi\pi^{00,+-}$) are collected simultaneously: this is achieved using simultaneous beams and the same fiducial region for K_L and K_S decays. One of the strategies to keep the data taking of $\pi^0\pi^0$ and $\pi^+\pi^-$ simultaneous is to apply offline the same dead time to all events: if there is a dead time condition affecting one mode the dead time is applied, offline, to the other to keep the symmetry between the modes. To reach the proposed statistical error of 1×10^{-3} on R a high number of CP violating decays $K_L \to \pi\pi$ is needed. The $K_L \to \pi^0\pi^0$ is the lower branching ratio channel (see Table (2.1)) therefore the most difficult to accumulate enough statistic.

The proposal intended to reach the desired error in three years of data taking, collecting 1.5x10^6 $K_L \to \pi^0\pi^0$ per year. The goal was reached collecting:

- 0.5 million good $K_L \to 2\pi^0$ in 1997,
- 3.3 million good $K_L \to 2\pi^0$ in 1998 and 1999,
- 1.5 million good $K_L \to 2\pi^0$ in 2001.

channel	decay ratio [7]
$K_{e3}: \pi^{\pm}e^{\mp}\nu$	$(38.78 \pm 0.27)\%$
$K_{\mu 3}: \pi^{\pm}\mu^{\mp}\nu$	$(27.17 \pm 0.25)\%$
$\pi^0\pi^0\pi^0$	$(21.12 \pm 0.27)\%$
$\pi^+\pi^-\pi^0$	$(12.56 \pm 0.20)\%$
$\pi^{\pm}e^{\mp}\nu\gamma$	(3.62 ± 0.22)x10^{-3}
$\pi^+\pi^-$	(2.067 ± 0.035)x10^{-3}
$\pi^0\pi^0$	(9.36 ± 0.20)x10^{-4}
$\gamma\gamma$	(5.92 ± 0.15)x10^{-4}

Table 2.1: Main KL decay channels

channel	decay ratio [7]
$\pi^+\pi^-$	$(68.61 \pm 0.28)\%$
$\pi^0\pi^0$	$(31.39 \pm 0.28)\%$
$\pi^+\pi^-\gamma$	(1.78 ± 0.05)x10^{-3}
$\gamma\gamma$	(0.178 ± 0.005)x10^{-6}

Table 2.2: Main KS decay channels

In November 1999, after the end of the run, all the four drift chambers were damaged by the beam pipe implosion. 2000 was devoted to systematic studies and high intensity K_S program, while the drift chambers reconstruction took place. The 1997+1998+1999 total uncertainty on $Re(\epsilon'/\epsilon)$ was 2.6x10^{-4} and adding the last run (2001) the low uncertainty suggested in the proposal has been reached.

2.2 NA48 beam lines

The NA48 K_L and K_S beams are nearly collinear, simultaneous and with very similar momentum spectra. This guarantee to the four modes, decaying in the same fiducial region, the best symmetry in Charge-Neutral and Long-Short ratio. Collinear beams minimize differences in acceptance between K_L and K_S while the simultaneous detection of $K_{L,S} \to \pi^0\pi^0, \pi^+\pi^-$ allows the four modes to see the same accidental activity and beam intensity variations and to apply the same dead time to all events.

As shown inFig. (2.6) the same primary proton beam from the CERN Super-Proton-Synchrotron (SPS) is used to produce both K_L and K_S beams. This proton beam impinge on a cylindrical beryllium target (2mm diameter, 400mm long corresponding to $1\lambda_{int}$ for protons) located 126m upstream from the last collimator. At this distance ($\approx 21c\tau_S$) we can assume that the K_L beam is free from K_S . The effect of $\pi\pi$ coming from pure K_S and K_S /K_L interference in the highest energy part of K_L beam has been studied in [26] where also the production asymmetry parameter [1]

[1] $K^0$and $\overline{K}^0$have different cross-section in matter. This, due to an interference term, gives a

D has been measured for NA48, and found to be in agreement with the NA31 value of 0.3. The obtained result was a negligible dilution ($Re(\epsilon'/\epsilon) \rightarrow Re(\epsilon'/\epsilon)$ $(1-\delta)$) of ϵ'/ϵ and a limited systematic effect (1×10^{-4}) on R from the uncertainty on D measure. It is important to keep the kaon beams as free as possible from unwanted particles (i.e. neutrons, muons, photons) produced in the target or along the beamline.

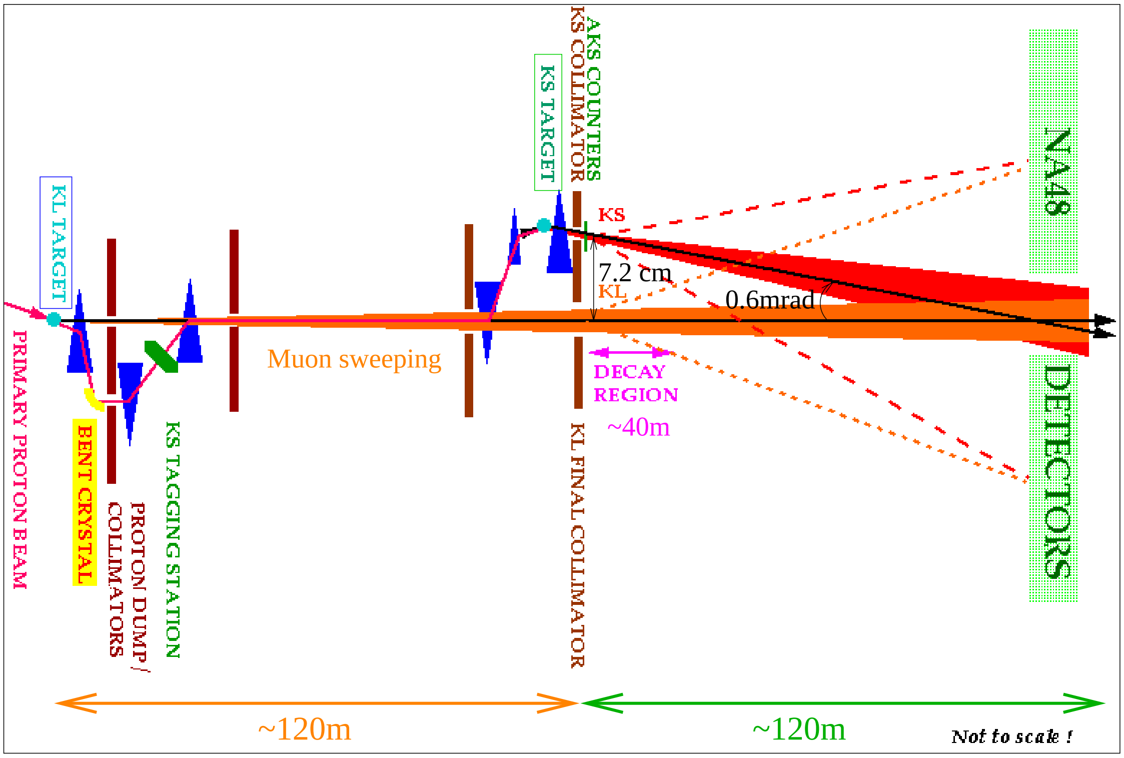

Figure 2.6: The simultaneous and almost collinear K_L and K_S beams, converging in the central detector

To reduce the neutron production at the target the protons impinge with an angle of 2.4mrad: in this way the neutron flux is a factor ≈ 4 reduced with respect to a $\theta = 0$ production angle. The price is a reduction factor (~ 0.25) for the K_L too. The muon flux is reduced by one order of magnitude using the sweeping magnet.

The K_L beam pass through three collimator named *defining, cleaning* and *final* placed at 40m, 100m and 125m downstream of the K_L target respectively. The first collimator *defines* the beam divergence, the second one *cleans* the particles produced

production probability different from 50% - 50%. The production asymmetry parameter, given by $D(P_K) = \frac{N_{K^0}-N_{\overline{K}^0}}{N_{K^0}+N_{\overline{K}^0}}$,is a function of K momentum but in NA48 energy range is quite constant.

or scattered by the previous collimator edges. Their position is such that there are no particles striking from the target to the second collimator. To prevent the products of a possible K_S regeneration on the *cleaning* edges to enter in the fiducial volume the *final* collimator is placed $\sim 3c\tau_S$ downstream, in this way the regenerated K_S are decayed and the products stopped. The beam pipe confines the high fluxes of neutrons and photons such that they do not reach the main detector.

The non-interacting part ($\approx 40\%$) of the primary proton beam is deviated to a secondary path where the protons are channeled by a mechanically bent silicon mono-crystal (Fig. (2.7)).

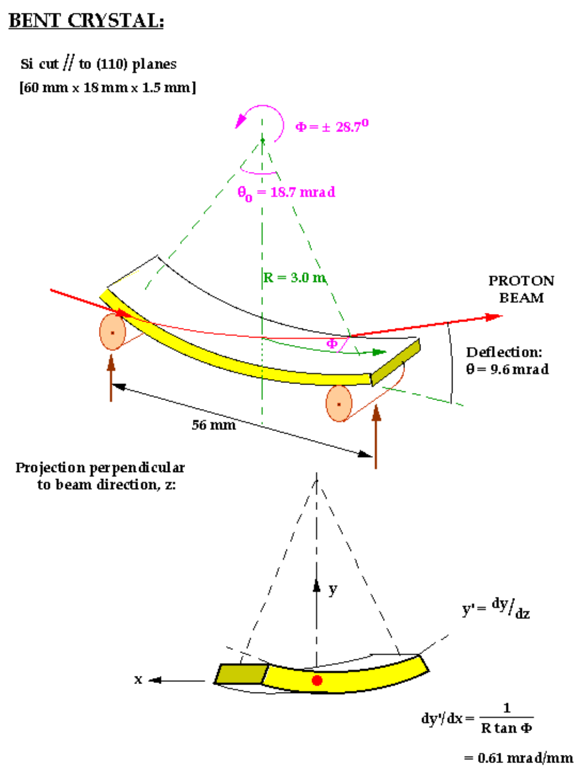

Figure 2.7: The bent crystal for protons deflection

Due to the collective Coulomb field a positive particle, entering in the crystal with a small critical angles to the crystal planes, can follow them and be deflected. Protons in a very selected phase space are obtained through the small transmission efficiency ($< 10^{-4}$). The crystal is designed, fine-tuning the deflection angle, to limit the emittance in both horizontal and vertical(bent) crystal plane, and to avoid heating due to the high incident protons rate. The guiding principle is to use a crystal bent through a fixed total angle θ_0, greater than that required, and then rotate the crystal about a vertical axis such that the beam impinges on one side edge, traverses the crystal diagonally and exits from the opposite edge [29]. The small fraction of protons selected ($\sim$ 5x10$^-$5) travel then toward the K_S target, passing through the tagging station where each proton's time is recorded to identify the decay as K_S or K_L .

The K_S target is identical to the K_L one, is located 120m downstream the K_L target and 7.2cm above the K_L beam. The production angle is 4.2mrad to have similar momentum spectra between K_L and K_S . The K_S collimator let the K_S beam converge with the K_L in the center of the detector. A finite separation of the K_S target with respect to K_L beam line is needed to permit different collimator apertures for the two beams with a minimum of shielding between them.

The beam intensities and their ratio are studied to reach the required number of $K_L \to \pi^0\pi^0$ collecting a similar number of $\pi\pi$ events from K_S and K_L . That is why high energy protons are used and why a K_S beam which intensity is $\approx 10^{-4} - 10^{-5}$ lower than K_L beam intensity is used. Once the two beams are both produced they enter simultaneously in the fiducial volume. This is far enough from the K_L target such that the K_S in this beam are vanished, but closed enough to K_S target to have a negligible amount of K_L decays in this beam [1] . The beginning of this decay volume is defined by an anti-counter (AKS) that vetoes the K_S decaying upstream of it. All the decay region is contained in a vacuum tank (89 length) to minimize interactions with air. The K_L beam continue his path in the beam pipe, evacuated to avoid accidental activity due to particle interactions.

Proton momentum and spill length changed from 1999 to 2001 data taking, as reported in Table (2.3). Until 1999 the proton momentum was 450 GeV/c and protons were delivered from SPS for a time of 2.4s (spill length) each 14.4s, corresponding to

[1] The $\pi\pi$ decays in K_S beam due to K_L "impurities" are at the level of few 10^{-3} [26]

a duty cycle of 0.17.

	98-99	2001
proton momentum (GeV/c)	450	400
SPS cycle time (s)	14.4	16.8
spill length (effective) (s)	2.4 (1.7)	5.2 (3.6)
duty cycle	0.17	0.31
K_L beam intensity (ppp)	$\approx 1.5\text{x}10^{12}$	$\approx 2.4\text{x}10^{12}$
K_S beam intensity (ppp)	$\approx 3\text{x}10^{7}$	$\approx 5\text{x}10^{7}$

Table 2.3: Beam proprieties in years 1998-99 and 2001

While in 2001, profiting of the end of LEP activity, the SPS provides a 5.2s spill each 16.8s. The better duty cycle allows to reach the needed amount of data with 400GeV proton momentum (Fig. (2.8)) giving lower instantaneous intensity in the detector.

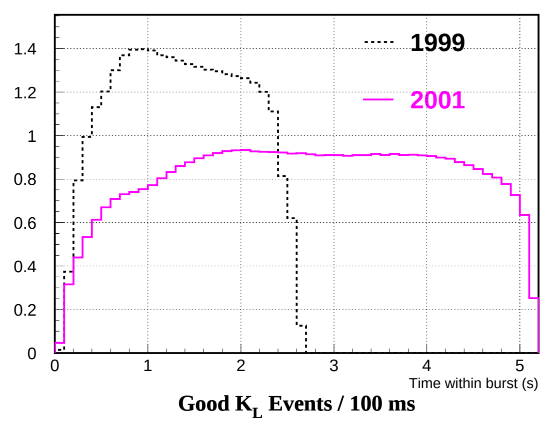

Figure 2.8: good $K_L \rightarrow 2\pi^0/100ms$ vs time in spill in 1999 and 2001 data

2.3 NA48 detector

[2, 3] In Fig. (2.9) and and Fig. (2.10) the different NA48 sub-detectors are drawn. Charged particles from K decays are measured by a magnetic spectrometer while a quasi-homogeneous liquid Krypton calorimeter (electromagnetic calorimeter) takes care of neutral particle decays. The charged hodoscope contribute to trigger de-

cision and gives the precise time for charged decays. The total energy is reconstructed by both electromagnetic (LKr) and hadronic (HAC) calorimeters.

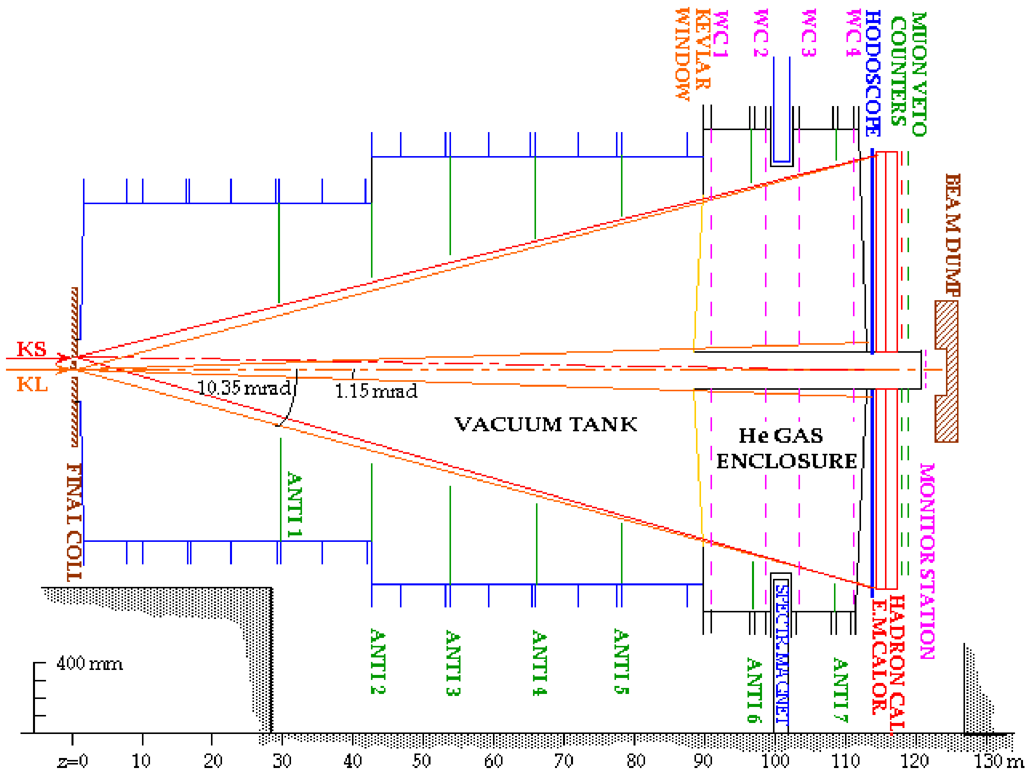

Figure 2.9: NA48 detector

Muon counters are used at the end of the beam line (MUV) to reduce the $K_{\mu 3}$ background vetoing the muons; while to reduce the $K_L \to 3\pi^0$ background anti-counters are placed at large solid angle (AKL). Upstream the spectrometer are located two fundamental devices: the AKS (anti-KS) to define the beginning of decay region, vetoing K_S decayed upstream it, and the TAGGER (or Tagging Station) along the proton beam secondary path, between the bent crystal and the AKS, to identify to which beam the decay belongs. The beam intensity is measured by two kinds of beam monitors both on K_S and K_L lines: counters and integrators.

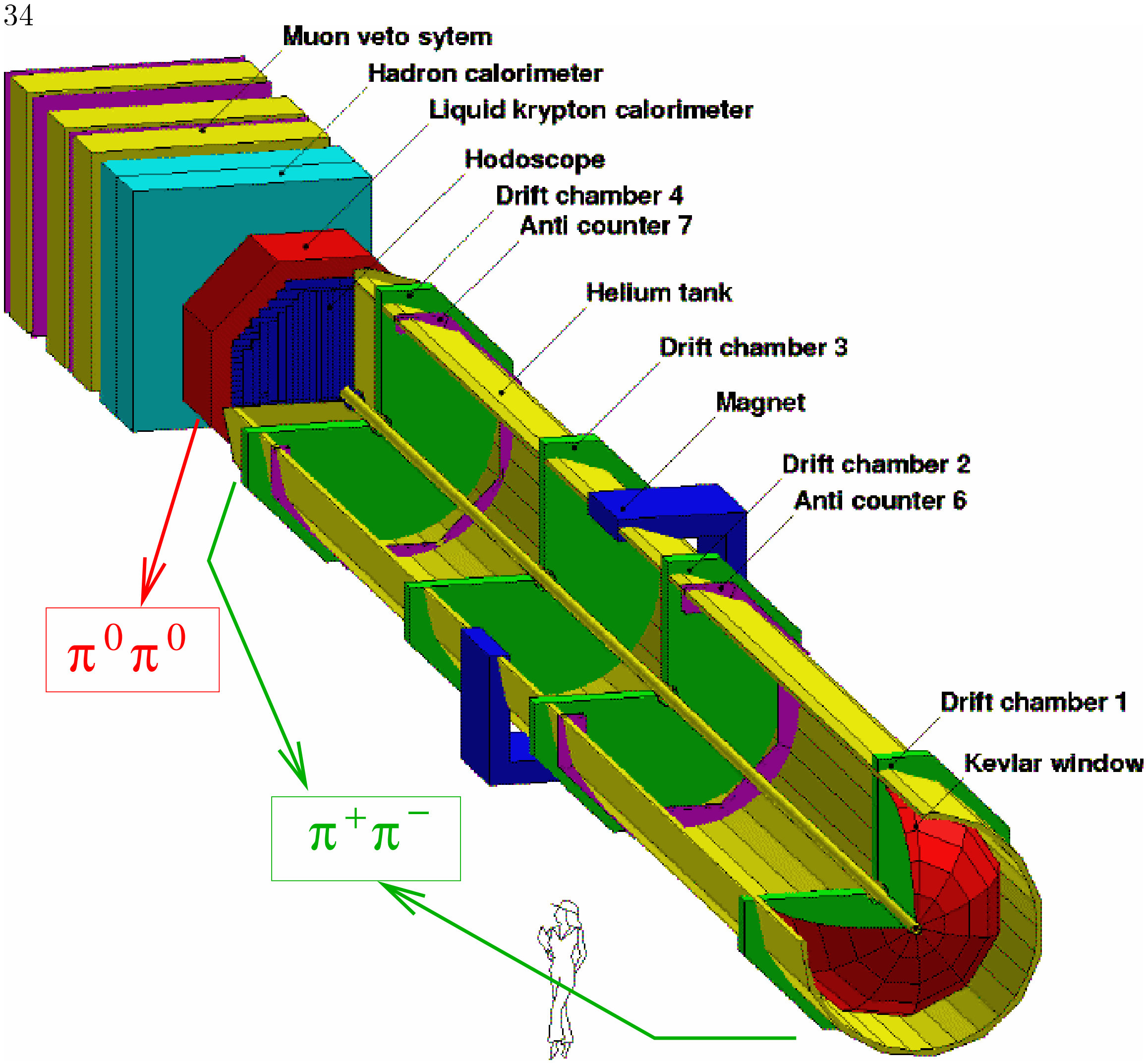

Figure 2.10: NA48 detector Geant picture

2.3.1 The Tagging Station or Tagger

The Tagging Station (Fig. (2.11)) is located after the bent crystal. Each proton traveling toward the K_S target pass through the Tagger where its crossing time is recorded. The station consists of two scintillator ladders, horizontal and vertical with a $50\mu m$ overlap to assure a complete covering of the proton beam, alternate such that a proton crosses at least one horizontal and one vertical scintillator. To equalize the proton counting rate in each channel both ladders are equipped with variable width scintillators. The proton time is defined combining offline the horizontal and vertical counters informations, where the reconstructed time per counter has resolution of

$\sim 140ps$ and the readout window is $\sim 100ns$ around the trigger time.

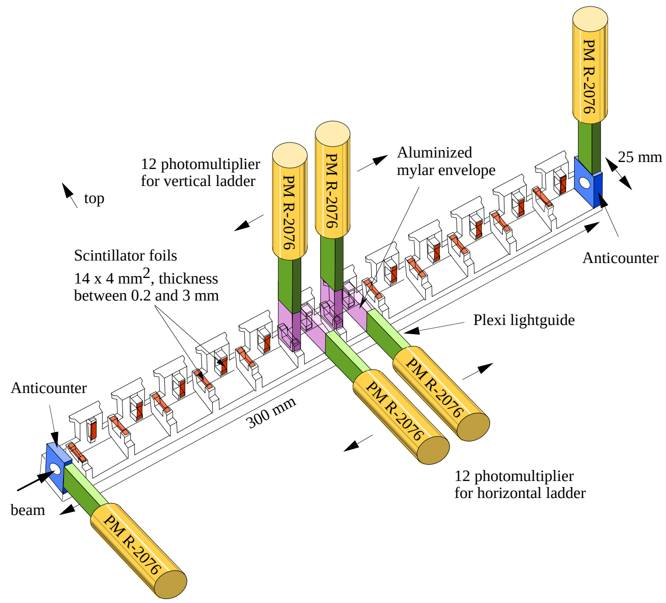

Figure 2.11: The Tagging Station or Tagger

The K_S or K_L decay assignment is based on the coincidence, in 4ns window, between the protons time and the event time: if least one proton is in coincidence with the event time the decay is assigned to K_S , otherwise it is tagged as K_L . The tagging is not needed for the charged decays, since they can be identified by the vertex position, but it is for the neutral decay. To avoid asymmetry on the double ratio measure the tagging is applied to every decay.

This principle is drawn in Fig. (2.12) where the two sources of possible asymmetries are also shown: one is related to the tagging inefficiency α_{SL} and the other one to the accidental tagging α_{LS}. The former (α_{SL}) is not very dangerous because the mistagging is due to the tagger inefficiency itself and affects equally charged and neutral decays. On the other side α_{LS} is related to an accidental coincidence with a proton that, as a consequence of the high rate, is not negligible. In this last case a K_L decay is identified as K_S . This kind of mistagging, named *dilution*, is of the oder

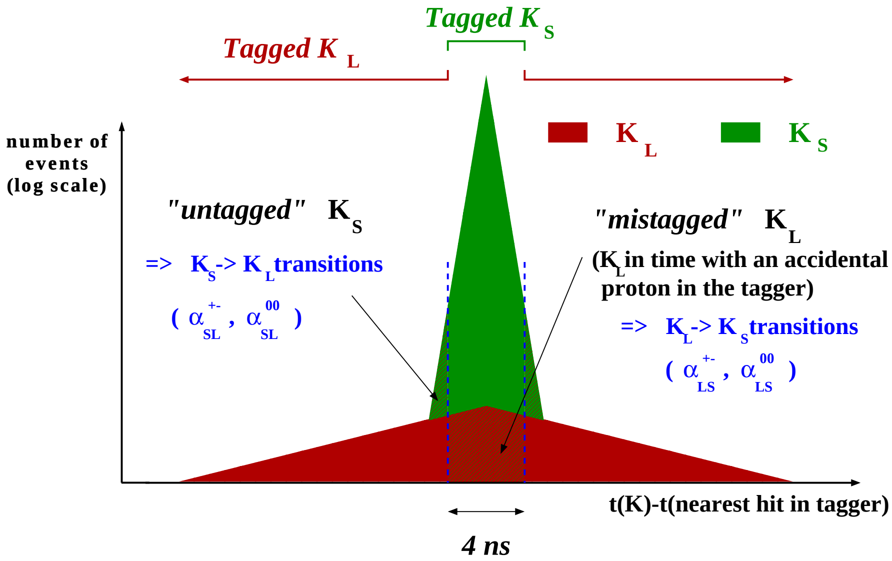

Figure 2.12: Tagging principle

of 10%. We are not afraid of the mistagging in itself but if a difference exists on it between charge an neutral events.

The measured difference $\Delta\alpha_{LS}$ between charged and neutral samples is mainly due to the higher sensitivity of charged events to accidental activity both in trigger and reconstruction. Due to drift chamber read-out overflow (see forward in trigger section) the charged events can be lost in trigger or in the reconstruction part giving the undesired asymmetry, although the same dead time conditions and trigger rejection are applied.

2.3.2 The anti-counters AKS and AKL

The anti-K_S (AKS) is located 607cm downstream of K_S target, at the exit of the K_S collimator. Its purpose is to veto all the upstream K_S decays thus defining the beginning of K_S decay region. Its component are a photon converter and, following it, three scintillator counters, as represented in Fig. (2.13).

The converter, 2.96mm thick iridium crystal ($1.8X_0$), converts photons ($\pi^0 \rightarrow \gamma\gamma$) into electron pairs to allow the vetoing of upstream neutral decay. To maximize the pair production the crystal axis is aligned to the beam axis. [1] . The scintillators counters detect charged particles coming from charged $\pi^+\pi^-$ decays or from photon conversion, In this way both charged and neutral decays are detected and vetoed: an event is rejected if there is an in-time hit in the second scintillator. The time is reconstructed offline with a resolution of $\sim 160ps$. Therefore is the second scintillator's crystal that gives the geometrical reference to define the beginning of the K_S decays fiducial region and to control the LKr energy scale.

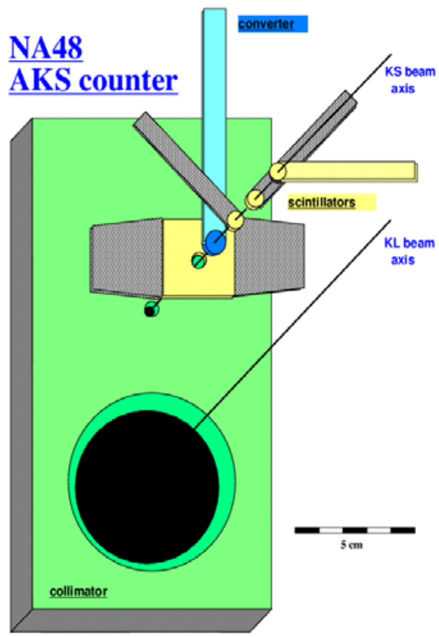

Figure 2.13: AKS scheme

The reduction of $K_L \rightarrow 3\pi^0$ is essential since the rate for this channel is 200 times the $K_L \rightarrow 2\pi^0$ rate. To study this background and the accidental activity seven rings of iron (acting as photon converter) and scintillator act like K_L anti-counter (AKL). The rings are placed at large solid angle in suitable position between the AKS and the end of the spectrometer: from ANTI1 to ANTI7, as are signed in Fig. (2.9).

[1] in crystalline materials the incident field experienced by an incident photon depends on the photon's direction to crystal axis, leading to a change in the pair production cross section [30]

2.3.3 The magnetic spectrometer

Charged events are detected by the magnetic spectrometric. It is housed in a tank filled with Helium, to lower the scattering probability, at atmospheric pressure. The spectrometer is defined by a central dipole magnet with two drift chambers on each side. The required purity in helium would be easily reached filling a balloon instead of the aluminum tank but the presence of the drift chambers and the beam pipe is a constraint leading to the tank choice. The tank is also a safer choice in case of outbreak or implosion, as happened in 1999 [31].

The requirements on momentum and space resolution, track acceptance and field uniformity leads to the magnet and chambers characteristics. The track positions, extrapolated downstream, are required to be within the acceptance of LKr and MUV system, in order to allow for proper electron and muon identification. The kaon energy is computed from the opening angle of the two tracks θ before the magnet and from the ratio of their momenta p_1, p_2:

$$E_K = \sqrt{\frac{\mathcal{R}}{\theta^2}(m_K^2 - \mathcal{R}m_\pi^2)} \quad \text{where} \quad \mathcal{R} = \frac{p_1}{p_2} + \frac{p_2}{p_1} + 2 \tag{2.7}$$

Computing the energy in this way, instead of the simple sum of the two tracks energy, the effects from uncertainties in magnetic field and multiple scattering in the definition of the fiducial region are reduced. That is the correction to the energy scale on momentum measurements is at the level of per mille [32].

As fast trigger requires easy momentum calculation, so the field must be as uniform as possible. Therefore a large magnet is needed to fulfill field uniformity and matching the acceptance of the electromagnetic calorimeter requirements. The integral of the magnetic field between the second and third chamber(Fig. (2.9)) is 0.83Tm, corresponding to an induced change in transverse momentum of 265 MeV/c in the horizontal plane. Nevertheless, in uniformity of the field, little imperfections remain. To avoid this to introduce a bias in the double ratio measure each weak of data taking the direction of the magnetic filed is inverted.

[34]In order to meet the $\approx 2MeV$ precision on reconstructed kaon mass and

good background rejection each chamber must have a detection efficiency closed to 100% and provide a reconstruction of hits with a resolution of about $100\mu m$. In addiction fine granularity with maximum drift distance restricted to few millimeters is necessary to have rate capability higher enough to cope with the high flux of incoming particle. Drift chamber have been constructed with minimal amount of material along the beam direction in order to minimize multiple scattering effects.

Each chamber is equipped with 4 views (Fig. (2.14)), in each view two 0.5cm staggered planes, to solve the left-right ambiguity, are grouped together. Chamber three represent a sort of *spare* chamber in which only four planes (2 views) are read-out, it is useful to reach a better resolution but is not as indispensable as the others: tracks are reconstructed by the first two chamber, before the magnet, and chamber four after the magnet. Each plane houses 256 grounded sense wires, spaced of 1cm, read-out in 16 group of 16 wires each. The central wires are half wires to allocate the beam pipe portion passing through the chamber, on this portion set of rings are located and the central wires soldered on these rings. The four views, named X,Y,U and V all orthogonal to the beam, follow different orientation as shown in Fig. (2.14): $0°, 90°, -45°, +45°$. This allows charged tracks reconstruction without ambiguities and, providing redundant information, the effect of inefficient wires is minimized.

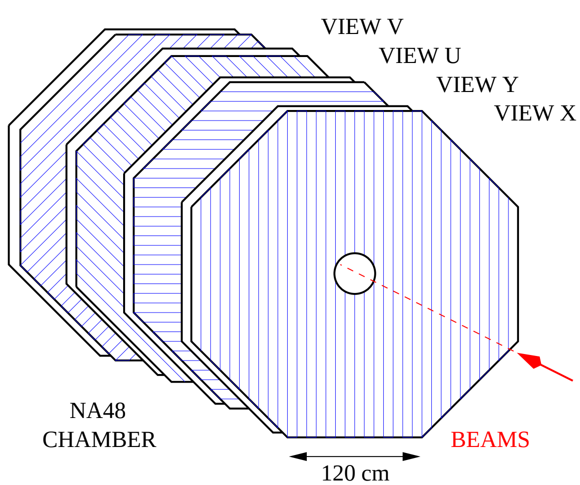

Figure 2.14: DCH: 4 views drawing

Sense wires, $20\mu m$ diameter, are made of gold-plated tungsten (that is stress resistant). The sense wire's plane is enclosed between two planes of potential wires (Ti-Cu) with a diameter of $120\mu m$ [34]. The spacing between two wires, both on the field and the sense wire planes (Fig. (2.15)), is 1cm therefore that the maximum transverse drift distance in a cell is 5mm, corresponding to $\sim 100ns$ drift time (180ns/cm). To shape the electric field and separating two consecutive views thin mylar foils ($22\mu m$) coated with graphite are used. The chambers, filled with a (50%)Argon-(50%)Ethane gas mixture, in usual operation conditions (-2250V applied on field wires) the space resolution is better than $100\mu m$. [34].

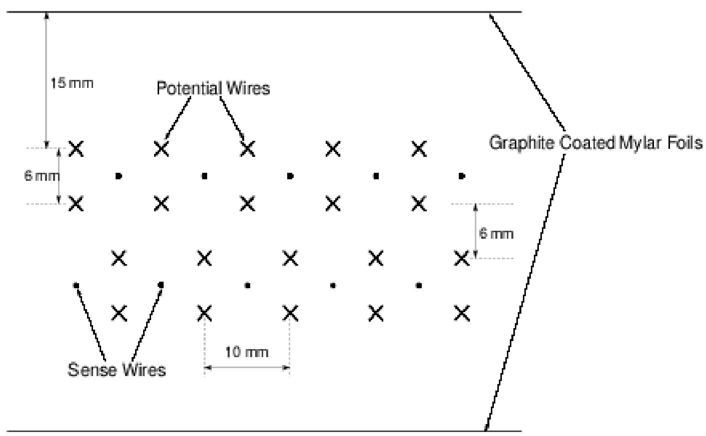

Figure 2.15: DCH sense and potential wires disposition

The track reconstruction provides an event time with a precision of 0.7ns used to cross-check the event time determined by the charged hodoscope. Track positions are reconstructed with a precision of $100\mu m$ per view and the momentum resolution (from special electron runs) is

$$\frac{\sigma(p)}{p} = 0.48\% \oplus 0.009p\% \quad \text{(p in GeV/c)} \tag{2.8}$$

where the first term is due to multiple scattering effects and the second term is due to the position resolution in the chambers. The resolution obtained on $\pi^+\pi^-$ invariant mass is $2.5MeV/c^2$.

The position of charged decay vertex is measured with high precision: ~500mm longitudinally and 2mm in the transverse plane [2]. The geometric accuracy due to the cumulative uncertainties on the wires position is better than 0.1mm/m.

Since in the decay region the K_S and K_L beams are vertically separated by about 6cm a clean identification of K_S and K_L decays into $\pi^+\pi^-$ from vertex position is possible and useful for many studies (e.g tagger inefficiency and dilution). The separation of the K_L and K_S beams gives a geometrical difference in the first chamber especially around the beam pipe, where the Monte-Carlo simulation is more difficult. But applying a cut on momentum asymmetry $A = |p_1 - p_2|/(p_1 + p_2)$, thus removing events with one track closed to the beam pipe, the acceptance error on R due to this geometrical difference is reduced.

2.3.4 The liquid Krypton calorimeter

The main detector for neutral decays is the electromagnetic calorimeter: it is a quasi-homogeneous detector with an active volume of $\sim 10m^3$ of liquid Krypton. Sever performances [35] are required since $2\pi^0$ decays are reconstructed through their 4γs detection. The photons' energy is in the 3GeV to 100GeV range and the average photon's energy is 25GeV. Furthermore $K_L \to 3\pi^0$ must be rejected and everything have to be done at the high K_L rate and minimizing potentials bias on R. The calorimeter is placed $\approx 100m$ downstream the decay region, it is not possible to have a direct measure of the photons' angles thus the distance to the decay vertex is calculated from the energies and positions in the calorimeter, assuming the Kaon mass for the 4γs ($E_k = \sum_i^4 E_i$):

$$D = z_{vtx} - z_{LKr} = \frac{1}{m_K}\sqrt{\sum_{i<j} E_i E_j d_{ij}^2} \tag{2.9}$$

$$d_{ij} = \sqrt{(x_i - x_j)^2 + (y_i - y_j)^2} \tag{2.10}$$

If there is a systematical energy error (α) in the measurement of photon energies such that $E_i \to \alpha E_i$, z_v will be affected on the same grounds and the effect will appear doubled in the proper time $\tau = m_K z_{vtx}/E_K$ determination.

The calorimeter must therefore fulfill the following requirements [25, 35]:

- space resolution $\approx 1mm$
- energy resolution $\approx 1\%$ for the detected photon of average energy 25GeV
- good uniformity
- non linearity bound to $\approx 0.1\%$ between few GeV and 100 GeV
- π^0 mass resolution $\approx$ 1MeV to reduce $K_L \to 3\pi^0$ background
- time resolution better than 500ps to cope with tagger rate
- recording multi-photon events standing the high K_L rate (500 KHz)
- stability over years
- initial current r/o technique to minimize the sampling fluctuations.

  This technique allows fast response and constant efficiency across the gap (except for a small region near the electrodes)
- segmentation to reduce ambiguity in pairing of photons coming from the same π^0 and get higher rate capability in relationship to accidental photons

A quasi-homogeneous Liquid Krypton Calorimeter operating as a ionization chamber has been finally chosen fulfilling the previous conditions. It is almost fully active, with high density sensitive medium, thus ensuring the good intrinsic resolution while as noble liquid has good stability. Referring to noble liquid proprieties Table (2.4): Argon density is not enough for a homogeneous calorimeter and concerning the liquid Krypton 127cm are needed to achieve a complete longitudinal containment of a shower ($27X_0$). Xenon has a similar Moliere radius (expressing the transverse size of showers) but a smaller radiation length. Liquid Krypton has then been chosen.

The segmentation is obtained by Cu-Be-Co ribbons defining $\approx$ 13000 cells in a structure of longitudinal projective towers pointing toward the center of the decay region. The cell cross section is about 2cm x 2cm and consists of a central anode between two cathodes. The electrodes, guided longitudinally through five spacer

noble liquid	Z	density (g/cm^3)	$X_0(cm)$	$R_{Moliere}(cm)$	T (K)
Ar	18	1.4	14.0	9.2	87.3
Kr	36	2.4	4.7	6.1	119.8
Xe	54	3.0	2.9	5.5	165.1

Table 2.4: Argon Krypton Xenon characteristics

plates, follow a $\pm 48mrad$ zig-zag to decrease the impact point position sensitivity on the energy (Fig. (2.17)).

Figure 2.16: LKr calorimeter

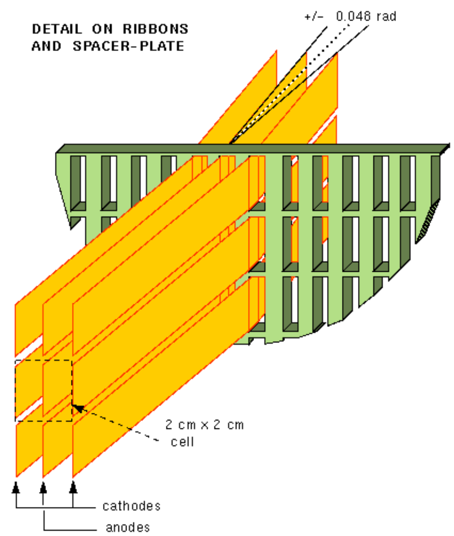

Figure 2.17: definition of a LKr calorimeter tower

The cluster radius r=*11cm* used in the shower reconstruction is a compromise between noise in the cluster (increasing with r) and the fluctuations dominating the sampling term (decreasing with r). The obtained energy resolution is:

$$\frac{\sigma(E)}{E} = \frac{(3.2 \pm 0.2)\%}{\sqrt{E}} \oplus \frac{(9 \pm 1)\%}{E} \oplus (0.42 \pm 0.05)\% \tag{2.11}$$

All the requirements are fulfilled and the $2\pi^0$ event time is known with a precision of $\sim 220ps$.

2.3.5 Hodoscopes, Hadron calorimeter and Muon Veto

Downstream the Helium Tank two planes, horizontal and vertical, of scintillators strips form the Charged Hodoscope (Fig. (2.18)). These are organized in four quadrants to give clear topological signals in the first level of charged trigger. The charged hodoscope informations are used offline to reconstruct the charged event time with a precision of $\sim 150ps$.

The neutral hodoscope (Fig. (2.19)) provides an independent neutral event time measure, that can be used to cross-check the LKr one, and take part in the neutral trigger decision. It is made of scintillating fiber counters located inside the LKr where the shower profile reaches its maximum ($\sim 9.5X_0$).

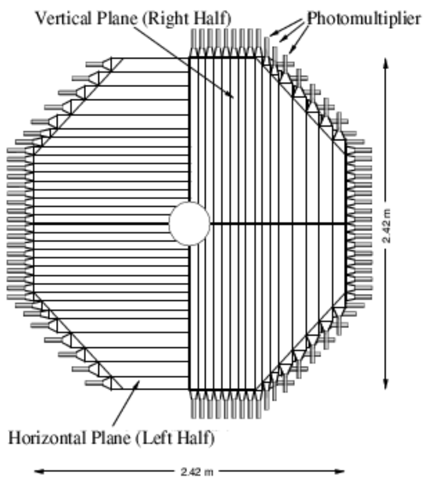

Figure 2.18: Charged Hodoscope

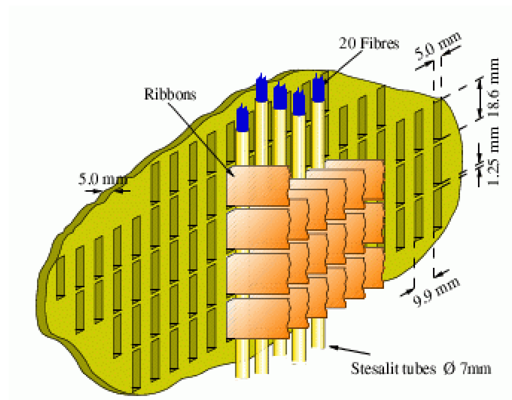

Figure 2.19: Neutral Hodoscope

The Hadron calorimeter, made of iron and scintillator, contributes together with the LKr to the total energy measure used in the trigger. Three planes of scintillators shielded by an iron wall (80 cm thick) constitute the Muon Veto, its informations are used to reject $K_{\mu 3}$ background.

2.3.6 Beam monitors

There are two sets of K_S and K_L beam monitors: a first one ,that we call standard, is a counter-like, and a second one named Ferrara is integration-based. The *standard beam monitors* are

- the K_S beam monitor placed alongside the K_S target. It consists of four plastic scintillators parallel to the target. The beam intensity is monitored counting particles emitted from K_S target in the direction orthogonal to the beam [36].

- the K_L monitor just before the beam dump. Consists of two orthogonal planes of scintillating fibers counting the activity in the K_L +K_S beams. The sensitive area is $18 \times 18 cm^2$ This activity is dominated by K_L beam: it is at the end of the detector and the K_L beam intensity is $10^4 - 10^5$ times the K_S intensity. The fiber size had been chosen such that the individual counting rates should not exceed a few MHz. The fibers are read by PhotoMultipliers, where each PM is coupled to 3 fiber bundles with a spatial binning of 2.5cm to measure the beam profile. [37].

The *standard* monitors are also used to trigger a special kind of events: the *random* triggers. These are very useful to study not only the accidental activity effect, through their overlay with data or Monte-Carlo events, but also the overflow incidence and distribution along the drift chambers. These special events, to be useful in the accidental activity study, must be:

- proportional to beam intensity
- independent from decay event but they have to record the same beam condition

These conditions are fulfilled if the random triggers are delayed by 3 SPS revolution cycle, equivalent to $69.3\mu s$. We will look in more detail at these special triggers in chapter four and five.

The *Ferrara beam monitors or Integrators* (Fig. (2.20)) installed for the 2001 run are:

- K_S Ferrara monitor, housed in the Tagger box
- K_L Ferrara monitor, placed between the standard K_L monitor and the beam dump

The main advantage is on the time scale we can study the instantaneous beam intensity. The informations coming from the standard monitors are read by continuous counters and the 'instantaneous' intensity is computed as the difference between two consecutive events divided by the time difference. In an optimistic estimation, taking into account the 2001 run condition of $\approx 30^{\cdot}000$ triggers collected in the $5s$ burst, with these informations we can investigate the instantaneous intensity behavior at time scale of $\approx 170\mu s$. In a more realistic picture, excluding the very high intensity beginning of the burst and taking into account the events distribution in the spill, the time scale can be estimated at $\approx 1ms$.

On the other side the Ferrara monitors have, for both K_S and K_L , a set of four integration times that in the 2001 run were chosen to be 200ns, $1\mu s$, $3\mu s$ and $15\mu s$. Instantaneous beam intensity behavior can thus be investigate down to 200ns time scale.

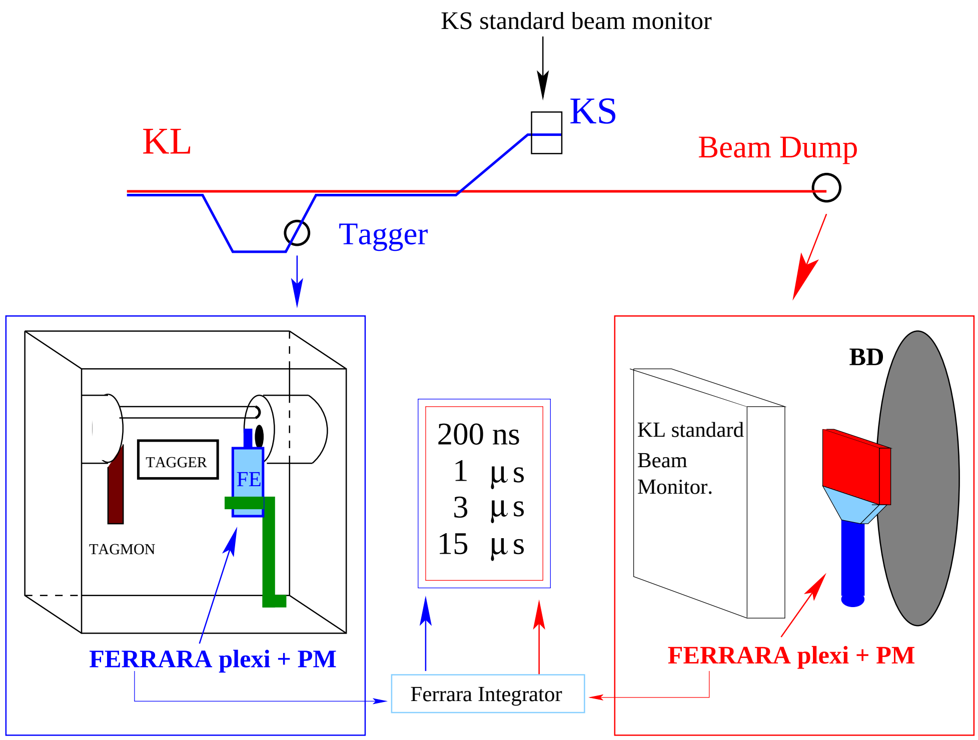

Figure 2.20: K_S and K_L Ferrara beam monitors

The Ferrara monitors are made of Plexiglas® as active medium read by a 10 stages photomultiplier. The K_S monitor replace a part of another device (Tagmon) used to monitor the proton beam in the Tagger box. The two Plexiglas sizes are suggested by the beam area to be covered, moreover the K_S monitor has to match the Tagmon thickness to not influence the proton beam: the K_S Plexiglas is $22 \times 22mm^2$ in area, and 10mm thick while the K_L Plexiglas is $121 \times 121 \times 10mm^3$. A more detailed description will be given in the next chapter, that is devoted to these beam monitors and their data quality.

2.4 Triggers and selection cuts

The trigger system is designed [3, 2] to reduce the high rate (500kHz) of particles reaching the detector, with minimal loss from dead time and inefficiencies, to less than 10kHz. A 40MHz clock signal is used to synchronize the entire experiment over its 250m length [38] and the Trigger Supervisor (TS) records the time of the accepted events relative to this clock. The Trigger Supervisor is an hardware system which correlates the trigger informations coming from the different trigger sources: L2C (level 2 charged trigger), L1TS (level 1 Trigger Supervisor) and NT (neutral trigger) [39] as shown if Fig. (2.21).

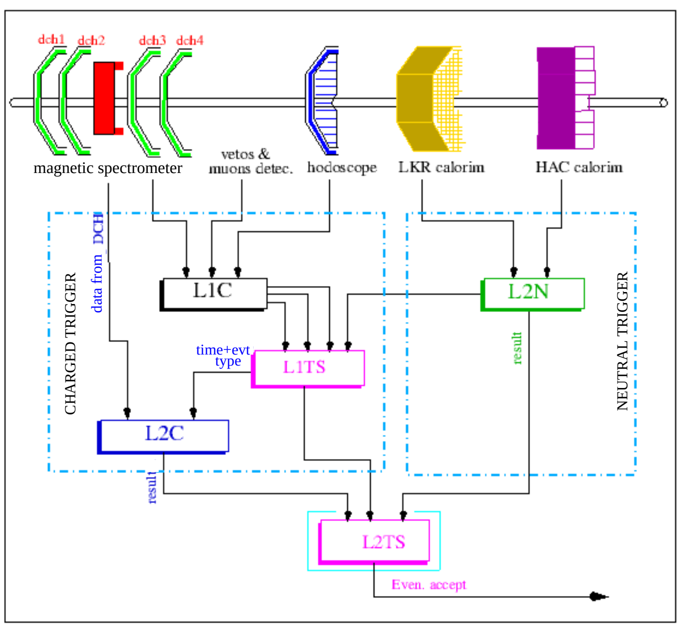

Figure 2.21: Trigger architecture

The neutral trigger operates on the information from the LKr such as energy deposit, number of energy peaks, and distance of the decay vertex from the calorimeter. The electronics is implemented in a pipeline which makes the trigger free of dead time. The efficiency is almost 100% (99.9there are no significant differences between K_S and K_L therefore none correction to R is needed.

The charged trigger (efficiency $\approx 98.7\%$)is made of two level triggers:

- a first level to reduce the rate to 100kHz by a coincidence of a) charged hodoscope signals in opposite quadrants, b) hit multiplicity in in the first chamber, integrated over 200ns and c) total energy from calorimeters (LKr+HAC)
- a second level trigger consisting of an hardware coordinate builder using the data from DCH 1,2 and 4 to reconstruct tracks.

An overflow conditions on the drift chambers readout affects both the second level trigger and the reconstruction: if the multiplicity in one plane is greater than 7 hits in 100ns the overflow condition is set, no hits are recorded for that plane and the memory is reseted. In this way events with high multiplicity are rejected but a safe rejection window of $\approx \pm 300ns$ around the overflow is needed in the selection to exclude possible influence in nearby events. The cut applied in the analysis is very tight: if there is at least one plane in overflow, in the extended $\approx \pm 300ns$ time window, the event is rejected. The analysis on random events shows an overflow incidence of $\sim$25% until 99 data and a reduction, due to better spill and lower instantaneous intensity, to $\sim$12% in 2001. We will examine later on the effect of this overflow on event losses while in App.A we will talk about the test on the new readout prototype in 2001 and its data taking in 2002. This new readout, commissioned for the 2002 K_S high intensity run , is overflow free.

There are various cuts to be applied in order to select the samples for the R analysis. Neutral selection K $\rightarrow 2\pi^0$ is based on LKr data on photons showers energy and position, minimum distance between photons, matching of photon pairs invariant mass with nominal π^0 mass. Charged selection K $\rightarrow\pi^+\pi^-$ is based on tracks, momenta and invariant mass that should be equal to the kaon mass. All the cuts have been studied for long time and the R stability with their variations has been checked.

An exhaustive description of these cuts can be found in [2, 1] while in the following chapters we will focus on some of them. The only anticipation is for a special 2001 cut to exclude the beginning of the burst: two fundamental detectors AKS and Tagger suffer from the unexpected very high intensity in the first 200ms, while for the rest of the burst the intensity was the expected one. This high intensity identification and related problem on AKS was the first Ferrara monitors' success.

2.5 Second order correction to R

The beam lines and detector are designed to reach the best symmetry between Long-Short and Charged-Neutral decays. Nevertheless existence of remaining asymmetries must be checked and, if there are, the relative corrections have to be applied on R. These small corrections are called of *second order*. Although the weighting principle is applied to minimize the acceptance differences there are still small geometric differences between the K_S and K_L . The two beams converge at the LKr center but at the spectrometer there is still a little separation. As a consequence a residual difference exists, between K_S and K_L charged decays, around the beam axis in the spectrometer.

This dissertation shall not cover all the complex subject of the second order corrections to R arising from years of study and analysis performed by the whole collaboration. Here we simply summarize the values of these corrections (Table (2.5)). The exhaustive explanation of the accidental effects and their correction is left to the next chapters.

We add here, as a final summary the corrected double ratio calculation $R = 1-$(ratio effects from 4modes numbers)+(corrections), the result for the 2001 run is $R_{2001} = 1-(1.169 \pm 0.147)\% + (0.350 \pm 0.111)\% = 0.99181 \pm 0.00147_{stat} \pm 0.00110_{syst}$. Part of the systematic error (± 0.00065) comes from the statistics on control samples.

The 2001 $Re(\epsilon'/\epsilon)$ value is $Re(\epsilon'/\epsilon) = (13.7 \pm 3.1) \times 10^{-4}$ that, combined with 97-98-99 result $(15.3 \pm 2.6) \times 10^{-4}$, gives the final result
$Re(\epsilon'/\epsilon) = (14.7 \pm 2.2) \times 10^{-4}$

	98-99	2001
$\pi^+\pi^-$ background	$16.9 \pm 3.0_{(syst.)}$	$14.2 \pm 3.0_{(syst.)}$
$\pi^0\pi^0$ background	$-5.9 \pm 2.0_{(syst.)}$	$-5.6 \pm 2.0_{(syst.)}$
beam scattering	$-9.6 \pm 2.0_{(syst.)}$	$-8.8 \pm 2.0_{(syst.)}$
Tagging inefficiency α_{SL}	$\pm 3.0_{(syst.)}$	$\pm 3.0_{(syst.)}$
Accidental tagging α_{LS}	$8.3 \pm 3.4_{(stat.)}$	$6.9 \pm 2.8_{(stat.)}$
$\pi^+\pi^-$ scale	$2.0 \pm 2.8_{(syst.)}$	$\pm 2.8_{(syst.)}$
$\pi^0\pi^0$ scale	$\pm 5.8_{(syst.)}$	$\pm 5.3_{(syst.)}$
AKS inefficiency	$1.1 \pm 0.4_{(syst.)}$	$1.2 \pm 0.3_{(syst.)}$
Acceptance	$26.7 \pm 4.1_{(stat.)}$ $\pm 4.0_{(syst.)}$	$21.9 \pm 3.5_{(stat.)}$ $\pm 4.0_{(syst.)}$
$\pi^+\pi^-$ trigger inefficiency	$-3.6 \pm 5.2_{(stat.)}$	$5.2 \pm 3.6_{(stat.)}$
Accidental activity intensity diff. illumination diff.	 $\pm 3.0_{(syst.)}$ $\pm 3.0_{(stat.)}$	 $\pm 1.1_{(syst.)}$ $\pm 3.0_{(stat.)}$
K_S in time activity	$\pm 1.0_{(syst.)}$	$\pm 1.0_{(syst.)}$
Total	$+35.9 \pm 8.1_{(stat.)} \pm 9.6_{(syst.)}$	$+35.0 \pm 6.5_{(stat.)} \pm 9.0_{(syst.)}$

Table 2.5: Different years corrections on R. Corrections and systematic uncertainties on R are reported in 10^{-4} units, pure statistical and pure systematic errors on corrections are labeled as (stat.) and (syst.) respectively.

Chapter 3

Beam Monitors in 2001 run

3.1 Beam monitors and SPS phases

In the second chapter the Ferrara beam monitors have been briefly introduced ((§ 2.3.6), Fig. (2.20)) together with the standard beam monitors. In this chapter they are presented in a more extensive way with a first look at their data quality. To distinguish their variables we will refer at them as (intKSMON, intKLMON) and (KSMON and KLMON) for Ferrara and standard monitors respectively. Apart from beam monitors other devices can give informations on the beam intensity, even if not designed for this purposes. I.e. extra activity measured in LKr, DCH and AKL used in accidental activity studies, or the scintillators closed to the Tagger (TAGMON) used to monitor the proton beam in the Tagger region.

The standard monitors signals are stored in a scaler read by continuous counters. The the difference between two consecutive events, divided by the time difference, is regarded as the instantaneous intensity they can measure. We are interested in the investigation of small time scale structure to study instantaneous intensity. A rough estimation (§ 2.3.6) indicates that these monitors can reach only a time scales of $\approx$ 1ms or few hundreds μs.

While the K_S and K_L Ferrara monitors can investigate smaller time scale according to the integration times chosen. The integration modules houses eight channels, 4 devoted to K_S and 4 to K_L monitor data, we can therefore choose four different integration time. In 2001 run the four times were chosen to investigate small time scales down to 200ns: 200ns,1μs,3μs,15μs.

The integration module was already there since 1999 run but, at that time, the input signals were taken splitting the signals of the TAGMON and standard KLMON. To investigate smaller time scales than standard monitors the integration times were chosen to be 2,15,30,60μs. But the resulting activity in the $2\mu s$ was very low and it was not possible to increment it (e.g. using converters in front of the TAGMON and standard KLMON) since both TAGMON and KLMON could not cope with higher rates. Moreover the TAGMON scintillators were suffering from radiation damage. A few times,roughly each 20 days, slight increments of High Voltage were needed to recover the efficiency.

It was thus clear that new devices were needed, especially if we want to investigate shorter time-scale to go toward 'as instantaneous as possible' activity. Moreover looking at LKr activity in random event there was an indication of existing small (in the μs to few hundred ns range) time scale structures, especially at the beginning of the bursts. As new monitors two Plexiglas -based devices (Plexiglas + air guide + PM) were chosen. There are several advantages in this choice [40]:

- the Cerenkov light is faster;

- it is not rate limited;

- the light guide in air is easy to build and is better than a Plexiglas guide especially in the K_S monitor case where the K_L beam halo would induce dangerous noise

- its radiation hardness, because scintillation is due to Cerenkov effect and not to molecular excitation;

- and, last but not least, is a easy-to-build device

The KS monitor is placed on the proton beam path through the Tagger box while the KL see neutral particle arriving at the beam dump. The Plexiglas dimensions are determined by the beam area they have to cover.

The signals, after an amplification stage, are sent to the integration module. The integrated signals, adjusted and shaped with the rise time of 50-100ns, are then readout by fast ADC and sent to a pipeline memory. From the Pipeline Memory Board

(PMB) card are readout in 12 timeslots (25ns each) around the trigger time. The charged hodoscope Q_X signal (coincidence of two opposite hodoscope's quadrants) has been used as the referring signal for the offset definition.

The first tests for the new beam monitors data quality is their matching with the SPS phase (defined below) and the SPS Main phase (50Hz governing the magnet for proton extraction). The behavior of these phases, affecting the proton intensity and magnets, should be reproduced in the event distribution. The beam monitors are expected to agree with these too. First of all we look at the SPS phase. [24]The SPS is filled up with two trains of bunches of protons circulating in it, the trains are separated by some empty bunches covering ∼10% of the SPS circumference(Fig. (3.1)). The protons take 23.3μs to complete an SPS circumference, equivalent to a revolution frequency of 43kHz. For each event the associate time with respect to a 43kHz clock signal, synchronized to the circulating protons, is recorded: this is the so called SPS phase. Protons are accelerated using RF system which kept the $\sim 5ns$ bunch

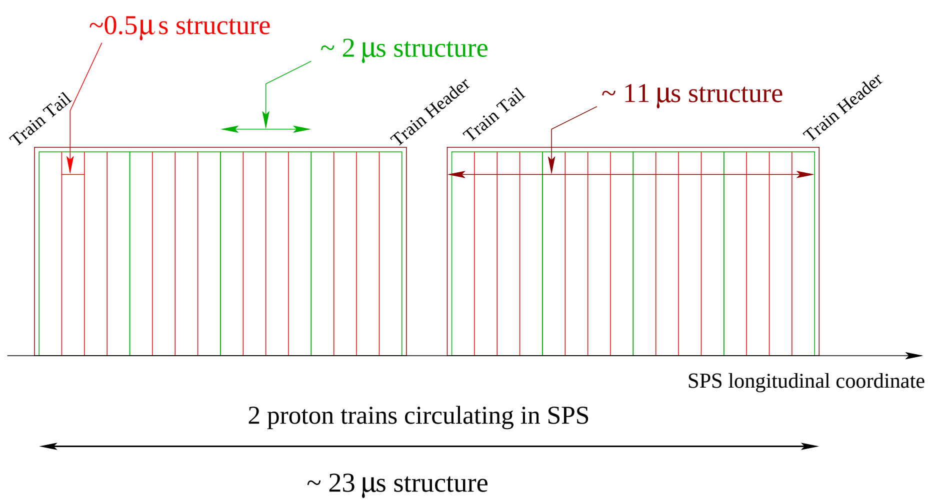

Figure 3.1: Two protons trains circulating in the SPS and their substructure

structure. The RF are then switched off to begin the extraction and protons start loosing their bunched structure (debunching). Ectracted protons are then delivered, to NA48, for a time of 5.2s (burst) each 16.8s.

We can have a look at the average behavior, over one hundred bursts, of the

SPS phase, recorded for each event, as shown in Fig. (3.2) and at the event time with respect to the same SPS phase in Fig. (3.3). The train structure and the holes between two trains are visible, but not as exactly as drawn in Fig. (3.1). In Fig. (3.3) a high populated region at the train tail is also visible. These features are related to

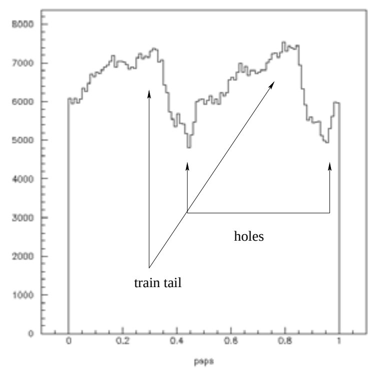

Figure 3.2: Events# vs SPS phase

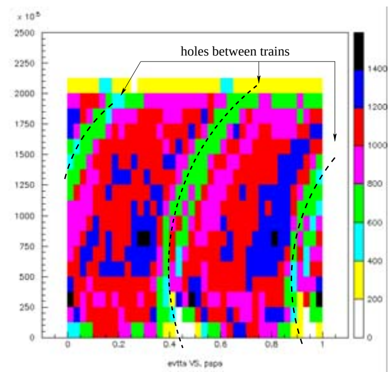

Figure 3.3: Event time vs SPS phase

the proton extraction and debunching in the SPS. The number of extracted protons from SPS is not stable but depends on their phase space distribution in the bunches, that changes along the train. A variation in the number of protons corresponds to a variation in the intensity and as a consequence on the number of events. The same behavior has to appear in our events. We can ask now if the monitors are in

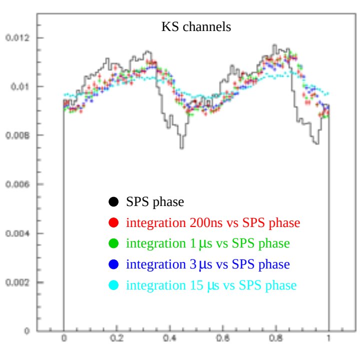

Figure 3.4: Ferrara KS channels vs SPS phase and SPS phase

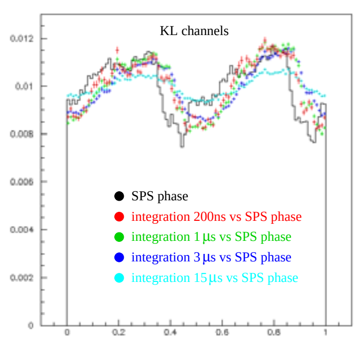

Figure 3.5: Ferrara KL channels and SPS phase

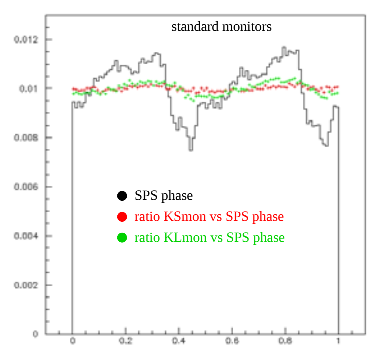

Figure 3.6: Standard monitor and PS phase

agreement with the SPS phase, their average behavior over one hundred bursts is shown in Fig. (3.4) and Fig. (3.5). The standard beam monitor too match the SPS phase (Fig. (3.6)) even if the agreement is a bit worse, as expected as a consequence of their bigger time-scale.

Nevertheless as we have mentioned earlier the SPS trains structure is not always exactly the same. To be sure of the SPS phase and monitors matching it is better to check it burst by burst. To show that we can take nine consecutive bursts as in Fig. (3.7) and notice that in fact the holes moves a little bit from one burst to the other. Moreover in the single burst picture the peaks at the beginning of the burst are

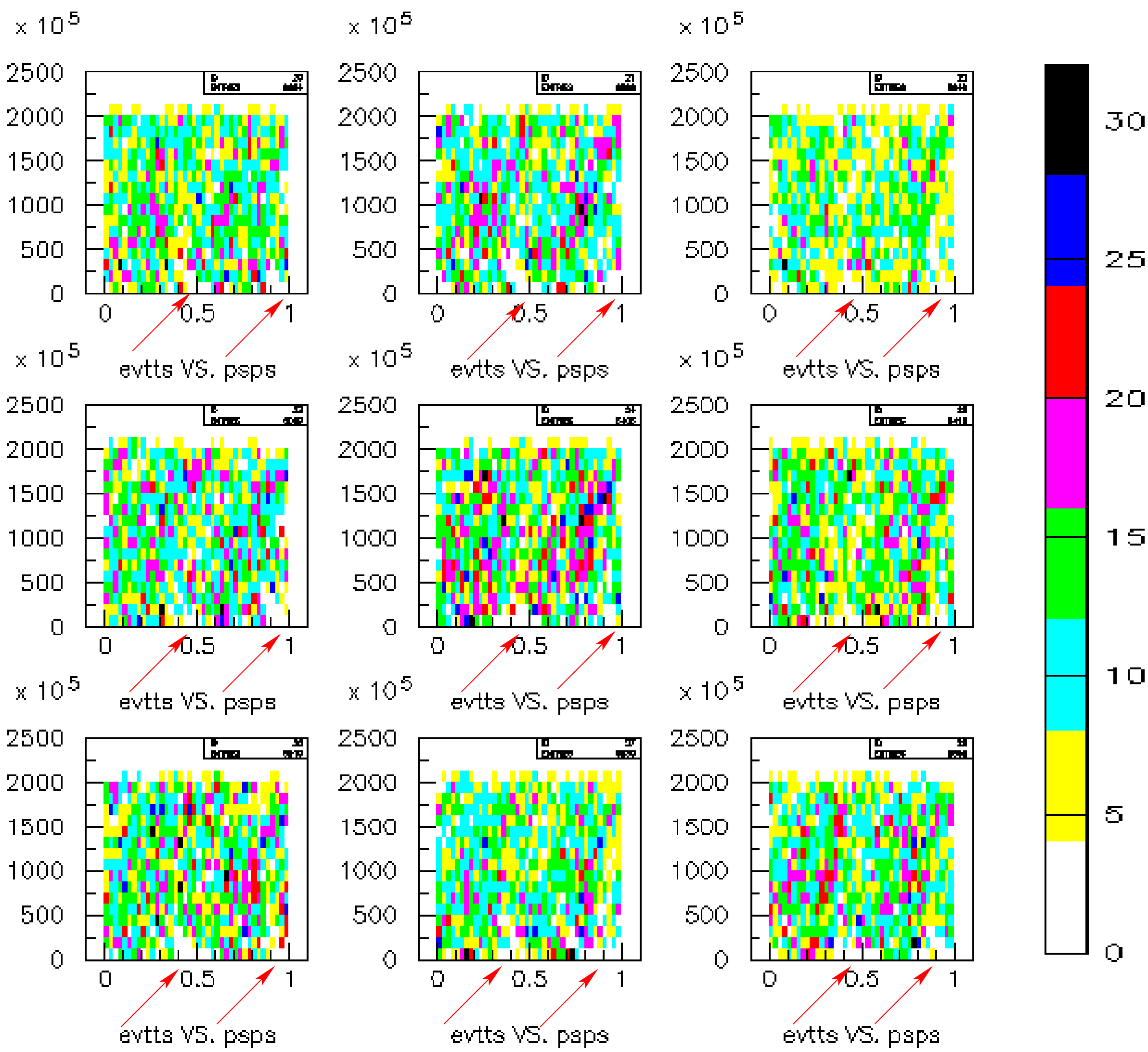

Figure 3.7: Event time vs SPS phase in nine consecutive single bursts

also visible, that was not clear in the average picture since the peaks position changes burst to burst. In order to check the monitor-phase matching we take the same nine bursts and look at the single burst monitor-SPS phase behavior: e.g. in Fig. (3.8) the Ferrara 200ns channels (green KS, red KL) are shown superimposed to the SPS phase.

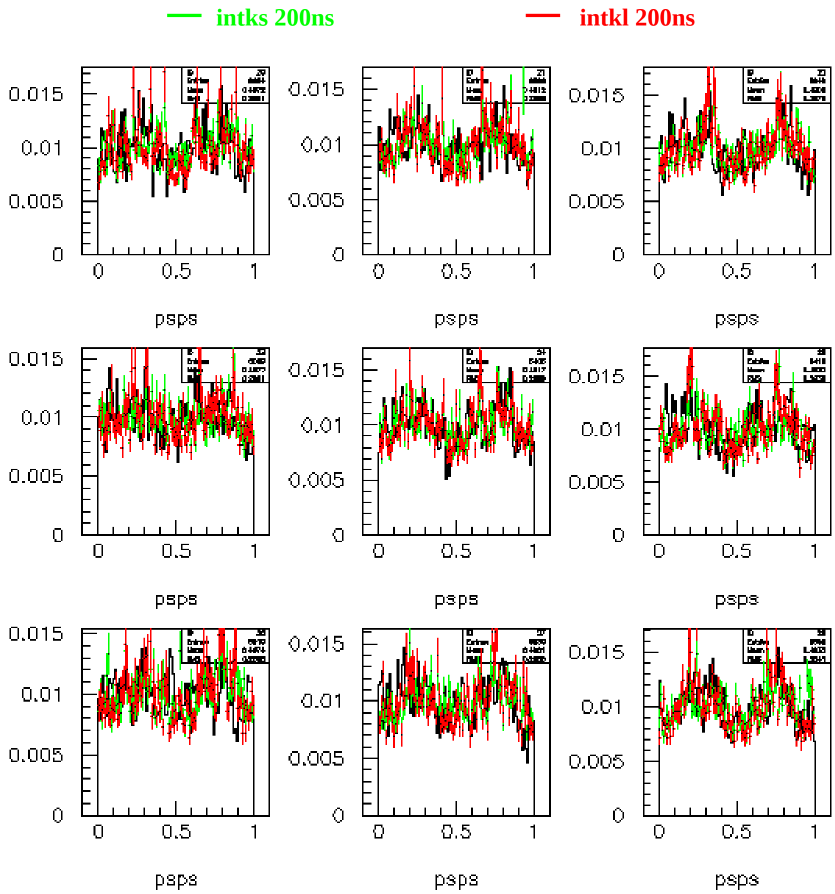

Figure 3.8: 200ns channels and SPS phase in nine consecutive single bursts

The same can be shown also for the other channels and the standard monitors, but obviously at higher time-scales the matching is less exact. In the same way we check the agreement between the beam monitors and the SPS Main phase. The average (100 bursts) matching between the Main phase and the beam monitor channels is shown for K_S (in Fig. (3.9)) and K_L (in Fig. (3.10)) four integration channels. The comparison with the SPS main phase for the standard monitors is shown in Fig. (3.11)

While looking at the single burst behavior Fig. (3.12) we take the same nine

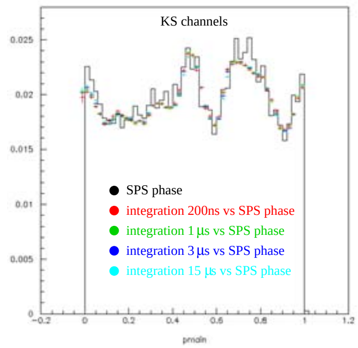

Figure 3.9: Ferrara KS channels and SPS main phase

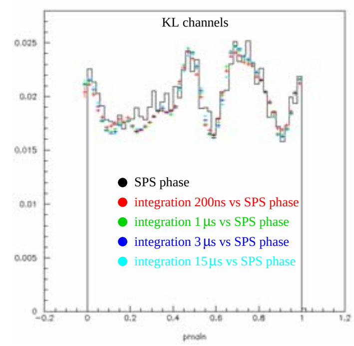

Figure 3.10: Ferrara KL channels and SPS main phase

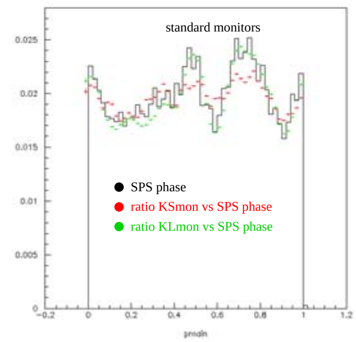

Figure 3.11: Standard monitor and SPS main phase

bursts shown in the SPS phase case and we superimposed at the SPS main phase the informations for the 200ns channels (K_S and K_L) only.

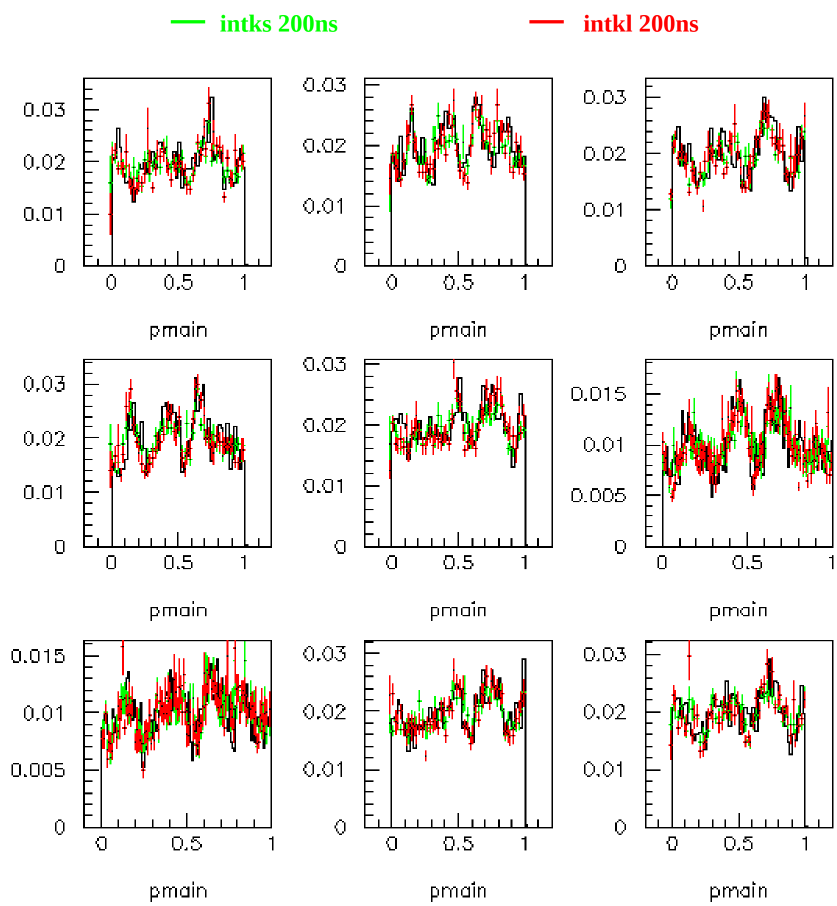

Figure 3.12: 200ns channels and SPS main phase in nine consecutive single bursts

3.2 Ferrara beam monitors: a special example

2001 run was a special for several reasons: drift chambers were repaired and re-installed, the end of LEP activities granted us a longer spill and lower proton momentum, and lower instantaneous beam intensity too. This was a very important chance to check the influence of beam related accidental activity on R. But it was also a unique opportunity to check the result stability in different experimental conditions. Of course beam monitors are strictly related to all of that, but now another subject was found pertaining to the Ferrara monitors.

Looking at the shapes of the four channels data during the burst an intensity as high as unexpected was seen in the very first part of the burst. It was clearly observable not only in the 200ns channels but also in the highest integration time, even if less shaped. The way the four channels looks like in a single burst can be seen in Fig. (3.13) for theK_L channels, analogous plots exist for the K_S channels.

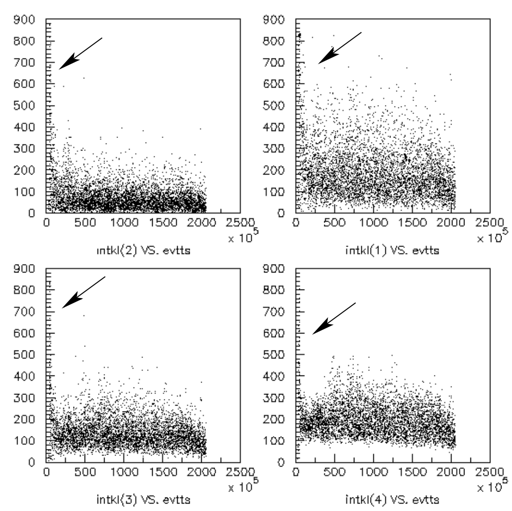

Figure 3.13: four KL channels along the burst time, single burst example The time in the burst is in timeslot of 25ns each

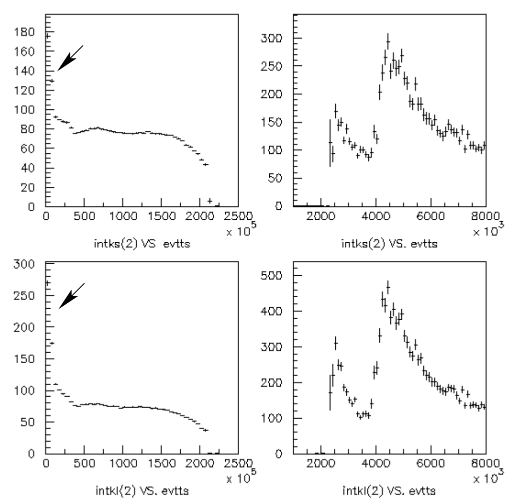

Figure 3.14: profile histograms of KL and KS 200ns channel versus time in burst. To the right the zoom of the very first part of the burst

The peak at the beginning of the burst is visible. This peak is not affecting few bursts but it is common to almost all the bursts as we can see from data taken on several bursts (100) as shown in Fig. (3.14). The entire burst (left side) and the zoom on the first part of the burst (right) are shown, for both KS and KL 200ns channels.

That high intensity peak was not a problem for the Ferrara monitors but it was for two fundamental detectors: the Tagger and AKS. The problem on AKS was discovered through the Ferrara monitors studies: as we have mentioned before the channels are read by a Pipeline Memory Board. This board is placed in a crate that is part of to two-crate decoding structure: the first crate houses our PMB, the standard monitor and SPS phase PMB and first part of the AKL's PMBs. The second crate of the structure houses the second part of AKL's PMBs and the AKS ones. Looking at our monitors variables surprisingly in roughly 10% of bursts there was a lack of informations in correspondence of the high intensity peak: this is shown by the green stars in Fig. (3.15). The rawdata decoding is structured in such a way that a problem on AKS's PMBs stops the bank filling also for the other PMBs variables. But forcing the decoding our values appear as shown by the red stars [41].

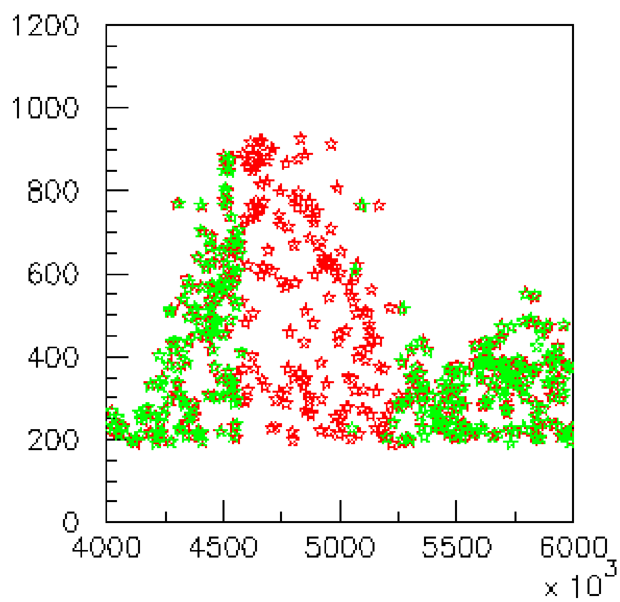

Figure 3.15: forced PMB rawdata decoding

Thus the monitor data are saved and informations are there but this was not the case for the AKS, that is a fundamental detector in the $Re(\epsilon'/\epsilon)$ measure. Looking directly at the events dump in raw data we discovered that part of the AKS words were missing together with the crate control word. Thanks to Davide Marras and his experience on PMBs the AKS problem was identified in the difficulty to send Xoffs to the Trigger Supervisor as frequently as required. Also the Tagger shew problems in the first part of the run related to the high intensity peak. Since $Re(\epsilon'/\epsilon)$ event selection cannot stand with problems in two fundamental detector (AKS and TAGGER) a cut was imposed: events in the first 200ms of the burst were excluded from the analysis.

Chapter 4

Formalism and methods to study accidental effects on $Re(\epsilon'/\epsilon)$ measurement

4.1 Extra activity

The NA48 experiment and its beam lines have been designed to minimize differences in both Long-Short and Charged-Neutral ratio, through the simultaneous data taking of the four decay modes and K_L events weighting [1] .

This imply a supposed zero correction to R due to extra activity, nevertheless this has to be checked with the best accuracy. Extra activity is related to the production of additional particles either *in time* or *out of time*: in the first case the additional particles can be produced at the target by the same protons producing the Kaons, while in the second case they come from the beam and are not correlated to Kaon decays therefore are also called accidentals.

In K_L decays the *in time* activity is suppressed by the beam collimation and shielding. In-time background from the K_S target may produce extra clusters in $K_S \to \pi^0\pi^0$ and cause a bias on R. This background has been studied in K_S only run to avoid accidental clusters coming from the $K_L \to 3\pi^0$ decays. The effect was found to be less than 1×10^{-4} [42].

The beam-induced, or *Out of time*, activity can be more dangerous since the pile-up of extra-particles may result in a good event loss in the reconstruction or selection [2] , also a bad event gain can happens but the probability is very low, compared to the loss.

[1] K_S and weighted K_L give almost the same illumination of the detector

[2] losses at trigger level are already taken into account in the trigger efficiency measurements

As already mentioned, due to the simultaneous four mode data taking the K_S and K_L events should be equally influenced by the accidental beam activity. Nevertheless residual asymmetries may result in a 'second order' correction to R. These potential asymmetry sources are the following:

- residual difference of the detector illumination by K_L and K_S beams. The two beams are by design almost but not perfectly collinear: a small angle is needed for K_S beam production and to allow the beams to intersect the LKr center. The distance between the two beam lines goes from 7.2 cm, at the K_S target, to zero at the LKr, this imply a small but non-zero separation in the spectrometer. An effect on R may arise if this small difference in detector illumination is not equal for charged and neutral events. The related correction to R is represented by the so called illumination or geometrical term: ΔR_{Geom}

- decorrelation of the two beams: differences in the four modes can show up if the instantaneous intensities of the two beams have variations that are not well correlated. The related correction to R is represented by the so called intensity term: ΔR_{Int}

Next sections are devoted to explain how we manage the study of the accidental activity and the correction to R related to it.

4.2 Accidental activity formalism

In order to study the accidental activity we look at the instantaneous intensity of the two beams. To study the time-varying intensity relations and effects we need a formalism to explicit the time dependent terms. This can be easily obtained since a time dependent function $f(t)$ can be written as:

$$f(t) = < f > (1 + \eta_f(t)) \tag{4.1}$$

Due to the $f(t)$ definition the following holds: the time varying term has zero average ($< \eta_f(t) >= 0$) and the relative variance is simply given by $\frac{\sigma_f^2}{<f>^2} = < \eta_f^2 >$;

as can be checked in the notation:

$$
\begin{aligned}
< f(t) > &\equiv \frac{1}{T}\int_T f(t)dt \\
\sigma_f^2 &= < (f - < f >)^2 > = \frac{1}{T}\int_T (f - < f >)^2 dt \\
&= \frac{1}{T} < f >^2 \int_T \eta_f^2 dt = < f >^2 < \eta_f^2 >
\end{aligned}
$$

Following the formalism developed by G.Unal and G.Collazuol [28, 24] the instantaneous beam intensity can be written, in the Eq. (4.1) notation, as:

$$I_k(t) = < I_k > (1 + \eta_k(t)) \quad k = L, S \tag{4.2}$$

where $I_k(t)$ represents the instantaneous rate for mode k decays at time t: $I_k(t) = \frac{dn_k}{dt}(t)$. Integrating over the beam time T we obtain the total number of observed events in mode k:

$$N_k^{(true)} = \int_T \frac{dn_k}{dt} dt = \int_T I_k(t)dt = T < I_k > \tag{4.3}$$

But the K_S and K_L selected events may be influenced by the accidental activity and a related probability to loose or gain events has to be taken into account. We use to refer to 'losses' meaning that the gains are already subtracted, while if we want to refer at losses and gains separately we will make it explicitly. The accidental losses are assumed to be dominated by the K_L beam, being its flux $10^4 - 10^5$ higher than the K_S one.

Now we state the fundamental hypothesis for our study: the linearity of losses with K_L beam intensity. This hypothesis has been finally confirmed on 2001 sample using the Ferrara beam monitors data, while standard monitors can only show an 'indication' of linearity. If the hypothesis hold, and it is, the losses probability due to accidental activity can be written as:

$$
\begin{aligned}
\Lambda_k^j &\times I_L(t) = \\
\Lambda_k^j &\times < I_L > (1 + \eta_L(t))
\end{aligned}
$$

where $k = L, S$ is the parent beam and $j = 00, +- = N, C$ the final state. Λ_k^j is the overall (gains already subtracted) probability of loosing an event.

The number of observed events is then changed, subtracting the number of lost events, in:

$$\frac{dn_k^j}{dt}(t)^{(obs)} = \frac{dn_k^j}{dt}(t)^{(true)} \times \left(1 - \Lambda_k^j I_L(t)\right) \propto I_k(t)(1 - \Lambda_k^j I_L(t)) \tag{4.4}$$

integrating the last over the beam time T (recalling that $< \eta >= 0$)

$$\int_T I_k(t)\left(1 - \Lambda_k^j I_L(t)\right)dt =< I_k > (1 - \Lambda_K^j < I_L >< 1 + \eta_k \eta_L >\big) \tag{4.5}$$

In terms of events free from losses due to accidental activity ($N_k^{j\ (true)}$), the observed number of events ($N_k^{j\ (obs)}$), can be expressed as:

$$N_k^{j\ (obs)} = N_k^{j\ (true)} \left(1 - \Lambda_k^j < I_L >< 1 + \eta_k \eta_L >\right) \tag{4.6}$$

Is worth notice that $< I_L >< 1 + \eta_k \eta_L >$ represents the average K_L beam intensity seen by $k = L, S$ mode decays, so we can define, for the generic k-mode:

$$\mathcal{I}_k = \frac{< I_k I_L >}{< I_k >} =< I_L >< 1 + \eta_k \eta_L > \tag{4.7}$$

The observed number of events in Eq. (4.6) can now be written in the equivalent and shorter way:

$$N_k^{j\ (obs)} = N_k^{j\ (true)} \left(1 - \Lambda_k^j \mathcal{I}_k\right) \tag{4.8}$$

We will make use of short or long notation, or both, depending on what we need to put in evidence. The observed double ratio can be written, in the short notation, as:

$$\begin{aligned} R^{(obs)} &= \frac{N_L^{00\ (true)}\left(1 - \Lambda_L^{00}\mathcal{I}_L\right)}{N_S^{00\ (true)}\left(1 - \Lambda_S^{00}\mathcal{I}_S\right)} \frac{N_S^{+-\ (true)}\left(1 - \Lambda_S^{+-}\mathcal{I}_S\right)}{N_L^{+-\ (true)}\left(1 - \Lambda_L^{+-}\mathcal{I}_L\right)} = \\ &= R^{(true)} \left[\frac{\left(1 - \Lambda_L^{00}\mathcal{I}_L\right)}{\left(1 - \Lambda_S^{00}\mathcal{I}_S\right)} \times \frac{\left(1 - \Lambda_S^{+-}\mathcal{I}_S\right)}{\left(1 - \Lambda_L^{+-}\mathcal{I}_L\right)}\right] \end{aligned} \tag{4.9}$$

While, defining the mean losses $\lambda_k^j = \Lambda_k^j < I_L >$, in the η's explicit from we obtain:

$$R^{(obs)} = R^{(true)} \left[\frac{1 - \lambda_L^{00} < 1 + \eta_L^2 >}{1 - \lambda_S^{00} < 1 + \eta_S \eta_L >} \times \frac{1 - \lambda_S^{+-} < 1 + \eta_S \eta_L >}{1 - \lambda_L^{+-} < 1 + \eta_L^2 >}\right] \tag{4.10}$$

where the true double ratio ($R^{(true)}$) and the accidental term (in square brackets) can be easily seen. Being $\Lambda_k^j \mathcal{I}_k < 1$ the denominator can be expanded to write the accidental term as:

$$
\begin{aligned}
[...] &= \left(1 - \Lambda_L^{00}\mathcal{I}_L\right)\left(1 - \Lambda_S^{+-}\mathcal{I}_S\right)\left(1 + \Lambda_S^{00}\mathcal{I}_S + \Lambda_L^{+-}\mathcal{I}_L + ...\right) \\
&= 1 + \mathcal{I}_S(\Lambda_S^{00} - \Lambda_S^{+-}) + \mathcal{I}_L(\Lambda_L^{+-} - \Lambda_L^{00}) + ... \qquad (4.11)
\end{aligned}
$$

while the explicit form is, at first order in λ and second order in η:

$$
\begin{aligned}
&\frac{1 - \lambda_L^{00} < 1 + \eta_L^2 >}{1 - \lambda_S^{00} < 1 + \eta_S\eta_L >} \times \frac{1 - \lambda_S^{+-} < 1 + \eta_S\eta_L >}{1 - \lambda_L^{+-} < 1 + \eta_L^2 >} = \\
&= 1 + (\lambda_S^{00} - \lambda_S^{+-}) < 1 + \eta_S\eta_L > + (\lambda_L^{+-} - \lambda_L^{00}) < 1 + \eta_L^2 > \\
&= 1 + \Delta
\end{aligned}
$$

The effect of accidental activity on R can thus be written as $R^{(obs)} = R^{(true)}[1 + \Delta]$ and the relative correction to R became $(R^{(true)} - R^{(obs)})/R^{(true)} = -\Delta = \Delta R$.

The different terms related to different sources of asymmetries are not yet disentangled, i.e. intensity variations, decorrelation between the beams and difference in the detector illumination. In order to do that we add and subtract $\lambda_S^{00,+-} < 1 + \eta_L^2 >$, moreover since $< 1 + \eta_S\eta_L > - < 1 + \eta_L^2 > = < \eta_L(\eta_S - \eta_L) >$ the effect on R can be written as:

$$
\Delta R = (\lambda_S^{00} - \lambda_S^{+-}) < \eta_L(\eta_L - \eta_S) > + \left[(\lambda_L^{00} - \lambda_s^{00}) - (\lambda_L^{+-} - \lambda_S^{+-})\right] < 1 + \eta_L^2 >
$$

Introducing the difference between Long and Short $\delta\lambda^j = (\lambda_L^j - \lambda_S^j)$ $(j = 00, +-)$ ΔR assumes the simplest form:

$$
\begin{aligned}
\Delta R &= (\lambda_S^{00} - \lambda_S^{+-}) < \eta_L(\eta_S - \eta_L) > + (\delta\lambda^{+-} - \delta\lambda^{00}) < 1 + \eta_L^2 > \qquad (4.12) \\
&= \Delta R_{Int} + \Delta R_{Geom}
\end{aligned}
$$

In the $\mathcal{I}_k$ view it reads:

$$
\Delta R_{Int} = (\Lambda_S^{00} - \Lambda_S^{+-})(\mathcal{I}_S - \mathcal{I}_L) \qquad (4.13)
$$

$$
\Delta R_{Geom} = (\delta\Lambda^{+-} - \delta\Lambda^{00})\mathcal{I}_L \quad ; \quad \delta\Lambda^j = (\Lambda_L^j - \Lambda_S^j) \qquad (4.14)
$$

It is now easy to see that different conditions must be satisfied to have non-zero correction to R:

- conditions on ΔR_{Int} :
  - $*$ difference in Charge and Neutral mean losses: $\lambda_S^{00} \neq \lambda_S^{+-}$
  - $*$ not-flat K_L beam intensity: $\eta_L(t) \neq 0$
  - $*$ decorrelation of the two beams: $\eta_L(t) \neq \eta_S(t)$
- conditions on ΔR_{Geom} :
  - $*$ different induced losses on K_L and K_S : $\delta\lambda \neq 0$
  - $*$ influence in induced losses not equal in charged and neutral events: $\delta\lambda^{00} \neq \delta\lambda^{+-}$

Back to Eq. (4.13) we can split the ΔR_{Int} correction in two parts:

$$\Delta R_{Int} = \Delta(C - N) \times \Delta(I)/I \tag{4.15}$$

where the $\Delta(C - N)$ accounts for difference between mean losses ($\lambda_k^j = \Lambda_k^j < I_L >$) in $\pi^0\pi^0$ and $\pi^+\pi^-$, and $\Delta(I)/I$ is the difference in the mean K_L beam intensity seen by K_L and K_S events ($\mathcal{I}_S - \mathcal{I}_L$). Due to the various way of measuring the corrections, as we will see in the next chapter, it is convenient to split ΔR_{Int} in these two different terms.

4.3 Accidental activity in detectors

Depending on their position on the beam lines there can be detectors whose activity is dominated by one of the two beam: i.e. the Tagger and K_S monitors are dominated by K_S beam while LKr, DCH, AKL and K_L monitors are dominated by K_L beam. Now let take a detector whose activity is dominated by beam m, the extra activity rate will be related to the beam m intensity

$m(t) \propto I_m(t) =< I_m > (1 + \eta_m(t))$. Defining $m_0 =< m >$, the extra-activity rate is given by:

$$m(t) = m_0(1 + \eta_m(t)) \tag{4.16}$$

If we consider now an un-biased sample of events in mode k, with probability $I_k(t)$ to have a K$\rightarrow\pi\pi$ decay in one of the four modes, the accidental rate in the detector is given by

$$p_k^m = \frac{< m(t) I_K(t) >}{< I_K >} = m_0 < 1 + \eta_m \eta_k > \tag{4.17}$$

Looking at the accidental activity of K_S and K_L events in the same detector we can investigate on the intensity correction:

$$\frac{p_S^m}{p_L^m} = \frac{1+ < \eta_m \eta_S >}{1+ < \eta_m \eta_L >} \approx 1+ < \eta_m(\eta_S - \eta_L) > \tag{4.18}$$

$$\frac{p_S^m - p_L^m}{p_L^m} = \frac{< \eta_m(\eta_S - \eta_L) >}{1+ < \eta_m \eta_L >} \tag{4.19}$$

$$\frac{p_S^m - p_L^m}{p_S^m} = \frac{< \eta_m(\eta_S - \eta_L) >}{1+ < \eta_m \eta_A >} \tag{4.20}$$

We can now measure from K_L and K_S beam indicators:

$$K_S \text{ indicator} \quad \rightarrow \quad \begin{aligned} \frac{p_S^S}{p_L^S} &\approx 1+ < \eta_S(\eta_S - \eta_L) > \\ \frac{p_S^S - p_L^S}{p_L^S} &= \frac{< \eta_S(\eta_S - \eta_L) >}{1+ < \eta_S \eta_L >} \\ \frac{p_S^S - p_L^S}{p_S^S} &= \frac{< \eta_S(\eta_S - \eta_L) >}{1+ < \eta_S^2 >} \end{aligned} \tag{4.21}$$

$$K_L \text{ indicator} \quad \rightarrow \quad \begin{aligned} \frac{p_S^L}{p_L^L} &\approx 1+ < \eta_L(\eta_S - \eta_L) > \\ \frac{p_S^L - p_L^L}{p_L^L} &= \frac{< \eta_L(\eta_S - \eta_L) >}{1+ < \eta_L \eta_L >} \\ \frac{p_S^L - p_L^L}{p_S^L} &= \frac{< \eta_L(\eta_S - \eta_L) >}{1+ < \eta_L \eta_S >} \end{aligned} \tag{4.22}$$

While if we have a sample of selected events in mode j suffering from accidental losses the resulting rate is:

$$\begin{aligned}
p_k^m(j) &= \frac{< m(t) I_K (1 - \Lambda_k^j I_L(t)) >}{< I_K (1 - \Lambda_k^j I_L(t)) >} = \qquad (4.23) \\
&= m_0 \frac{< (1+\eta_m)(1+\eta_k)[1 - \lambda_k^j (1+\eta_L)] >}{< (1+\eta_k)[1 - \lambda_k^j (1+\eta_L)] >} = \\
&= m_0 \frac{< (1+\eta_m)(1+\eta_k) > - \lambda_k^j < (1+\eta_L)(1+\eta_k)(1+\eta_m) >}{1 - \lambda_k^j < (1+\eta_L)(1+\eta_k) >} = \\
&= m_0 \frac{< (1+\eta_m)(1+\eta_k) > \left[1 - \lambda_k^j \frac{<(1+\eta_L)(1+\eta_k)(1+\eta_m)>}{<(1+\eta_m)(1+\eta_k)>}\right]}{1 - \lambda_k^j < (1+\eta_L)(1+\eta_k) >} = \\
&= p_k^m \frac{1 - \lambda_k^j \frac{<(1+\eta_L)(1+\eta_k)(1+\eta_m)>}{<1+\eta_m)(1+\eta_k>}}{1 - \lambda_k^j < (1+\eta_L)(1+\eta_k) >} \qquad (4.24)
\end{aligned}$$

as usual at first order in λ and second in η

$$\begin{aligned}
p_k^m(j) &\approx m_0 < (1+\eta_m)(1+\eta_k) > \times \\
&\quad \left[1 - \lambda_k^j \frac{< (1+\eta_L)(1+\eta_k)(1+\eta_m) >}{< (1+\eta_m)(1+\eta_k) >}\right] \times \\
&\quad \left[1 + \lambda_k^j < (1+\eta_L)(1+\eta_k) >\right] = \\
&= m_0 \left[< (1+\eta_m)(1+\eta_k) > - \lambda_k^j < (1+\eta_k)(1+\eta_L)(1+\eta_m) >\right] \times \\
&\quad \left[1 + \lambda_k^j < (1+\eta_L)(1+\eta_k) >\right] \\
&= m_0 < 1 + \eta_m \eta_k > - m_0 \lambda_k^j < (1+\eta_k)(1+\eta_L)(1+\eta_m) > \\
&\quad + m_0 \lambda_k^j < 1 + \eta_m \eta_k >< 1 + \eta_L \eta_k > \\
&= m_0 \left[1 + < \eta_m \eta_k > - \lambda_k^j < \eta_L \eta_m >\right] + \\
&\quad - m_0 \left[\lambda_k^j \left(< \eta_k \eta_L \eta_m > - < \eta_m \eta_k >< \eta_L \eta_k >\right)\right] \qquad (4.25) \\
&\approx m_0 \left[1 + < \eta_m \eta_k > - \lambda_k^j < \eta_L \eta_m >\right] \qquad (4.26)
\end{aligned}$$

In this equation accidental activity and event losses are related by intensity variation only, direct effect on event reconstruction and selection are not taken into account, this imply that to avoid bias on accidental activity measurements the indicators directly connected to the losses have to be excluded.

This is the case of extra-tracks or clusters in the drift chambers: the amount of activity observed around the event time is an estimation of the beam instantaneous intensity but in the DCHs the out of time tracks are related to the overflow presence, that cause losses and a bias in the measure. Detectors which are not used in trigger or reconstruction decisions and are not in the central detectors (e.g. Tagger) are un-bias estimator, but also central detectors (e.g. LKr) can well measure the extra activity in good events (e.g. out of time clusters in LKr), provided the sidebands are far enough from the event time to exclude direct connection to event losses and avoid correlations with event's induced activity.

In the past (on 1998-99 data) a big effort to measure the auto-correlation $< \eta_k^2 >$ and cross-correlation $< \eta_L \eta_S >$ terms has been done [24] through extra-activity measures in the sidebands closed to the event time. The auto-correlation terms were found to be $\approx 25\%$ with huge r.m.s. ($\approx 50\%$) on I_k, while the difference between auto-correlations and cross-correlation terms $< \eta_k^2 > - < \eta_L \eta_S >$ (k=L,S) were found to be very small (order of few per mill) pointing to a small intensity effect on R and r.m.s $\lesssim 10\%$ on I_S I_L.

In this contest we can look at the ratio between $p_k^m(j)$ and $p_{k'}^{m'}(j')$ where $m, m' = L, S$ is the dominant beam in a chosen detector, $k, k' = L, S$ and $j, j' = C, N$ refer to the decay mode. Therefore the general form is given by:

$$\frac{p_k^m(j)}{p_{k'}^{m'}(j)} = \frac{1+ < \eta_m \eta_k > -\lambda_k^j(\cdots)}{1+ < \eta_{m'} \eta_{k'} > -\lambda_{k'}^j(\cdots)} \tag{4.27}$$

If we study the extra activity in the same detector ($m = m'$), for the same k-decay mode (k, k') we can look at the charged-neutral ratio ($j = N, j' = C$) or difference:

$$\begin{aligned} \frac{p_k^m(N)}{p_k^m(C)} &= \frac{1+ < \eta_m \eta_k > -\lambda_k^N(\cdots)}{1+ < \eta_m \eta_k > -\lambda_k^C(\cdots)} && (4.28) \\ &\approx 1 + (\lambda_k^C - \lambda_k^N)(\cdots) && (4.29) \\ p_k^m(N) - p_k^m(C) &= m_0(\lambda_k^C - \lambda_k^N)(\cdots) && (4.30) \end{aligned}$$

Another possibility is to use the same detector ($m = m'$) the charged decays ($j, j' = C$) on different k mode ($k = S, k' = L$)

$$\frac{p_S^m(C)}{p_L^m(C)} = \frac{1+ < \eta_m \eta_S > -\lambda_S^C(\cdots)}{1+ < \eta_m \eta_L > -\lambda_L^C(\cdots)} \tag{4.31}$$

that ,neglecting the geometrical effect (thus $\lambda_S = \lambda_L$), can be written as:

$$\frac{p_S^m}{p_L^m} = \frac{1+<\eta_m\eta_S>}{1+<\eta_m\eta_L>} \tag{4.32}$$

$$\approx 1+<\eta_m(\eta_S-\eta_L)> \tag{4.33}$$

In the LKr (AKL,DCH ...) case the K_L is the dominant beam ($m = L$) therefore the last equation became $\frac{p_S^L}{p_L^L} \approx 1+<\eta_L(\eta_S-\eta_L)>$.

This is an indication of the methods we can use to derive informations and how to measure the correction to R due to accidental activity. In the past the information from extra activity in AKL, DCH, Lkr have been investigated, unfortunately the AKL turns out to be biased but was in any case useful to put an upper limit on the correction we want to measure.

4.4 Correlation measured with beam monitors

The informations from the beam counters, the K_S and K_L monitors, can be used computing the intensity as the difference of counting, divided by the time difference Δt_i, of two consecutive events. Defining N_k^i the counts collected in Δt_i, we can compute the auto-correlation and cross-correlation in each burst:

$$<\eta_k^2> = \frac{<I_k^2>}{<I_k>^2} = \frac{\sum_{i=1}^n (N_k^i)^2\Delta t_i}{(\sum_{i=1}^n N_k^i\Delta t_i)^2} \tag{4.34}$$

$$<\eta_S\eta_L> = \frac{<I_SI_L>}{<I_S><I_L>} = \frac{\sum_{i=1}^n N_S^iN_L^i\Delta t_i}{(\sum_{i=1}^n N_S^i\Delta t_i)(\sum_{i=1}^n N_L^i\Delta t_i)} \tag{4.35}$$

where n is the number of sampling in the burst, in the counters case this is the number of events in which the counters difference can be computed: the first event and the events where there is an overflow in the counter scale are excluded.

While in the Ferrara integrator channels the informations are directly given event by event as $I_k(t)$, and there is no need to compute the difference between consecutive events. From both counters and integrators we can have more complex information like the following:

$$\frac{< 1+\eta_S\eta_L >}{< 1+\eta_L^2 >} = \frac{< I_S I_L >}{< I_S >} \times \frac{< I_L^2 >}{< I_L >} = \frac{\mathcal{I}_S}{\mathcal{I}_L} = A \tag{4.36}$$

$$\frac{< \eta_L(\eta_S-\eta_L) >}{< 1+\eta_S\eta_L >} = \frac{\frac{<I_S I_L>}{<I_S>} - \frac{<I_L^2>}{<I_L>}}{\frac{<I_S I_L>}{<I_S>}} = \frac{\mathcal{I}_S - \mathcal{I}_L}{\mathcal{I}_S} = B = \frac{A-1}{A} \tag{4.37}$$

Where $\mathcal{I}_k$ represents the average K_L beam intensity seen by k-mode decays, as defined in Eq. (4.7). The two quantity A and B are obviously related between them and to the classical correlation

$$\begin{aligned} C &= \frac{< I_S I_L > - < I_S >< I_L >}{\sqrt{(< I_S^2 > - < I_S >^2)\,(< I_L^2 > - < I_L >^2)}} \\ &= \frac{< \eta_S\eta_L >}{\sqrt{< \eta_S^2 >< \eta_L^2 >}} \end{aligned} \tag{4.38}$$

As already mentioned the informations from integrator channels are in very shorter time scale than counters channels so their use to study both correlation (A,B,C type) and auto-correlation terms gives hints on shorter time scale structures and with higher precision.

4.5 Random Events

Special events to study accidental activity are collected through dedicated trigger, these events have to show the detector noise and accidental activity being, at the same time, decorrelated from $K_{\pi\pi}$ events: they have to be randomly triggered but proportionally to the beam intensity to represent the accidental activity in the detector as it is seen by $K_{\pi\pi}$ events. These special events are the random triggers, ~ 10 K_L and ~ 10 K_S randoms are collected per burst.

Due to the SPS extraction mode the same extraction position in the SPS ring is reached by protons with same conditions on SPS phase only every 3 SPS revolutions. This correspond to a delay time of 69.3 ns to apply at the trigger so that the intensity condition recorded are independent to $K_{\pi\pi}$ events but representing the same intensity conditions. The random triggers coming from K_S monitor (placed at K_S target) and K_L monitor (placed at the beam dump) are thus delayed by 3 SPS cycle and recorded in two different streams: K_S random and K_L random.

These special events can be used in two ways to measure the accidental activity effects: overlay method (see next section) and measuring the activity on different detectors registered in these events. Randoms don't suffer from losses so we can measure the activity as in Eq. (4.17) where now k=Random:

$$p_R^m = \frac{< m(t) I_R(t) >}{< I_R >} = m_0 < 1 + \eta_m \eta_R > \tag{4.39}$$

If random events represent properly the $K_{\pi\pi}$ intensity condition then $< \eta_R >=< \eta_k >$, therefore we can compare the detector response in k-mode and k-type randoms.

4.6 Data Overlay and Monte Carlo Overlay

Random events are used to produce new events of two kinds:

- Data overlay (DO): k-mode events are overlaid with k-type randoms
- Monte-Carlo overlay and double-overlay (OMC): Monte-Carlo generated events are overlaid (once and twice) with randoms events

In the Data Overlay case the noise in the detector is doubled since it is present both in random and real data, while in MC only the random event are noise-affected. A DOMC event is obtained by the overlay of an OMC event and a random, in this case we have doubled the noise too. So the OMC would be compared to the original data while the DOMC can be compared to DO.

In both cases the information from each detector are summed to produce the informations for the overlaid event. Overlay procedure accounts for accidental effects on reconstruction and selection, but does not account for in-time accidental effects (induced by $K_{\pi\pi}$ events), that are negligible, anyway. The original and overlaid events then pass through the analysis cuts and true losses (gains not subtracted) and gains are measured. We can now identify different classes with respect to the selection cuts:

- losses: bad overlay coming from good original
- gains: good overlay coming from bad original

- common good events: both the original and overlay are good events

Moreover

- common events = good originals + good overlay events
- good original events = common events + losses
- good overlay events = common events + gains

The overall loss probability is obtained looking at the number of true losses (gains not subtracted) minus gains normalized to the number of good originals:

$$P = \frac{n_{loss} - n_{gain}}{n_{goodorig}} \geq 0 \tag{4.40}$$

If weighted K_L are accounted for then the weights can be different for original (w_i) and overlaid events (w_i'), and the loss probability became:

$$P = \frac{\sum_i (w_i)_{loss} - \sum_i (w_i')_{gain} - \sum_i (w_i' - w_i)_{common}}{\sum_i (w_i)_{goodorig}} \tag{4.41}$$

In principle both Intensity and Geometrical effects can be measured overlaying K_S random with K_S event and K_L random with K_L event (Brute Force Overlay). But up to 1999 the delay on random events was not precise as expected: there was a bias, different for K_S and K_L randoms, in the delay. This, inducing a few % bias in the intensity difference seen by K_S and K_L randoms, invalidate the $\Delta(I)/I$ measure whose expected value is few % too. On the other side this is not a problem to study ΔR_{Geom} and the $\Delta(C-N)$ term in ΔR_{Int} , as a consequence different methods to study the corrections separately have been found in the past and used in 2001 run too.

In 2001 run the bias on delay has been adjusted rendering valid the procedure to evaluate the correction all in once but the limited number of randoms available induce a big statistical uncertainty. As a consequence of all considerations above to obtain a more precise evaluation all the methods developed in the past are used obtaining better results thanks to the new informations from integrator channels. Another way to improve the use of randoms in OMC is to use both type (K_S and K_L) for the overlay without care of k-mode of the original event, this is called mixed overlay and is useful to compute ΔR_{Geom} as will be explained in next chapter.

4.6.1 Data Overlay formalism

To investigate the data overlays we have to take into account:

- losses in original events $\rightarrow \Lambda_k^j I_L(t) = \lambda_k^j (1 + \eta_L(t))$
- losses in overlays $\rightarrow \overline{\Lambda}_k^j I_L(t') = \overline{\lambda}_k^j (1 + \eta_L(t'))$

As we have already seen the number of good original suffers from losses:

$$\begin{aligned}(N_{goodorig})_k^j &= c \int_T I_k(t)(1 - \Lambda_k^j I_L(t))dt \\ &= (N_{true})_k^j (1 - \lambda_k^j < 1 + \eta_L \eta_k >)\end{aligned}$$

but this is true also for the overlay events, where also the original losses have to be taken into account:

$$(N_{goodovly})_k^j = c \int_T I_k(t) \left(1 - \Lambda_k^j I_L(t)\right) \left(1 - \overline{\Lambda}_k^j I_L(t')\right) dt \qquad (4.42)$$

If, for every original event, a random event can be found such that $t' = t$ is satisfied then we can write:

$$\begin{aligned}(N_{goodovly})_k^j &= (N_{goodorig})_k^j \left(1 - \overline{\lambda}_k^j < 1 + \overline{\eta_L \eta_k} >\right) \qquad (4.43) \\ &= (N_{true})_k^j \left(1 - \lambda_k^j < 1 + \eta_L \eta_k >\right) \left(1 - \overline{\lambda}_k^j < 1 + \overline{\eta_L \eta_k} >\right) \\ &= (N_{true})_k^j \left[1 - \lambda_k^j < 1 + \eta_L \eta_k > - \overline{\lambda}_k^j < 1 + \overline{\eta_L \eta_k} >\right] \\ &\quad + (N_{true})_k^j \left[\lambda_k^j \overline{\lambda}_k^j < 1 + \eta_L \eta_k >< 1 + \overline{\eta_L \eta_k} >\right] \\ \frac{(N_{goodovly})_k^j - (N_{goodorig})_k^j}{(N_{goodorig})_k^j} &= -\overline{\lambda}_k^j < 1 + \overline{\eta_L \eta_k} > \\ \frac{(N_{goodovly})_k^j - (N_{true})_k^j}{(N_{true})_k^j} &= -\lambda_k^j < 1 + \eta_L \eta_k > - \overline{\lambda}_k^j < 1 + \overline{\eta_L \eta_k} > + ...\end{aligned}$$

Comparing the double ratio obtained from good overlay modes and good original we can estimate the accidental activity corrections:

$$R^{(goodovly)} = R^{(goodorig)} \frac{1 - \overline{\lambda}_L^{00} < 1 + \overline{\eta_L^2} >}{1 - \overline{\lambda}_S^{00} < 1 + \overline{\eta_L \eta_S} >} \times \frac{1 - \overline{\lambda}_S^{+-} < 1 + \overline{\eta_L \eta_S} >}{1 - \overline{\lambda}_L^{+-} < 1 + \overline{\eta_L^2} >} \tag{4.44}$$

Moreover if the $\overline{\lambda}_k^j < 1 + \overline{\eta_L \eta_k} >$ term is a good estimator for $\lambda_k^j < 1 + \eta_L \eta_k >$ we know also the double correction:

$$R^{(goodovly)} = R^{(true)} \frac{1 - 2\lambda_L^{00} < 1 + \eta_L^2 >}{1 - 2\lambda_S^{00} < 1 + \eta_L \eta_S >} \times \frac{1 - 2\lambda_S^{+-} < 1 + \eta_L \eta_S >}{1 - 2\lambda_L^{+-} < 1 + \eta_L^2 >} \tag{4.45}$$

To found these relations we have used $t' = t$ and $\overline{\lambda}_k^j < 1 + \overline{\eta_L \eta_k} >= \lambda_k^j < 1 + \eta_L \eta_k >$, and this holds if the overlay procedure

1) overlap each original events with a random event with equal trigger time within the burst

2) use randoms providing an accidental activity 'picture' as closed as possible to $K_{\pi\pi}$ events 'picture'

3) not be biased by non linearity of losses with beam intensity.

However these requirements are not completely fulfilled: in the first case the random chosen is the closest in time to the original event, but a small difference in time remains so that $t' - t \neq 0$. This results in a small difference between $< \overline{\eta_L \eta_k} >$ and $< \eta_L \eta_k >$. The overlay, doubling the noise, introduces non-linearities in the losses. The way to escape from these problems has been found in Monte-Carlo Overlay method.

4.6.2 Monte Carlo Overlay formalism

In this procedure Monte-Carlo events are generated and then overlaid with random events collected during the run. The generated events are free from noise and accidental activity that are only related to randoms. The overlay event resulting from the superposition of MC event and random event is thus not affected by double noise. Double overlay is the same procedure as OMC but applied to overlay MC instead of original MC. DOMC events have double noise (coming from the 2 randoms) like data-overlay so if everything is well simulated the difference between the double and single overlay should be the same as data overlay. DOMC were first introduced to check possible non linear effect due to the overflow cut.

Once more the formalism is the same, where the original events are free from losses and acts like the true events in the previous picture.

$$\begin{aligned}
N_{goodorig} &= N_{goodMC} \\
(N_{goodovly})^j_k &= (N_{goodorig})^j_k \left[1 - \overline{\lambda}^j_k < 1 + \eta_L \eta_R >\right] \\
(N_{gooddblovly})^j_k &= (N_{goodovly})^j_k \left(1 - \overline{\lambda}^j_k < 1 + \eta_L \eta_R >\right) \\
(N_{gooddblovly})^j_k &= (N_{goodorig})^j_k \left(1 - 2\overline{\lambda}^j_k < 1 + \eta_L \eta_R > + ...\right)
\end{aligned}$$

From the double ratio of these numbers we can compute the overall corrections ΔR if random events can satisfy two conditions needed to represents exactly the same intensity seen by $K_{\pi\pi}$ events: $< \eta_L \eta_{Rk} >=< \eta_L \eta_k >$ and $< I_{Rk} >=< I_k >$. Even if this is not perfectly true, as in the past due to the bias on random delay, we can exclude from the useful computation the $\Delta(I)/I$ part and compute $\Delta(C-N)$ and ΔR_{Geom} .

If k-mode decays are overlaid with their k-mode random (Brute Force overlay) and $< \eta_L \eta_{Rk} >=< \eta_L \eta_k >$we can write:

$$R_{goodovly} = R_{goodorig} \left[\frac{1 - \overline{\lambda}^{00}_L < 1 + \eta_L \eta_L >}{1 - \overline{\lambda}^{00}_S < 1 + \eta_L \eta_S >} \times \frac{1 - \overline{\lambda}^{+-}_S < 1 + \eta_L \eta_S >}{1 - \overline{\lambda}^{+-}_L < 1 + \eta_L \eta_L >} \right] \tag{4.46}$$

while in the mixing random procedure, in which we do not care of the random's k-mode, we can have

$$\begin{aligned}
R_{goodovly} = R_{goodorig} \quad &\times \quad \frac{1 - \overline{\lambda}^{00}_L (< 1 + \eta_L \eta_L > \text{ or } < 1 + \eta_L \eta_S >)}{1 - \overline{\lambda}^{00}_S (< 1 + \eta_L \eta_S > \text{ or } < 1 + \eta_L \eta_L >)} \\
&\times \quad \frac{1 - \overline{\lambda}^{+-}_S (< 1 + \eta_L \eta_S > \text{ or } < 1 + \eta_L \eta_L >)}{1 - \overline{\lambda}^{+-}_L (< 1 + \eta_L \eta_L > \text{ or } < 1 + \eta_L \eta_S >)}
\end{aligned}$$

as a consequence in this case we can not measure the overall ΔR as in the BF case, but we can ignore the k-type random and focus on the difference in charged and neutral losses between Long and Short, $(\delta\lambda^{+-} - \delta\lambda^{00}) =< I_L > (\delta\Lambda^{+-} - \delta\Lambda^{00})$, that means measure ΔR_{Geom} .

4.6.2.1 OMC and DOMC sequences

[43]The MC basic package to generate events is NASIM, developed for the detailed simulation of NA48 setup. For each random event four MC events, corresponding to the four decays modes, are simulated and overlaid with the random event. Two randoms events are needed to start the DOMC sequence. Due to the finite number of randoms collected the number of sequences is finite too: 80% are OMC and 20% DOMC sequences.

An OMC sequence contains 17 events:

- random event, used for all the overlays in the sequence
- for each one of the four modes (K_S^{+-}, K_S^{00}, K_L^{+-}, K_L^{00})

  * MC original 1

  * overlay random-MC original 1

  * MC original 2 (same mode as original 1)

  * overlay random-MC original 2

  Two events are generate for the same random to use the random in a more effective way, one of the two couple original-overlay can be rejected passing trough the analysis cuts.

A DOMC sequence contains 26 events:

- random event 1
- random event 2
- for each one of the four modes (K_S^{+-}, K_S^{00}, K_L^{+-}, K_L^{00})

  * MC original 1

  * overlay random 1 - MC original 1

  * overlay random 2 - Overlay 1

  * MC original 2 (same mode as original 1)

* overlay random 1 - MC original 2

* overlay random 2 - Overlay 2

Chapter 5

Accidental effects corrections on $Re(\epsilon'/\epsilon)$ measurement

5.1 Introduction to the measurements

The correction to R (ΔR) due to possible asymmetries induced by accidental activity has been introduced in the previous chapter, along with the formalism to show explicitly its Intensity and Geometrical terms. Now we are going to see the methods developed to measure them, and their results. We have also to verify the linearity dependence of losses on K_L beam intensity (losses probability $= \Lambda_k^j I_L(t)$), that is the fundamental hypothesis we have used to derive the ΔR as:

$$
\begin{aligned}
\Delta R &= \Delta R_{Int} + \Delta R_{Geom} \\
\Delta R_{Int} &= (\lambda_S^{00} - \lambda_S^{+-}) < \eta_L(\eta_S - \eta_L) > \\
&= (\Lambda_S^{00} - \Lambda_S^{+-})(\mathcal{I}_S - \mathcal{I}_L) \\
&= (\Lambda_S^{+-} - \Lambda_S^{00})(\mathcal{I}_L - \mathcal{I}_S) \\
&= \Delta(C-N) \times \Delta(I)/I \\
\Delta R_{Geom} &= (\delta\lambda^{+-} - \delta\lambda^{00}) < 1 + \eta_L^2 > \quad ; \quad \delta\lambda^j = (\lambda_L^j - \lambda_S^j) \\
&= (\delta\Lambda^{+-} - \delta\Lambda^{00})\mathcal{I}_L \quad ; \quad \delta\Lambda^j = (\Lambda_L^j - \Lambda_S^j)
\end{aligned}
$$

where $\mathcal{I}_k$ is the average K_L beam intensity seen by k-mode (L,S) decays, $\mathcal{I}_k = \frac{<I_k><I_L>}{<I_k>} =< I_L >< 1 + \eta_k\eta_L >$.

By means of Overlay Monte Carlo techniques we could measure the accidental activity induced correction $\Delta R = \Delta R_{Int} + \Delta R_{Geom}$ all in once, if the random triggers satisfy all the requirements needed to represent the activity seen by $K_{\pi\pi}$ events.

However randoms were not perfectly triggered up to 1999 run, with different biases on K_L and K_S random delay, introducing a few % effect on the average intensity seen by random events. As a consequence the $\Delta(I)/I$, being of the same order of few % was estimated in different ways. OMC, and other methods, were used to evaluate the $\Delta(C-N)$ term and the ΔR_{Geom} correction. As it was in the past the different contributions to ΔR are estimated separately also in 2001 data, and with different methods to verify our results. In addiction in 2001 data the overlay technique has been used to compute the overall correction, but it is used as a cross-check being dominated by the statistical error of the overlay procedure (§ 5.4). The different measurements are divided as follow:

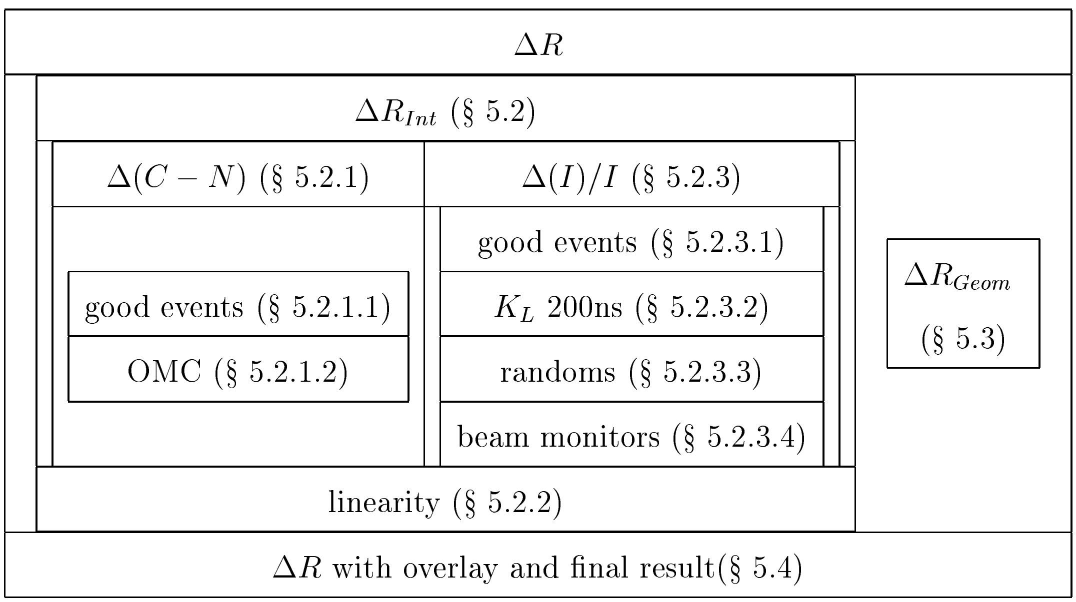

5.2 ΔR_{Int} measurements

We are going to see the different methods developed in the past and in the 2001 run to evaluate this correction in its $\Delta(C-N)$ and $\Delta(I)/I$ terms. The final result, taking into account all the following methods, is $\Delta R_{Int} = (0 \pm 1.1) \times 10^{-4}$ [3]. It was $(0 \pm 3) \times 10^{-4}$ in 1998-98.

5.2.1 $\Delta(C-N)$ or $\Delta\lambda$ measurements

The $\Delta(C-N)$ is also called $\Delta\lambda$ being the difference of neutral and charged mean losses. Several methods are involved to measure this term and the final results from them is $\Delta(C-N) = (1.0 \pm 0.5)\%$. [3] This value is 30% lower than 1998-99 value ($(1.4 \pm 0.7)\%$) thanks to the lower average beam intensities in 2001, allowed by the longer spill length.

5.2.1.1 $\Delta(C-N)$ from good events

We can compare the ratio of charged and neutral K_S events in ($K_S + K_L$) to pure K_S beam. In the K_S only case the accidentals are one order of magnitude smaller than $K_S + K_L$, because the K_L beam is absent, therefore following the previous chapter's formalism we can measure:

$$\begin{aligned}
(C/N)_{K_S} &= N_S^C/N_S^N \\
(C/N)_{K_S+K_L} &= (C/N)_{K_S}\frac{1-\lambda_S^C < 1+\eta_L\eta_S >}{1-\lambda_S^N < 1+\eta_L\eta_S >} \\
\frac{(C/N)_{K_S+K_L}}{(C/N)_{K_S}} &\approx 1-(\lambda_S^C-\lambda_S^N) < 1+\eta_L\eta_S >
\end{aligned}$$

From that measure $\Delta(C-N)$ is also called $\Delta(C/N)$ and the resulting value is found to be $\Delta(C-N) = (0.9 \pm 0.6)\%$ [45]. Evaluating then the $\Delta(I)/I$ as $\frac{<\eta_L(\eta_L-\eta_S)>}{<1+\eta_L\eta_S>} = (\mathcal{I}_L - \mathcal{I}_S)/\mathcal{I}_S$ we can obtain the full ΔR_{Int} correction.

5.2.1.2 $\Delta(C-N)$ with overlay method

We can estimate separately the Losses (not gains subtracted) and Gains on charged and neutral events in Overlaid Monte Carlo events checking the results with Double Overlay Monte Carlo and Data Overlay. To evaluate the charged-neutral difference we refer to losses meaning Losses-Gains. The difference between charged and neutral losses (Losses-Gains) [1] is found to be, after noise (correlated with 50Hz phase) subtraction in LKr, 0.65% in OMC, 0.7% in DOMC and 1% in Data Overlay [46, 47, 48, 49]. In 98+99 sample the difference in (C-N) losses was 1% in OMC, 1.1 % in DOMC and 1.4% in DO, where the lower percentage of losses in 2001 is due to the lower intensity.

[1] we consider here that there is no difference between K_L and K_S losses in the same mode (charged or neutral) being this involved in the lower order geometrical correction

The major discrepancy between DOMC and DO is on the charged losses due to the overflow cut, in which the DOMC losses are $\approx 30\%$ lower than DO. Is useful to recall what this overflow condition is, because it is also the main cause of losses in charged events and of the difference with neutral losses. The overflow cut has to be set due to the imposed limit on drift chambers' readout. The overflow condition is set, in a plane, if there are more than 7 hits in 100ns to be readout. If this happens the hits for that plane are not recorded, instead of the hits' words only the overflow word is sent out and the readout memory in that plane is reseted. Hits from neighbor events can be deleted too by the memory reset, as a consequence to avoid bias on R measure a tight cut is applied in the analysis: the event is flagged in overflow, and rejected in the selection phase, if at least one plane, in the first or second or fourth chamber, is found in overflow condition in a [-312.5,312.5]ns time window around the event time. In charged events the overflows are enhanced by the good $\pi^+\pi^-$ two hits per plane. The main difference between data and DOMC is in DCH4 where the MC lacks in reproducing the true overflow distribution. It has been checked by D.Madigojine [43] that the overlay procedure is correct and the remaining suspect is on NASIM simulation at hits level.

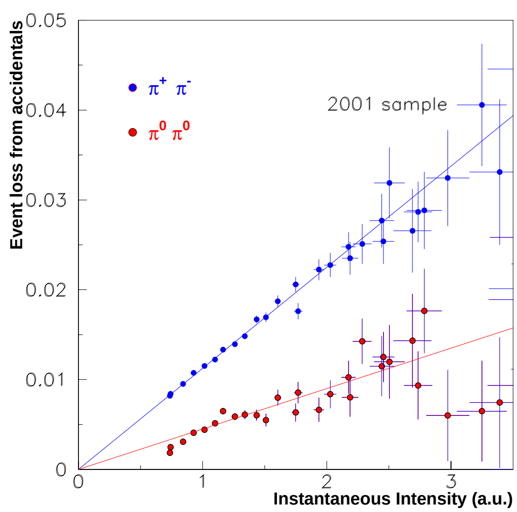

Figure 5.1: linearity of losses with K_L beam intensity, 200ns K_L integrator

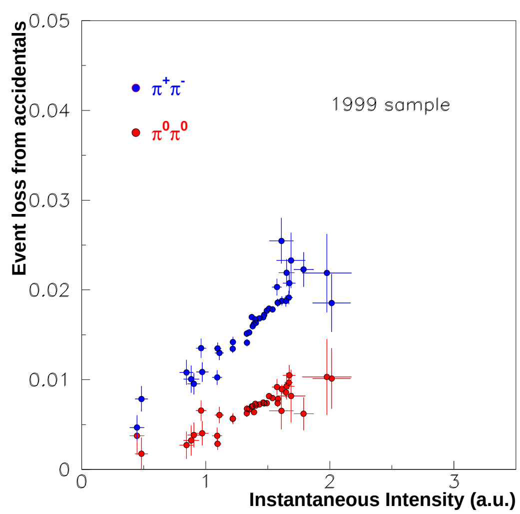

Figure 5.2: linearity of losses with K_L beam intensity 1999 sample, K_L counter

The losses in 2001 sample are shown in Fig. (5.1) in which there is also a clear evidence of linearity of losses with K_L beam intensity. The OMC variables, cut and losses will be exhaustively treated in the ΔR_{Geom} section.

5.2.2 Linearity of losses with K_L beam

Looking at the overlay losses as a function of the K_L beam monitors the linearity of losses with K_L beam intensity can be verified. Before the K_L Ferrara monitor installation (in 2001) the referring monitor was the K_L counter at the beam dump. With the new Ferrara monitor data the linearity has been not only verified in a more precise way but also on a bigger range as shown in Fig. (5.1) and Fig. (5.2) were the charged and neutral losses in OMC are shown. The K_L beam intensity are in arbitrary units obtained rescaling the beam monitor data to the Lkr extra-cluster probability.

5.2.3 $\Delta(I)/I$ measurements

Different methods are involved to measure $\Delta(I)/I$, resulting in a final estimation in agreement to a zero value within 1%. [3]

5.2.3.1 $\Delta(I)/I$ with good events

$\Delta(I)/I$ can be measured in good events using as estimator of the intensity the probability to have one extra cluster (out of time) in Lkr. It can be done also with extra-tracks but taking care of the bias introduced by the overflows in DCHs. The K_L beam in the dominant one therefore the extra-activity in good K_S and K_L events is a measure of the K_L beam intensity seen by these events. That means we are measuring $\mathcal{I}_S$ and $\mathcal{I}_L$. The few centimeters separation between K_S and K_L beams at the K_S target allow the charged decays to be easily identified, as K_S and K_L , through the vertex position. The few centimeters separation between K_S and K_L beam at the K_S target and the path throughout the spectrometer Therefore ks and K_L $\pi^+\pi^-$

selected by the vertex are used, avoiding correlation between mis-tagging probability and beam intensity. Long range variations in K_L / K_S ratio are excluded wighting the K_S to equalize the K_L / K_S ratio. [44]

The good events suffer from losses so that are not a perfect unbiased sample but at first order in the ratio this method gives a good estimation of accidental activity difference between K_L and K_S . We are applying to Lkr (m=L) we have seen in Eq. (4.31) and Eq. (4.33).

Comparing the rate of extra-cluster in Lkr in good K_S and K_L events selected by vertex, the $\Delta(I)/I$ is found to be less than 1% ($(+0.4 \pm 0.4_{stat})$% [44]), after K_S weighting. Without K_S weighting the value is higher ($\approx 1.2\%$) as a consequence of the higher K_S / K_L ratio at the beginning of the burst. [1] This is shown in Fig. (5.3) while in Fig. (5.4) the accidental activity probability seen by Lkr is compared between 1999 (red) and 2001 (blue). In this last is clearly shown the difference in burst structure and time.

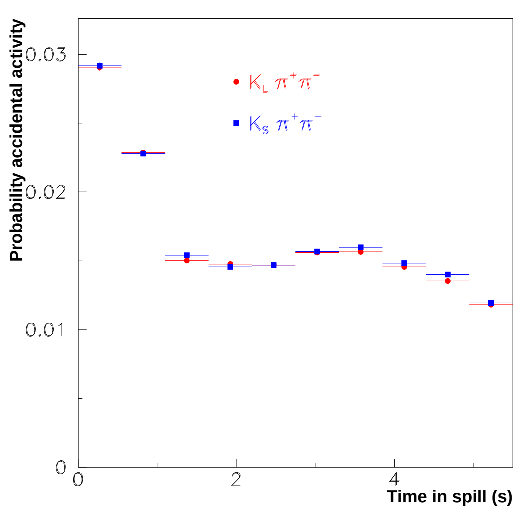

Figure 5.3: accidental activity probability in Lkr: K_L and $K_S \rightarrow \pi^+\pi^-$ versus time in the burst

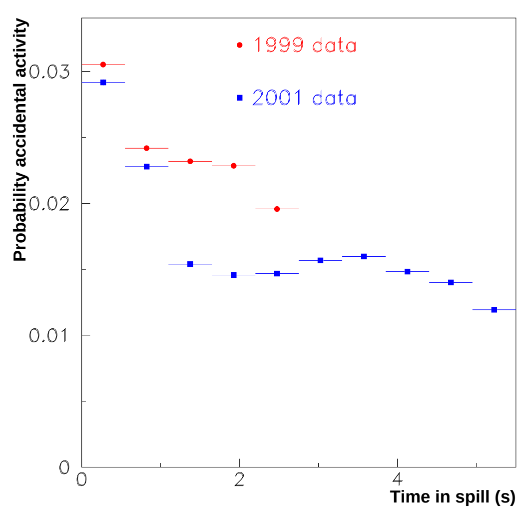

Figure 5.4: accidental activity probability in Lkr in 1999 and 2001 sample, K_L and $K_S \rightarrow \pi^+\pi^-$ versus time in the burst

[1] Analogous result is obtained looking at the extra-tracks in DCHs. [44]

5.2.3.2 $\Delta(I)/I$ with K_L 200ns integrator in good events

The beam intensity from the 200ns K_L integrator channel recorded for each event are used to evaluate the difference in average K_L intensity seen by good K_S and K_L events. As in the previous method charged events selected by the vertex are used to measure:

$$\frac{K_S}{K_L} - 1 = \frac{\mathcal{I}_S}{\mathcal{I}_L} - 1 = \frac{< 1 + \eta_S \eta_L >}{< 1 + \eta_L^2 >} - 1 \approx < \eta_L(\eta_S - \eta_L) >$$

The resulting value, after the K_S weighting to equalize K_L /K_S ratio, is again found to be less than 1% ($(-0.08 \pm 0.04_{stat})\%$) [44]. The 200ns K_L integrator channel for K_S and K_L to $\pi^+\pi^-$ (vertex selected) events is shown in Fig. (5.5) and Fig. (5.6) respectively.

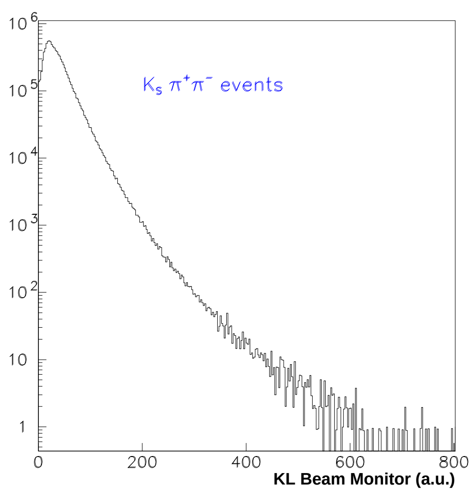

Figure 5.5: 200ns K_L integrator in $K_S \to \pi^+\pi^-$ vertex selected

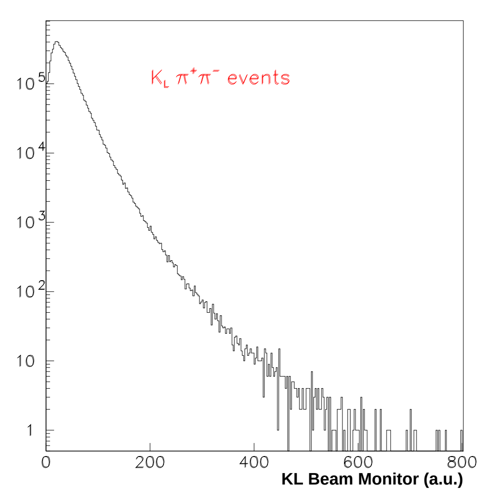

Figure 5.6: 200ns K_L integrator in $K_L \to \pi^+\pi^-$ vertex selected

5.2.3.3 $\Delta(I)/I$ with K_S and K_L randoms

The ratio $(\mathcal{I}_L - \mathcal{I}_S)/\mathcal{I}_S$ has been measured (by G.Unal) on random events too. A small bias was found in K_L random trigger giving a decrease of the number of K_L random during the burst. After K_L random re-weight the $< \eta_L(\eta_{rndmL} - \eta_{rndmS}) > / < 1 + \eta_L \eta_{rndmS} >$ from Lkr cluster and DCH tracks has been found to be, again, less than 1% [45].

Moreover looking at LKr clusters in random events ($L_0 < 1 + \eta_L \eta_R >$) we can have an estimation of the agreement with K_L beam integrator channels and their capacity to see instantaneous intensity. The 200ns channel turns out to be the best correlated to Lkr activity, as it should be.

5.2.3.4 $\Delta(I)/I$ with beam monitors

Decorrelation of the beams is measured by means of beam monitors, counters and integrators.

To investigate beam structures at small time scale we can look at

- beam counters through the difference in counts between two consecutive events: we can investigate down to ms scale
- beam integrators at 15μs, 3μs, 1μs, 200 ns.
- Lkr cluster in random events (down to $\approx$ 100ns readout window). This has shown in 1999 data that structures at time scale smaller than 2 μs were involved, especially at the beginning of the burst. This was one of the reasons to have smaller integration times and new devices in 2001 run.

We can compute the variables A and B defined in Eq. (4.37) to compute $\Delta(I)/I$ and other informations like auto-correlation ($< \eta_k^2 >$, k=L,S) and cross-correlation ($< \eta_L \eta_S >$). In order to do that both K_S and K_L have been reweighted since during the run the intensity of their response decreased, because of growing of pedestal values. Another kind of special triggers has been used, the Lydia Pulser ($\sim$ 37/burst) that are taken uniformly in time. All the four channels are used to evaluate, burst by burst, the $\Delta(I)/I$ and the other terms like cross and auto-correlation but to avoid statistical fluctuation in the rate measurements the 15μs result is taken. The $(\mathcal{I}_L - \mathcal{I}_S)/\mathcal{I}_S$ is found to be $\approx$ -1% with same order of uncertainty.

Looking at the single term of auto and cross correlation, burst by burst, their values can not be disentangled by the statistical component. This means that the autocorrelation value changes according with its uncertainty: from $\approx$ 40% in the 200ns channel to $\approx$ 15% in the 15μs channel, being compatible with zero within their uncertainty.

5.3 ΔR_{Geom} measurements

The illumination difference effect can be estimated using OMC computing Losses and Gains for K_S and K_L events. Mixed K_L and K_S randoms are used to produce the overlay events. This, respect to the Brute Force method (used in DO), improves the statistics of randoms since we can overlay all of them without take care if are Long or Short random (§ 4.6.2). We do not introduce bias on ΔR_{Geom} measure, being the correction sensitive only to the average intensity times the difference in illumination of K_L and K_S events ($\Delta R_{Geom} \approx < I_L > (\delta\Lambda^{+-} - \delta\Lambda^{00})$)

Random events presenting overflows, killing also the following overlay events, are of course excluded from the analysis. Original, overlay and double overlay are good events if they satisfy the $Re(\epsilon'/\epsilon)$ cuts:

- general cuts

  * event time in the burst > 200ms, to avoid the very high intensity peak at the beginning of burst
  * $c\tau/c\tau_S$ less than 3.5
  * $c\tau/c\tau_S > 0$ for K_L events, $c\tau = 0$ is the AKS position
  * no overflow in any plane of DCH1 or DCH2 or DCH4 within [-312.5,+312.5]ns around the event time
  * total energy between 70GeV and 170GeV

  The proper time τ is related to the vertex and AKS position by $\tau = \frac{(z_{vtx} - z_{AKS})m_k}{p_k}$

- neutral cuts

  * Z cut ($Z_{vertex} = z_{Lkr} - d_{vertex}$): the origin of K_L fiducial region is at the iridium crystal (607.2 cm, AKS region). The distance between decay vertex

and Lkr is computed assuming that the four photons invariant mass is the Kaon mass (m_K)

$$d_{vertex} = \sqrt{\sum_{i}^{4}\sum_{j>i}^{4} E_i E_j[(x_i - x_j)^2 + (y_i - y_j)^2]/m_K} \qquad (5.1)$$

It is used to determine the proper time of the decay

* photon (shower in Lkr) candidate energies between 3GeV and 100GeV

* fiducial cuts to ensure well measured energies of the photon candidates:

  - photons candidates in the Lkr acceptance region

  - distance from the center of beam tube $> 15cm$

  - distance from Lkr edges $> 11cm$

  - photon candidate distance to closest dead cell in Lkr$> 2cm$

* distance between any two photon candidates $> 10cm$

* absolute time difference between photon candidate and 4 photons average time $< 5ns$

* Center Of Gravity (COG) of 4 photons candidate $< 10cm$

* no extra-cluster (more than 4) with Energy$> 1.5GeV$ within $\pm 3ns$ (to reduce $3\pi^0$ background)

* $R_{ellipse}$ < 1.5 (to choose the best pairing of 4 photons in $2\pi^0$, reduce $3\pi^0$ background) This is a χ^2-like variable on the two couples of photons to form the two π^0 mass, it is defined as:

$$R_{ellipse} \quad = \left[\frac{(m_1 + m_2)/2 - m_{\pi^0}}{\sigma_{m_1+m_2}}]^2 + [\frac{(m_1 - m_2)/2}{\sigma_{m_1-m_2}}\right]^2 \qquad (5.2)$$

It is well represented by the ellipses in Fig. (5.7) where the two reconstructed $m_{\gamma\gamma}$ masses (m_1 and m_2) are shown. Where for each couple of photons their invariant mass is

$$m_{\gamma a \gamma b} = \sqrt{E_a E_b[(x_a - x_b)^2 + (y_a - y_b)^2]}/d_{vertex} \qquad (5.3)$$

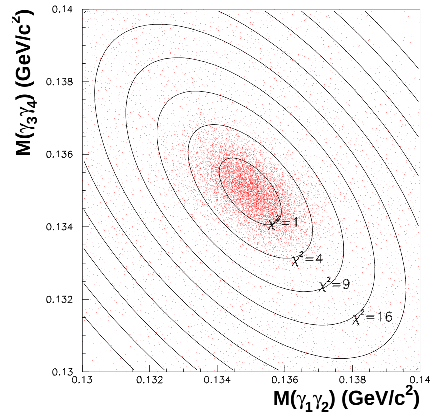

Figure 5.7: $R_{ellipse}$ view in the (m_1, m_2) plane

- charged cuts
  - the origin of K_L fiducial region is at the scintillator (609.4 cm, AKS region)
  - track distance to the center of the beam pipe $> 12cm$
  - both track with $E/p < 0.8$ (to exclude electrons from K_{e3} background). The kaon energy is computed through the opening angle of the two tracks before the magnet and their momenta assuming the Kaon invariant mass:

$$E = \sqrt{\frac{\mathcal{R}}{\theta^2}(m_K^2 - \mathcal{R}m_\pi^2)}, \text{ where } \mathcal{R} = \frac{p_1}{p_2} + \frac{p_2}{p_1} + 2 \tag{5.4}$$

  - no hits in the MUon Veto (to exclude electrons from $K_{\mu 3}$ background)
  - tracks momenta $p > 10GeV/c$
  - Closest Distance Approach (CDA) $< 3cm$
  - COG $< 10cm$
  - Track impact point within Lkr acceptance
  - asymmetry cut to exclude asymmetric decay in which one track is closed to the beam tube (where the MC is more critical) ASP $< min(0.62, 1.08 - 0.0052 \times p[GeV])$; where $ASP = |p_1 - p_2|/(p_1 + p_2)$ is related to the decay orientation in the kaon rest frame

* invariant mass $m_{\pi\pi}$ closed ($\pm 3\sigma_m$, σ_m is typically $2.5MeV/c^2$) to Kaon mass
* cut on high p'_T event: $p'^2_T < (200MeV/c)^2$, to reduce K_L semileptonic decays background in a symmetric way between K_L and K_S . p'_T , as shown in Fig. (5.8), is the p_K component orthogonal to the line joining the production target and the point where the kaon trajectory crosses the DCH1.

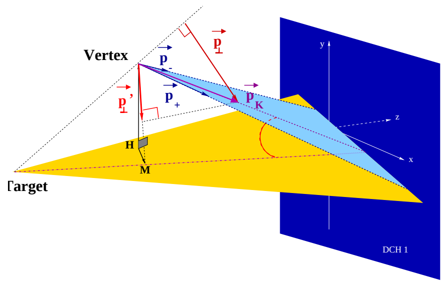

Figure 5.8: p'_T definition

The COG cut, both in neutral and charged event is to reject, in K_S beam, the beam halo formed by re-scattering at K_S collimator or in the AKS. In neutral events is computed from four photons energy and position:

$$COG = \sqrt{(\sum_i E_i x_i)^2 + (\sum_i E_i y_i)^2}/E \tag{5.5}$$

In the charged events the positions are obtained from the tracks extrapolation to the Lkr plane. In true data there are more cuts needed as AKS veto on K_S , tagging, bad burst rejection both in trigger and detectors that are described in detail elsewhere [2, 3].

The agreement between overlaid MC and true data variables is pretty good, a better agreement on $R_{ellipse}$ variable has been reached in 2001 MC while up to 1999 it was underestimate. This can be seen in Fig. (5.9) where the $R_{ellipse}$ for original, overlaid and double overlaid is shown compared to the true data spectra for 1998 sample. The agreement between overlay and data is not very good, and a better agreement is reached only with the double overlay showing clearly that there is some underestimate effect in MC.

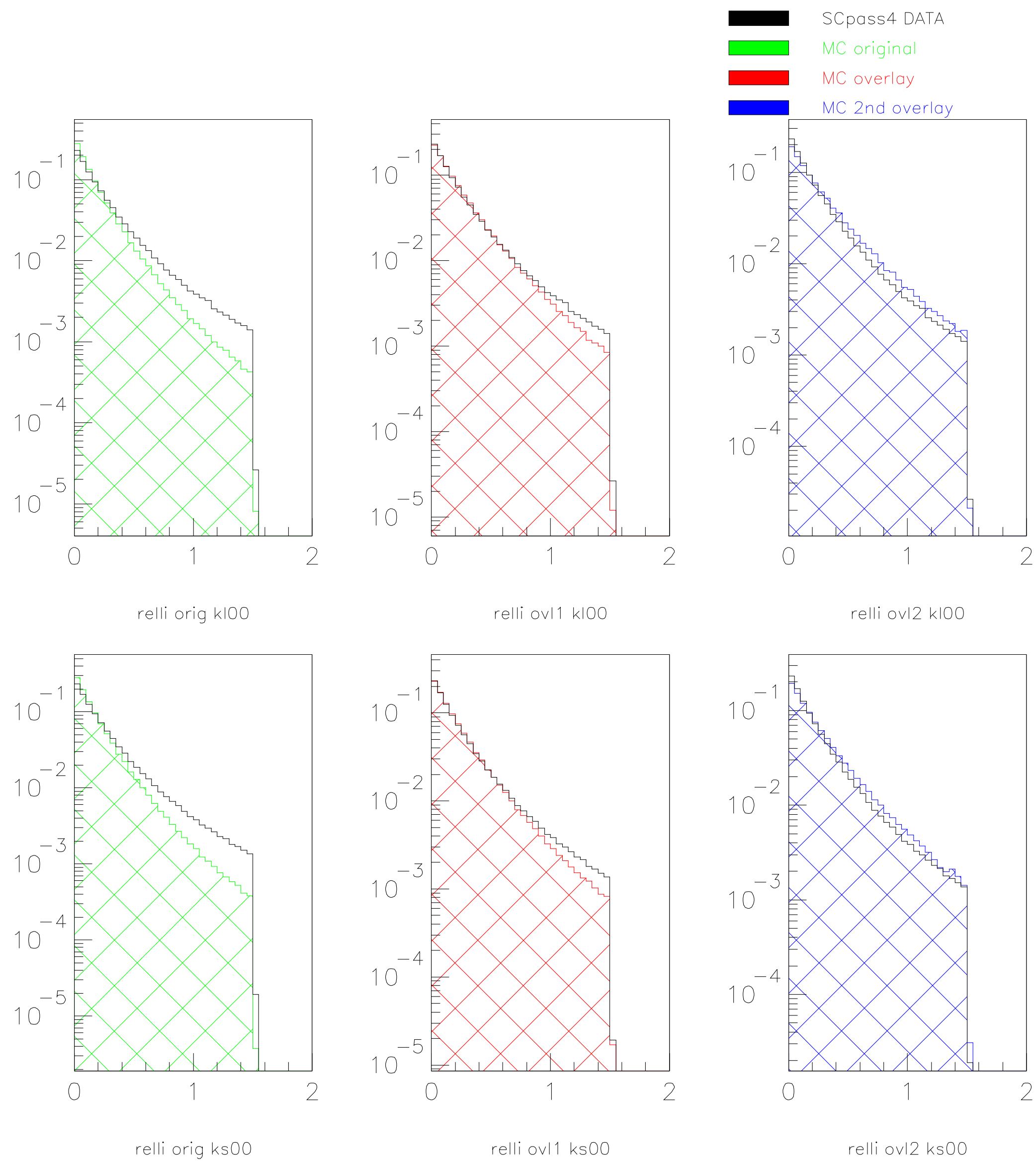

Figure 5.9: K_L and K_S $R_{ellipse}$ comparison in data and original MC, overlay, double overlay; 1998 sample

In 2001 the the good agreement has been reached, with the introduction in MC of non-gaussian tails in Lkr response, as shown in Fig. (5.10)

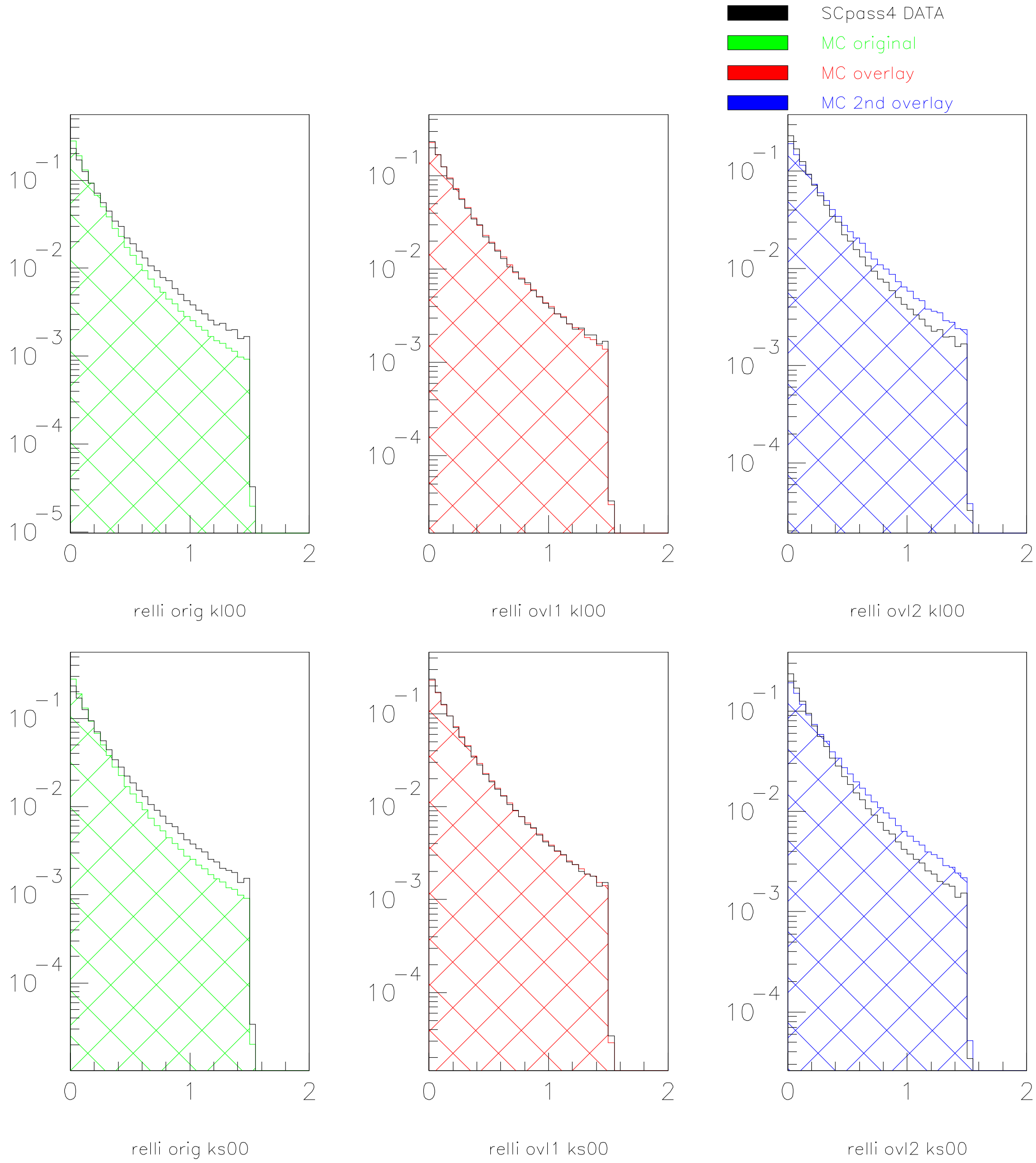

Figure 5.10: K_L and K_S $R_{ellipse}$ comparison in data and original,overlay, double overlay; 2001 sample

On charged events small discrepancies remain e.g.on p'_T as shown in (Fig. (5.11)) where the overlay, and double overlay too, are underestimate.

Losses and Gains are then evaluated and the Losses-Gains (giving λ_k^j) are used to compute $\delta\lambda^j = (\lambda_L^j - \lambda_S^j)$ where j=C,N and $(\delta\lambda^{+-} - \delta\lambda^{00})$.

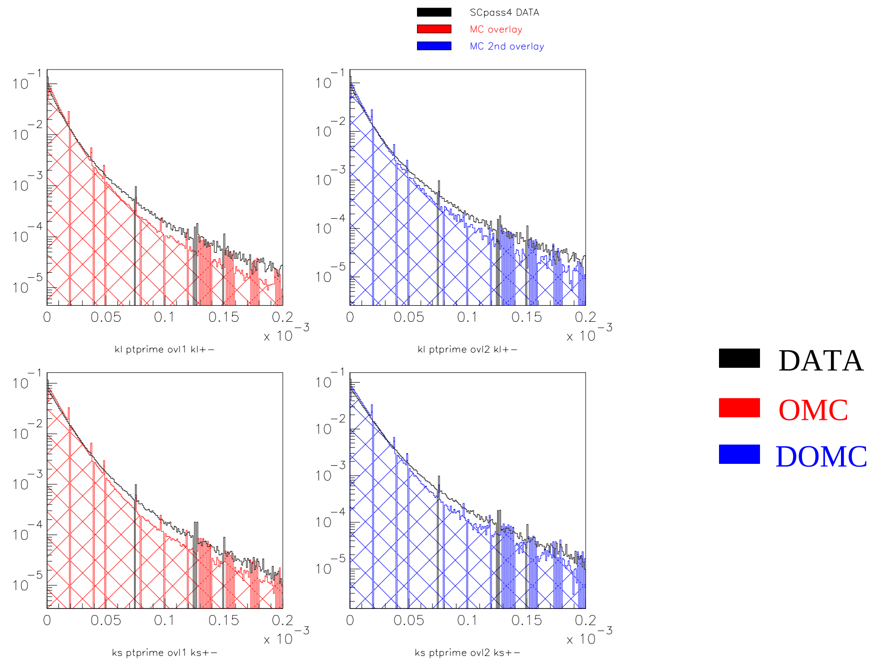

Figure 5.11: K_L and K_S p'^2_T comparison in data , overlay and double overlay; 2001 sample

An OMC event can be identified as:

- loss: bad overlaid coming from good original event
- gain: good overlaid coming from bad original event
- common: good overlaid coming from good original event

in the same way a DOMC event can be identified as:

- loss: bad double overlaid coming from good overlay event
- gain: good double overlaid coming from bad overlay event
- common: good double overlaid coming from good overlay event

The major source of event losses is in the charged mode and it is the overflow cut in DCHs. This cut reject the event if for at least one plane in DCH1,2,4 is found to satisfy the overflow condition (more than 7 hits in 100ns in one plane) in a 625ns time window around the event time. The overflow incidence is obviously higher in charged than neutral since in the first the overflow is enhanced by the 2 hits (per plane) related to the charged event itself. On the neutral side, in 2001 $\approx$ 0.7% of neutral losses are due to noise in the Lkr, but once it is subtracted the charged losses are higher than neutral, as they were in the past.

Losses due to noise in the detector are not intensity depend and certain cuts are sensitive to noise e.g. in the overflow case a group of noisy wires enhance the overflow probability. But the overflow is insensitive to illumination difference since the cut is set looking over all the spectrometer, as a consequence if there is an effect of illumination difference it is well below the % we measure. As already explained in (§ 5.2.1.2) the main difference in losses between Data Overlay and DOMC is due to the overflow cut probably due to MC hits simulation [43]. [1]

In the neutral case the main sources of losses is the $R_{ellipse}$ cut but also in this case the DOMC losses are underestimate with respect to DO, despite the good agreement of the OMC and data variable.

The measure of this correction involve a wide group of people [46, 47, 48, 49] and all agree on a difference in losses between K_S and K_L at the per mille level. The effect computed with weighted or un-weighted K_L (in which the illumination difference is bigger), is found to be compatible with zero. The correction to R is therefore, both on OMC and DO, consistent with zero with the uncertainty of $\pm 3.0 \times 10^{-4}$ as it was in the past, being dominated by the statistical error of the overlay procedure.

5.4 Accidental activity correction result

Combining the results from the intensity and geometrical terms the effect on R is found to be consistent with 0 with $\pm 3.1 \times 10^{-4}$ uncertainty. The overall correction is also computing all in once using OMC Brute Force overlay, but the statistics is worse with respect to mixed overlay since K_S randoms are used only for K_S events and K_L randoms only for K_L events. The resulting correction to R is $(4.7 \pm 4.9) \times 10^{-4}$, where the quoted error is statistical. While the systematic uncertainty from random triggers accuracy is expected to be $\approx 1 - 2 \times 10^{-4}$.

[1] DCH4 in random events presents almost the same overflow rate and hit multiplicity than DCH2, as shown in (§ A.2) and (§ A.5)

5.5 Conclusions

The 1998-99 result on the ΔR due to accidental activity was $(0 \pm 4.2) \times 10^{-4}$, where both ΔR_{Int} and ΔR_{Geom} corrections had zero value but the uncertainties were $\pm 3 \times 10^{-4}$. It is true that these were not the only high value uncertainties, but it was possible to reach a lower value, at least on ΔR_{Int} , with a better understanding of accidental activity influence. This was one of the 2001 proposed items and we succeed on it obtaining a better measure on ΔR, lowering the error to $\pm 3.1 \times 10^{-4}$, and obtaining also the verification of the linearity of losses with K_L beam intensity.

The improvement on ΔR uncertainty comes from the ΔR_{Int} part, being the geometrical error dominate by overlay procedure statistics. This has been achieved through the informations of the new Ferrara beam monitors with four integration times each: 200ns, $1\mu s$, $3\mu s$, $15\mu s$. They had shown the capability to represent the instantaneous beam intensity and their use gave us very good results: the correlation with Lkr clusters (K_L beam dominated detector), especially the (K_L) 200ns channel, their use in the accidental related correction and to verify the linearity of losses with K_L beam intensity, the clear identification of a very high intensity first period in the burst. I have participated to the analysis of this correction, in particular in the correlation part and OMC related items (both in 1998-99 and 2001 sample). But the big effort was in the installation of the monitors and have them properly working.

By June 2001 the devices have been installed by P.L. Frabetti and myself, with the help of Marco Contalbrigo. We have performed all the test needed to have the proper calibrations, gains, rising time, integration time and offset definition. I have adapted the decoding software for the raw data and I have then written the common routine for proper pedestal subtraction in the reprocessed data ('Compact' level). I have studied the monitors data quality and the AKS problem, explained in the third chapter.

Besides, I have joined the project of new DCH readout (App.A), performed by the Ferrara group. On this subject I have studied the old readout overflow statistics, useful for the design of the new electronics. In 2001 run, I have worked to the test of prototypes implementing the decoding software and analyzing the data. During the 2002 run the whole new readout was installed and I was involved in each step of the work. My special contributions were the decoding, the raw data analysis and the software error handling at Compact level.

Appendix A

New drift chambers' readout

A.1 Why a new readout

The drift chambers' readout we have token about up to now is the one involved up to 2001 run. In 2002 a new readout has been installed. In order to distinguish between them we will refer to *old readout*, the first, and *new readout*, the second one. In Fig. (A.1) the four chambers are represented.

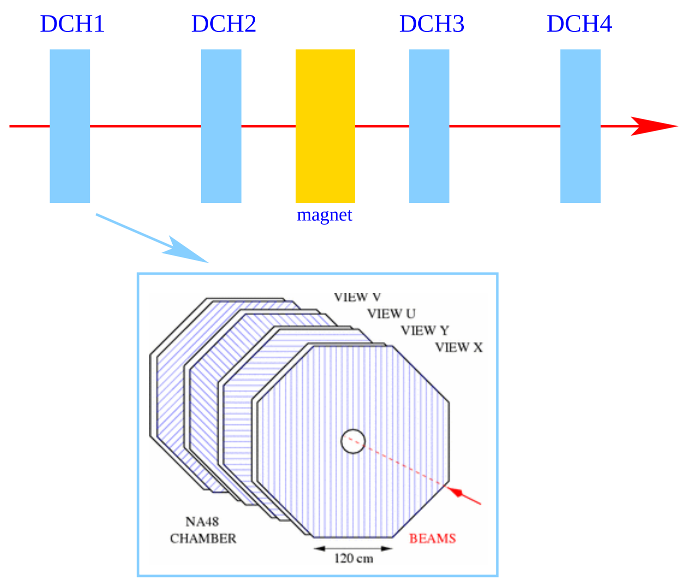

Figure A.1: Four chambers drawing

Each chambers houses 8 planes instrumented to be read out, except the third chamber in which only four planes are instrumented. One centimeter is the distance between two consecutive planes, defining a view. Each old-readout card houses 16 TDC cards to read the 256 wires in the plane. The central wires are divided in two groups, 16 wires each, of half wires soldered on rings at the beam pipe surface. In the old-readout a limit is imposed on the number of hits that can be read in each plane, if more than 7 hits are collected in 100ns, an overflow condition is imposed. If this happens the only information from the plane in overflow is a special word (the overflow word) that means there is no way to read out the hits' informations. To be safe in the analysis the overflow flag is set on a bigger time window of 625ns around the event time. In this way not only there is enough time to empty the readout memory but losses on informations of events closed to the overflow condition are excluded. The cut is imposed if at least one plane in DCH1 or DCH2 or DCH4 shows an overflow. The overflow condition can induce losses also at charged trigger level so to have an indication of the true estimation of overflows we look at them in random events. The percentage of events flagged by the overflow cut is far from being negligible, moreover the project to have a K_S high intensity (KSHI) run in 2002 and the KSHI run took in 1999 (see next) highlight the necessity to built a new readout free from overflow.

A.2 Old readout overflows in 1999 K_S high intensity run

In 1999 $\sim$ 9000 bursts were taken with the K_S only beam at 200 times the usual K_S only run, $\sim$ 10 randoms per burst have been collected. The analysis of overflow incidence on random events has shown a $\approx$ 30% [50, 51] of overflows in at least one plane in DCH1 or DCH2 or DCH4. An overflow can be induced by [2]

- a noisy group of wires or amplifier card,
- showers, induced by interaction of electrons or photons in the material surrounding the beam pipe in the spectrometer region,
- δ rays, coming from interaction of charged particles with the drift chamber gas.

In the first case only one or two planes are affected by the overflow, but in the other cases, since the spacing between planes is only 1cm, it is not difficult for a shower or δ ray to enhance the overflow probability over the whole chamber.

The overflows distribution in the four chambers is shown in Fig. (A.2) (on the left) with the relative percentage per chamber. Looking an the distribution per plane shown in Fig. (A.3) it is clear that a noisy group of wires enhances the overflow probability.

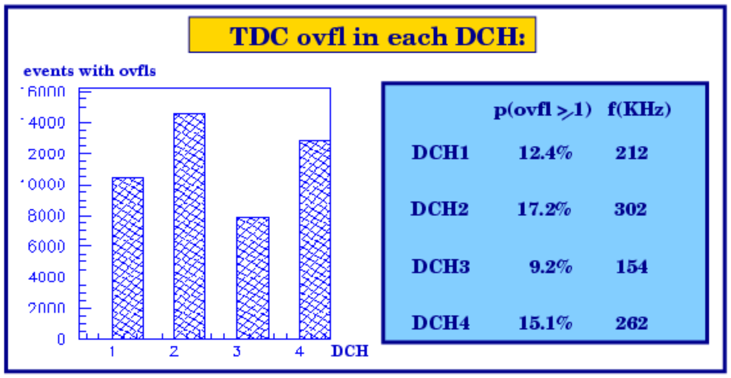

Figure A.2: Overflows distribution in the four chambers (left) and their percentage (right). Third chamber is only half instrumented

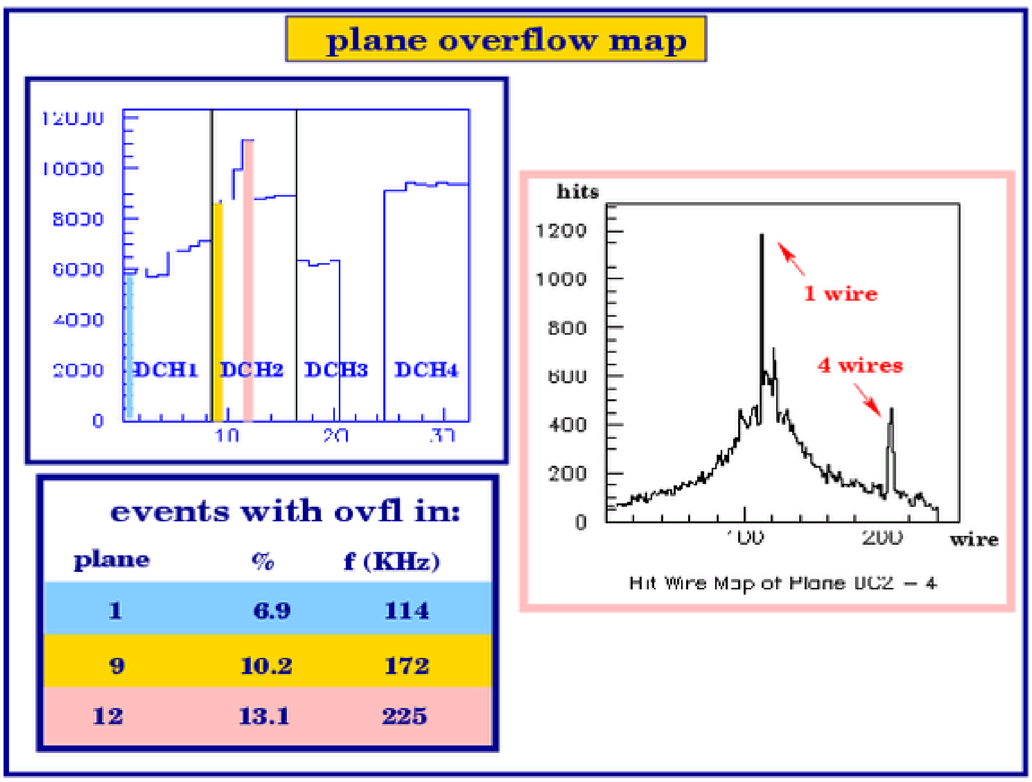

Figure A.3: Overflows plane map (left) and wire map for an 'overflow-hot' plane (right)

A.3 New readout prototype test in 2001 run

The new readout project has been designed in Ferrara by Angelo Cotta Ramusino, Stefano Chiozzi, Roberto Malaguti and Chiara Damiani. The basic component is the TDC-F1 chip developed for the COMPASS experiment at CERN but it is flexible to fit for the NA48 application too [52]. Each chip reads eight channels, four chips are placed on a compact mezzanine card (CMC) as it is in the COMPASS experiment but with a modified design for NA48 purposes. Eight CMCs, 32 channels each, are needed for each plane and mounted on the front end modules. In Fig. (A.4) a drawn of a new readout is shown: one Master and one Slave card per plane, each card housing 4 CMCs. From the chamber front end the 256 channels are grouped in 16 channels connectors so that 2 connectors are read by one CMC.

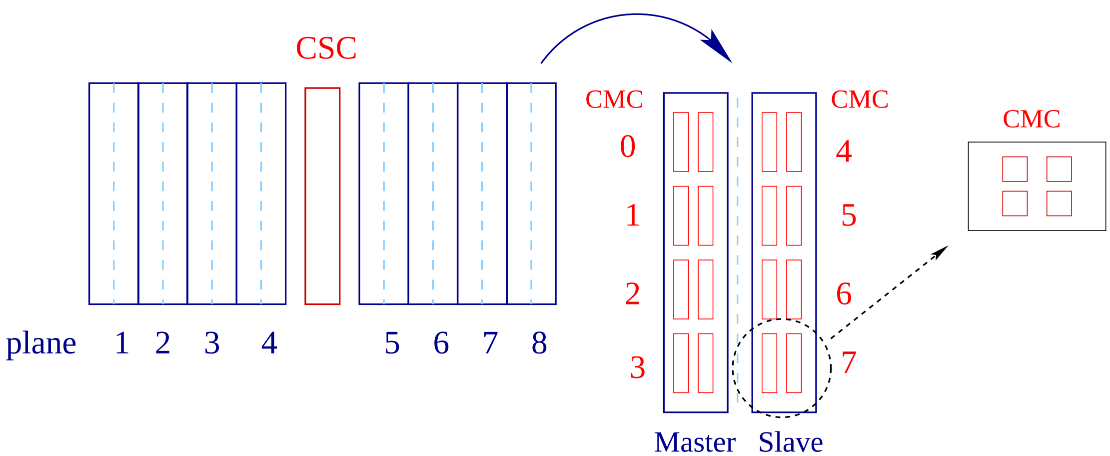

Figure A.4: New dch readout drawing, 8 planes per crate, 1 Master and 1 Slave card per plane, 8 CMCs per plane, 4 chips per CMC

The first eight CMCs prototype cards has been delivered in March 2001 and the beam test has been done during the 2001 run using the two ready master cards. Tests in two position were done:

- two masters to read plane 2, DCH3
- half plane 1 and half plane 2 (half X-view),on DCH4

Both position were equipped with splitters to have a parallel reading of both old and new readouts.

Comparison between the two required:

- the exclusion of old readout overflows

- the same readout time window.

  Both new and old were using a $1.2\mu s$ readout time window but in different ways: the new-readout's windows is simmetric around the trigger time while the old-readout works in three slots of 400ns each, taking the slot in which the trigger is and its nearest neighbors (before and after) (Fig. (A.5)).

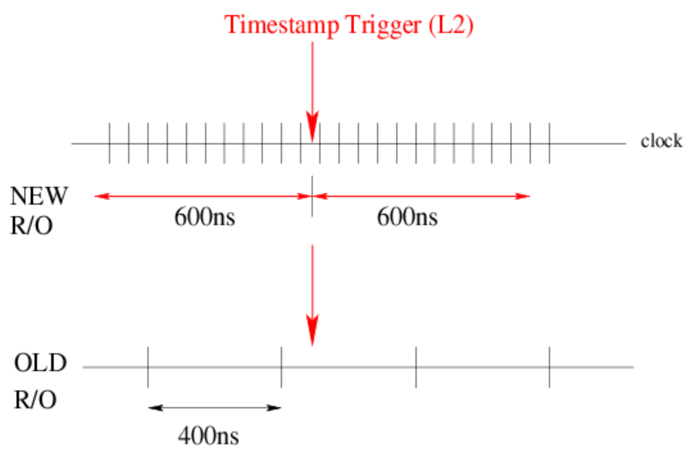

Figure A.5: New and Old readout time window

The comparison between the two readouts gave very good results both in the $Re(\epsilon'/\epsilon)$ run and in the KSHI run, as shown in Fig. (A.6) and Fig. (A.7). Some bursts showed us some problems as bit errors or time mismatch that had been investigated and solved.

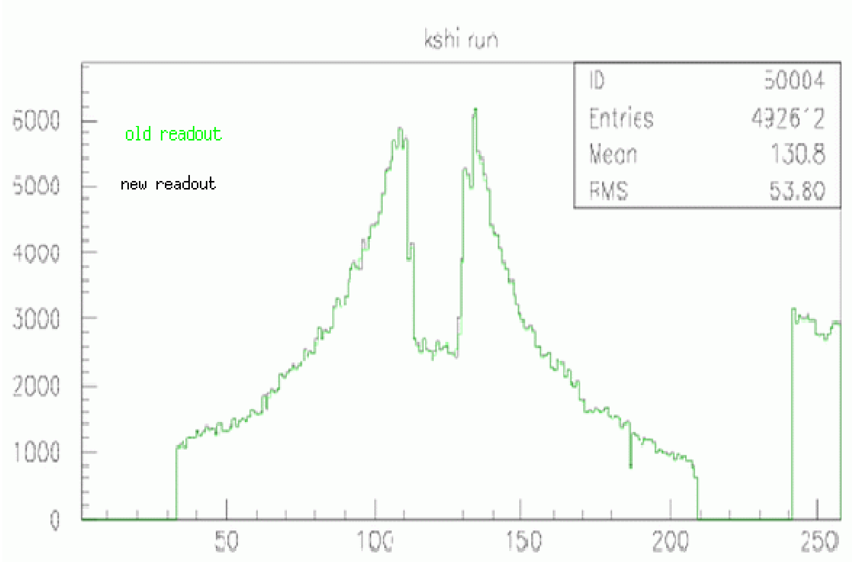

Figure A.6: KSHI New and Old readout wiremap in plane 2,DCH3. The flat zones at the edges are due to the 2 CMCs not installed

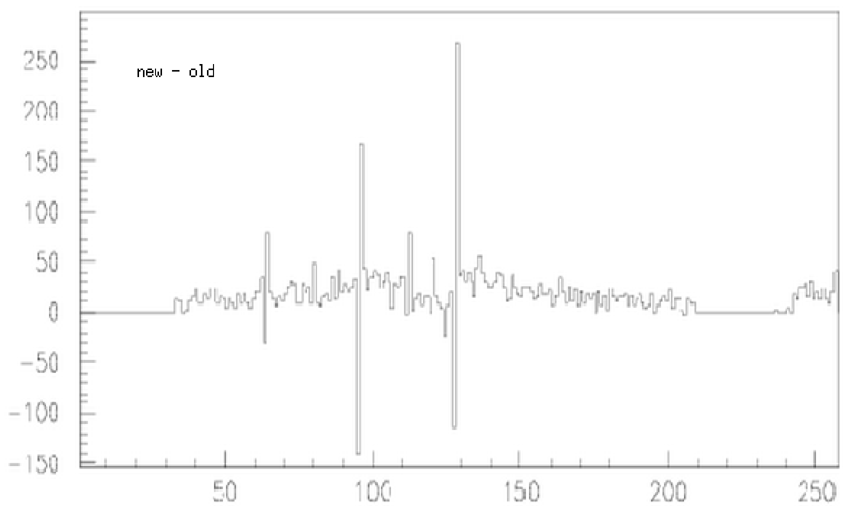

Figure A.7: KSHI New and Old readout difference in plane 2,DCH3. Bit errors are present. The holes at the edges are due to the 2 CMCs not installed

A.4 New readout at work in 2002 run

The full new readout as described in Fig. (A.4) has been installed in April 2002 and took data in the 2002 KSHI. The new readout can take high multiplicity events, the only limit on plane multiplicity (63hits/plane) being required by the DAQ system. As shown in Fig. (A.8) and Fig. (A.9), two pictures taken from the online event display , the new readout was able to see the big events illuminating a whole chamber (e.g. DCH2 in Fig. (A.8) and DCH4 in Fig. (A.9)).

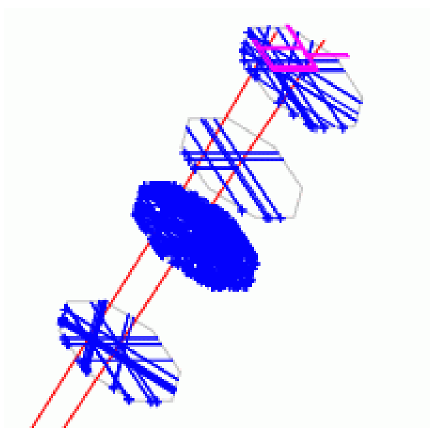

Figure A.8: New dch readout at the online event display. Splash event in DCH2

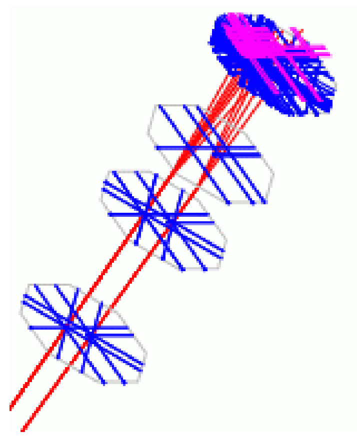

Figure A.9: New dch readout at the online event display. Splash event in DCH4

Anyway it is difficult to reconstruct this very high multiplicity events illuminating a whole chamber, especially if this happens in DCH4 Fig. (A.9). In this case as a consequence of the full illumination the DCH4's point association to tracks takes too much time and we cannot be confident in its accuracy.

The upgrades done on the experiment, mainly new readout installation and the software improvements on the Lkr readout, had allowed to take data at the very high intensity of $\approx 5 \times 10^{10}$ protons from SPS per pulse and to collect ≈ 50000 triggers per burst. To take data at this very high intensity the drift chambers HV has been reduced by 50V, the $\pi^+\pi^-$ mass resolution had thus worsen a little from 2.5 to 3.1 MeV/c^2, but it is good enough for the 2002 rare decays.

In Fig. (A.10) an example of the hits distribution (wire map) in four DCH2's planes is given, while in Fig. (A.11) the efficiency per plane (top) and the number of inefficient wires per plane (bottom) are shown. The efficiency is computed using tracks extrapolation, the third chamber has only four planes instrumented and is used as a sort of 'spare' chamber. That is why its planes have the worse efficiencies.

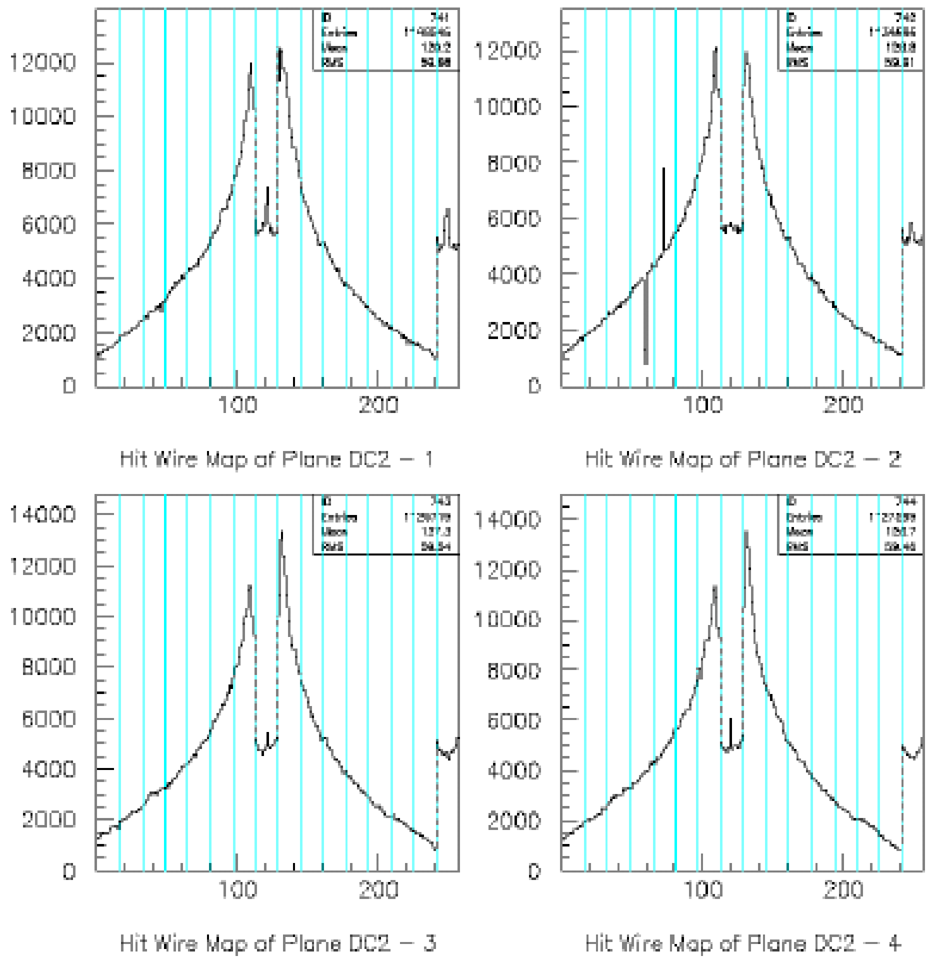

Figure A.10: Example of new dch readout wire maps in chamber 2. Hits are from rawdata control triggers, 50 bursts

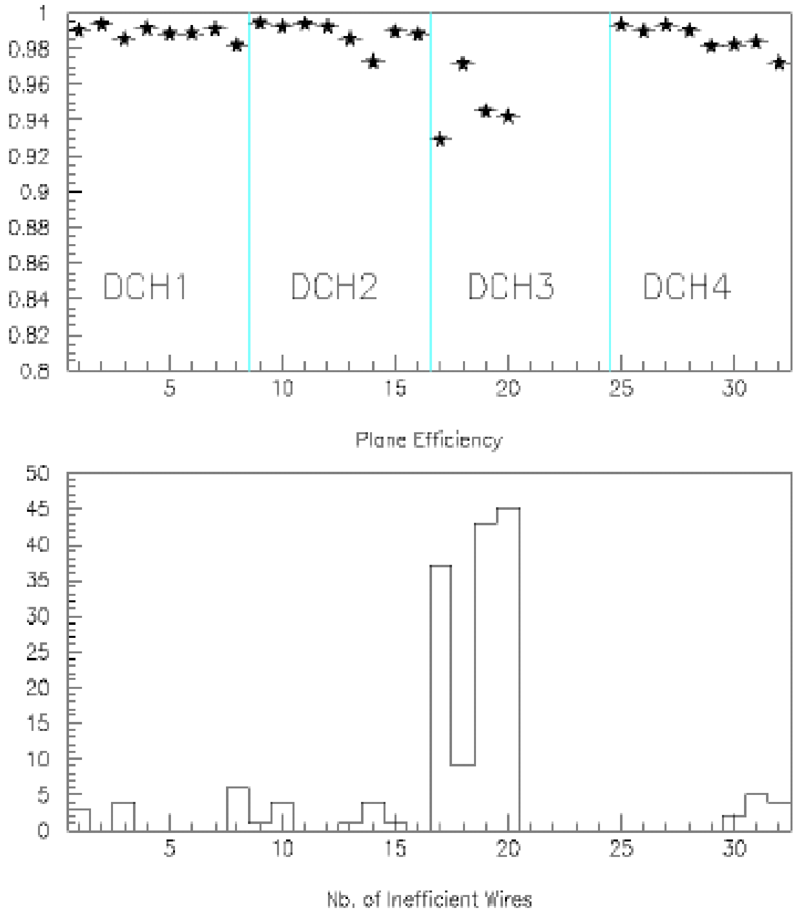

Figure A.11: Example of new dch readout efficiency per plane (up) and number of innefficient wires per plane (down). Hits are from rawdata control triggers, 50 bursts

A.5 Multiplicity studies in 2002 random events

Studying the old readout overflows we have seen that they were induced by noise, showers and δ rays. In the noise-induced case we had one or two plane at most in overflow, while showers and δ rays were responsible for overflows in many planes. So far we have studied the overflow rate and distribution in random events, both in $Re(\epsilon'/\epsilon)$ and KSHI runs. Now we can profit, from the new readout capability to collect up to 63hits/plane (DAQ limit), to investigate the multiplicity in random events ($\sim$ 30 per burst). As already mentioned, to cope with the high 2002 intensity ($\sim 5 \times 10^{10}$ppp) the drift chamber voltage has been lowered. On the new readout (and trigger) side to lower the noise and accidental rate the time window, that in 2001 tests was $\pm 600ns$ around the trigger time, has been reduced to $[-100, 300]ns$. With the new readout we can see, for the first time, the whole activity responsible for the old readout overflows.

Far from being negligible, the multiplicity in randoms can reach the upper limit of 63hits/plane, not only in a single plane but also in the whole chamber. In Fig. (A.12) the multiplicity per chamber is shown, here we can see that chamber two and four have few events reaching the highest limit (63×8). Of course DCH3 has the lowest multiplicity, since only 4 planes are instrumented.

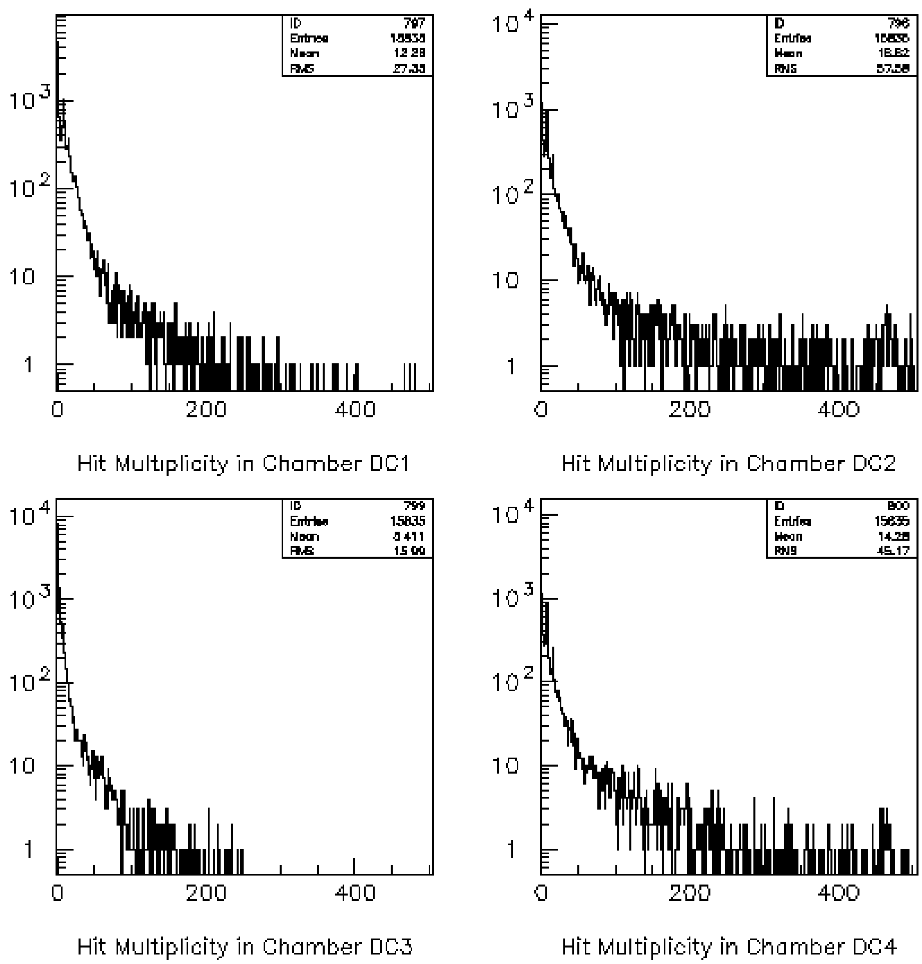

Figure A.12: New dch readout chambers multiplicity in random events, 500 bursts

The plane multiplicity plots are shown in Fig. (A.13), Fig. (A.14), Fig. (A.15), Fig. (A.16). Recalling the MC underestimation of overflows in DCH4 (§ 5.2.1.2) we can observe that this chamber is populated only slightly less than DCH2.

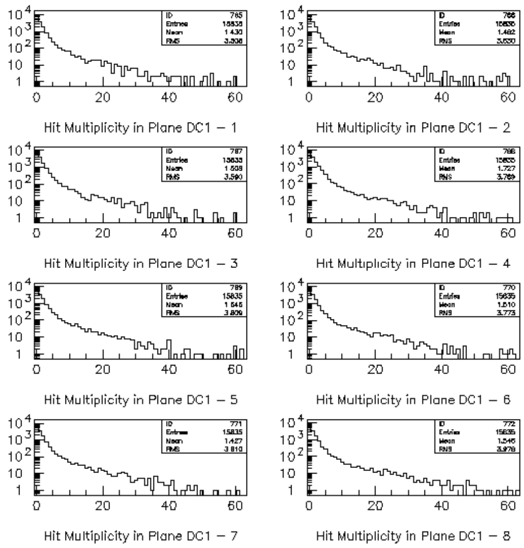

Figure A.13: DCH1 Plane multiplicity in randoms events, 500 bursts

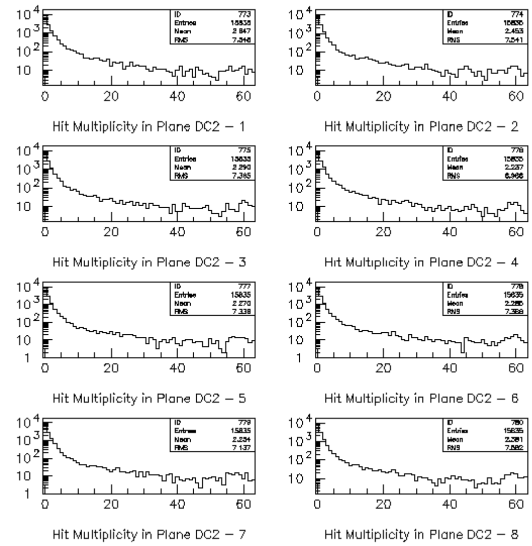

Figure A.14: DCH2 Plane multiplicity in randoms events, 500 bursts

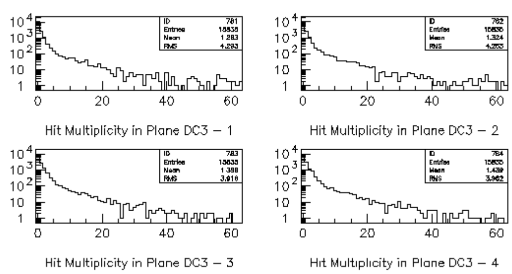

Figure A.15: DCH3 Plane multiplicity in randoms events, 500 bursts

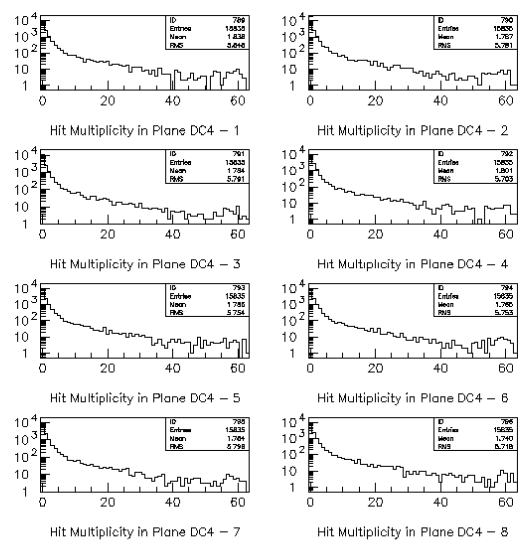

Figure A.16: DCH4 Plane multiplicity in randoms events, 500 bursts

Moreover we can try to estimate the overflow rate we would have observed using the old readout. Since the two electronics work in different ways, and with different readout windows, this can only be a rough evaluation. To 'simulate' the old readout behavior we follow the usual definition and selection cut:

- a plane is overflow-flagged if there are more than 7 hits in 100ns

- an event is overflow-flagged if there is at lest one plane in overflow, in a [-300,300]ns around the event time, in DCH1 or DCH2 or DCH4

The 'overflow' plane map obtained is shown is Fig. (A.17). A check of this procedure is the enhanced 'overflow' level in noisy plane, like plane 1 in DCH2 (Fig. (A.18)), as plane 4 in DCH2 in 1999 KSHI (Fig. (A.3))

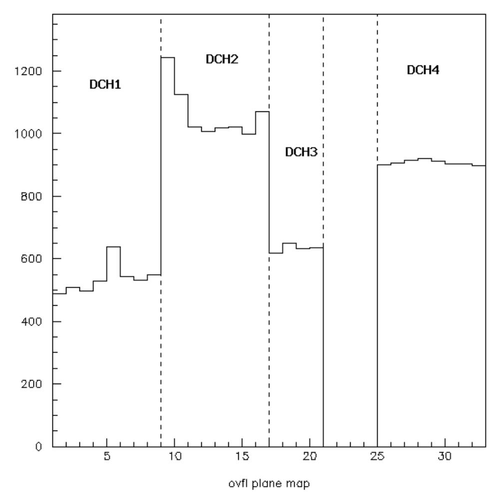

Figure A.17: Plane map of reproduced old-readout overflow in random events

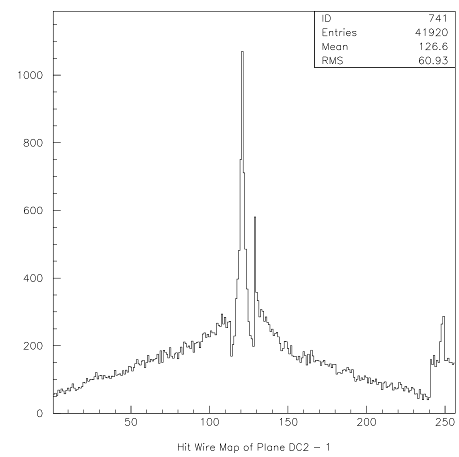

Figure A.18: DCH2 first plane: example of noisy wires inducing reproduced 'old-readout' overflow, random events, 500bursts

The resulting 'overflows' rate is $\sim 20\%$ [1]. Recalling that

- the new-readout window has been reduced to $[-100, 300]ns$ around the trigger time and

- the old-readout window was $1.2\mu s$.

If we assume the linearity of overflows in random with the readout window, the overflow rate should be tripled.

[1] In 1999KSHI we obtained an overflow rate of $\sim 30\%$. In 2001 and 2002 runs, compared to 1999, a lower instantaneous intensity was achieved thanks to the better SPS duty cycle, a longer spill and lower momentum of primary protons. But 2002 intensity (5×10^{10} ppp) was higher than 1999KSHI ($\sim 6 \times 10^9$ ppp).

Bibliography

[1] V.Fanti et al. A new measurement of direct CP violation in two pion decays of the neutral kaon. Phys.Lett. B, 465:335–348, 1999.

[2] A.Lai et al. A precise measurement of the direct CP violation parameter Re(epsilon prime/epsilon). Eur. Phys. J. C, 22:231–254, 2001.

[3] J.R.Batley et al. A precision measurement of the direct CP violation in the decay of neutral kaons into two pions. Physics Letters B, 544:92–112, 2002.

[4] J.R.Batley et al. ADDENDUM 2 TO THE PROPOSAL A high sensitivity investigation of KS and neutral hyperon decays using a modified KS beam. CERN/SPSC 2000-002, 2000.

[5] J.R.Batley et al. ADDENDUM 3 TO THE PROPOSAL For a Precision Measurement of Charged Kaon Decay Parameters with an Extended NA48 Setup. CERN/SPSC 2000-003, 2000.

[6] J.H.Christenson et al. Evidence for the 2π Decay of the K(2)0 Meson. Phys. Rev. Lett., 13:138, 1964.

[7] K.Hagiwara et al. 2002 Review of Particle Physics. Phys. Rev. D, 66, 2002.

[8] M.Battaglia and L.Gibbons. Determination of $|V_{ub}|$. in Review of Particle Physics,K. Hagiwara et al., Phys. Rev. D, 66, 2002.

[9] F.Halzen A.D.Martin Quarks & Leptons: an introduction course in Modern Particle Physics. John Wiley & sons, 1984.

[10] A.Masiero. CP violation for pedestrians. In 1993 European School of High-Energy Physics, number 94-04. CERN, 1994.

[11] J.L.Rosner. Present and Future Aspects of CP Violation. In VIII J.A. Swieca Summer School Proceedings, number hep-ph/9506364. World Scientific, 1995.

[12] V.A.Rubakov Cosmology and Astrophysics. In 2001 European School of High-Energy Physics, number 2002-002. CERN, 2002.

[13] D.Wyler. Flavour Physics: what, why and how. In 2001 European School of High-Energy Physics, number 2002-002. CERN, 2002.

[14] C.T.Sachrajda. Flavour Physics. In 1997 European School of High-Energy Physics, number 98-03. CERN, 1998.

[15] P.Nason and G.Ridolfi. An introduction to CP violation. PhD lessons, Milan, 2000.

[16] P.Nason and G.Ridolfi. An Introduction to the Standard Model of Electroweak Interactions. PhD lessons, Milan, 2000.

[17] B.Winstein and L.Wolfenstein. The Search for Direct CP Violation. Rev. Mod. Phys., 65:1113–1147, 1993.

[18] V.Novikov. Field Theory and the Standard Model. In 1998 European School of High-Energy Physics, number 99-04. CERN, 1999.

[19] Y.Nir. Flavour Physics and CP violation. In 1998 European School of High-Energy Physics, number 99-04. CERN, 1999.

[20] C.Jarlskog. Commutator of the quark mass matrices in the standard electroweak model and a measure of maximal CP violation. Phys. Rev. Lett., 55:1039–1042, 1985.

[21] C.Jarlskog. Introduction to the Standard Model. In 1989-1990 CERN Academic Training Lectures, number AT00000327. CERN, 1990.

[22] A.J.Buras, M.E. Lautenbacher and G. Ostermaier. Waiting for the top quark mass, $K^{+-} \to \pi + \nu\overline{\nu}, B_s^0 - \overline{B}_s^0$ mixing, and CP asymmetries in B decays. Phys. Rev. D, 50:3433–3446, 1994.

[23] Roberta Arcidiacono. Effetti sistematici sulla misura di ϵ'/ϵ nell'esperimento NA48 al CERN: efficienze di trigger e correzioni per accidentali. PhD thesis, Universitá degli Studi di Torino, Jan. 1999.

[24] Gianmaria Collazuol. Rate Effects in the Measurement of the Direct CP Violation with the NA48 Experiment at CERN. PhD thesis, Universitá degli Studi di Firenze, Dec. 2000.

[25] NA48 collaboration. Proposal for a precision measurement of ϵ'/ϵ in CP violating $K \to \pi\pi$ decays. CERN/SPSC/90-22, 1990.

[26] G.Graziani and S.Palestini. K_L/K_S interference and pure K_S in the "K_L" beam. NA48 Note/99-29, 1999.

[27] Giacomo Graziani. Stability of the $Re(\epsilon'/\epsilon)$ result. NA48 Note/2002-16, 2002.

[28] Guillame Unal. Accidental effects on R. NA48 Note/2001-09, 2001.

[29] N.Doble, L.Gatignon and P.Grafstr$\ddot{o}$m. A novel application of bent crystal channeling to the production of simultaneous particle beams. NA48 Note/1995-13, 1995.

[30] M.A.Parker, R.Moore, A.Baurichter, K.Kirsebom, R.Medenwaldt, U.Mikkelsen, S.P.Møller, E.Uggerhøj, T.Worm, N.Doble et al. Measurement of pair-production by high energy photons in an aligned tungsten crystal. Nucl. Inst. and Methods B, 119:149–155, 1996.

[31] Jean Duclos. CP-violation in the kaon system: recent results obtained by the NA48. Seminar Ferrara, October 21, 2002.

[32] Victoria Jane Martin. A measurement of the CP Violation Parameter $Re(\epsilon'/\epsilon)$. PhD thesis, University of Edinburgh, Aug. 2000.

[33] E.Griesmayer, G.Neuhofer, F.Bergsma, J.P.Grillet, P.F.Dalpiaz, J.Duclos and F.Petrucci. Comparison of field calculations and measurements of a spectrometer magnet. Nucl. Inst. and Methods A, 361:466–471, 1995.

[34] D.Bédereède, J.B.Chèze, M.De Beer, P.Debu, D.Durand, S.Edard, L.Gosset, J.Heitzmann, F.Louis, E.Mazzucato. High resolution drift chambers for the NA48 experiment at CERN. Nucl. Inst. and Methods A, 367:88–91, 1995.

[35] Guillame Unal. Performances of LKR. CALOR2000, Annecy, October 9-14, 2000.

[36] A. Bizzeti, M. Calvetti, M. lenti and A. Michetti. The NA48 Ks Monitor. NA48 Note/97-29, 1997.

[37] H.Blümer. The NA48 Beam Intensity Monitor. NA48 Note/95-08, 1995.

[38] M.Jeitler, I.Mikulec, G.Neuhofer, M.Pernicka, S.Schmied and M.Steininger. The clock and control signal distribution system for the NA48 experiment. Nucl. Inst. and Methods A, 400:101–106, 1997.

[39] R.Arcidiacono, P.L.Barberis, F.Benotto, F.Bertolino, G.Govi and E.Menichetti. The Trigger Supervisor of the NA48 experiment at CERN SPS. Nucl. Inst. and Methods A, 443:20–26, 2000.

[40] M. Contalbrigo. Beam integrators upgrade. NA48 Collaboration Meeting, April 5, 2001.

[41] M.Scarpa, presented by G.Anzivino. Problems in AKL PMB crates. NA48 Analysis Meeting, March 26, 2002.

[42] P.Grafstrom. In-time accidentals. NA48 Analysis Meeting, June 6-7, 2002.

[43] A.Gaponenko, P.Hristov, D.Madigojine. Overlaid Monte Carlo calculation for run 2001. NA48 Note/02-09, 2002.

[44] G. Unal. Tagging inefficiency, $K_L - K_S$ intensity difference. NA48 Analysis Meeting, March 26, 2002.

[45] G. Unal. Overlay losses, Lkr noise. NA48 Collaboration Meeting, February 22, 2002.

[46] G. Unal. R corrections and value, Accidental effects in 2001. NA48 Analysis Meeting, May 3, 2002.

[47] D. Madigojine. results from OMC. NA48 Analysis Meeting, May 3, 2002.

[48] L. Incomidou Fayard. Losses by accidentals and $\Delta\alpha_{LS}$. NA48 Analysis Meeting, May 3, 2002.

[49] M.Scarpa. Ferrara monitors. NA48 Analysis Meeting, May 3, 2002.

[50] R.Sacco. Study of the random events in the high intensity Ks beam. NA48 Collaboration Meeting, February 16, 2000.

[51] M.Scarpa. Overflow rate studies related to new readout. NA48 Collaboration Meeting in Wien, October 5, 2000.

[52] Angelo Cotta Ramusino. NA48 new drift chamber readout (DCHRO): report on the inefficiencies of the "Front End Buffer Block" based on the TDC-F1 ASIC. NA48 Note/2002-18, 2002.